Technische Universität München
TUM School of Medicine and Health

The role of CDC42 in cellular dynamics: Implications for stress, aging, and hematopoiesis

Theresa Landspersky

Vollständiger Abdruck der von der TUM School of Medicine and Health der Technischen Universität München zur Erlangung einer

Doktorin der Naturwissenschaften (Dr. rer. nat.)

genehmigten Dissertation.

Vorsitz: Prof. Dr. Hendrik Sager

Prüfende der Dissertation:

1. apl. Prof. Dr. Robert Oostendorp
2. apl. Prof. Dr. Ralph Kühn

Die Dissertation wurde am 04.09.2024 bei der Technischen Universität München eingereicht und durch die TUM School of Medicine and Health am 04.12.2024 angenommen.

Für all jene, die mit Leidenschaft und Neugier die
Grenzen des Wissens erweitern.

TABLE OF CONTENTS

LIST OF ABRREVIATIONS

5-FU	5-Fluorouracile
AGM	Aorta-gonad-mesonephros region
ALCAM	Activated leukocyte cell adhesion molecule
ALL	Acute Lymphocytic Leukemia
alloHSCT	Allogenic hematopoietic stem cell transplantation
ALP	Alkaline phosphatase
AML	Acute Myeloid Leukemia
AMPK	Adenosine monophosphate-activated protein kinase
BM	Bone marrow
BMP	morphogenetic protein
BV	Bone volume
CASIN	CDC42 Activity-Specific Inhibitor
CDC42	Cell division control protein 42
CLL	Chronic Lymphocytic Leukemia
CLP	Common lymphoid progenitor
CML	Chronic Myeloid Leukemia
CMP	Common myeloid progenitor
CRIB	CDC42/Rac1-interactive binding
EC	Endothelial cell (CD45- TER119- CD31+ SCA-1+)
ECM	Extracellular matrix
EHT	Endothelial-to-hematopoietic transition
ERα	Estrogen receptor alpha
FACS	Fluorescence-Activated Cell Sorting
FGF	Fibroblast growth factor
GAP	GTPase-activating protein
G-CSF	Granulocyte-Colony Stimulating Factor
GEF	Guanine nucleotide exchange factor
GAP	GTPase-activating proteins
Hh	Hedgehog
HSC	hematopoietic stem cell
HSCT	Hematopoietic stem cell transplantation
IF	Immunofluorescence

IFN-α	Interferon-α
IGF1	Insulin-like growth factor 1
IL-1	Interleukin-1
IL-6	Interleukin-6
JNK	C-Jun N-terminal kinase
LPS	Lipopolysaccharide
LT-HSCs	Long-Term hematopoietic stem cells (Lin− Sca-1+ c-Kit+ CD34- CD48- CD150+)
Micro-CT	Micro-computed tomography
MPP	Multipotent progenitor
MSPC	Mesenchymal stem and progenitor cell (CD45- TER119- CD31- SCA-1+ Alcam$^{-/low}$)
mTOR	Mammalian target of rapamycin
Myo6	Myosin 6
O5A$^{\Delta/\Delta}$	Wnt5a deleted mutants
OBC	Osteogenic lineage (CD45- TER119- CD31- SCA-1- Alcam+)
OPTN	Optineurin
PAK4	p21-activated kinase 4
PCK	Protein kinase C
PECAM	Platelet endothelial cell adhesion molecule
pI:pC	PolyInosine- polycytosine
PRKN	Parkin
Rhot-1/Miro-1	Ras Homolog Family Member T1/ Mitochondrial Rho GTPase 1
ROS	Reactive Oxygen Species
Sca1	Stem cell antigen 1
SCF	Stem Cell Factor
TAX1BP1	Tax1 Binding Protein 1
TER-119	Glycoprotein A
TGFβ	transforming growth factor-beta
TLR4	Toll-like receptor 4
TNF	Tumor necrosis factor
TOCA	Transducer of Cdc42-dependent actin assembly
WNT	wingless-type MMTV integration site
Wnt5a	Wingless-type MMTV integration site family member Wnt5a

ABSTRACT

This dissertation identifies the small Rho GTPase CDC42 as a key regulator of cytostatic stress responses, particularly in hematopoiesis and the skeletal system. Overactivation of CDC42 (CDC42-GTP) plays a central role in causing functional defects in both hematopoietic stem cells (HSCs) and mesenchymal stem and progenitor cells (MSPCs), significantly impairing hematopoiesis and skeletal integrity.

Regardless of the method of activation — whether by cell stress in a stress-susceptible mouse model ($O5A^{\Delta/\Delta}$) using the chemotherapeutic agent 5-FU or by lethal irradiation of wildtype mice followed by hematopoietic stem cell transplantation (HSCT) — overactivation of CDC42 consistently resulted in defective F-actin fiber formation in MSPCs. This disruption of the cytoskeleton led to irregular or completely disorganized F-actin fibers, which, in turn, impaired critical cellular maintenance processes, such as autophagy, impacting HSC behavior.

This research shows that pharmacological *in vivo* inhibition of CDC42 with CASIN in mice attenuates elevated CDC42 activation, prevents defective actin-anchored autophagy in MSPCs and protects against lethal cytopenia under stress, as well as skeletal degeneration after HSCT. This makes CDC42 a promising therapeutic target, especially in scenarios where stress, aging, or treatments such as HSCT impair cytoskeletal and HSC function.

ZUSAMMENFASSUNG

In dieser Dissertation wird die kleine Rho GTPase CDC42 als Schlüsselregulator für zytostatische Stressreaktionen identifiziert, insbesondere in der Hämatopoese und im Skelettsystem. Eine Überaktivierung von CDC42 (CDC42-GTP) spielt eine zentrale Rolle bei der Entstehung funktioneller Defekte sowohl in hämatopoetischen Stammzellen (HSCs) als auch in mesenchymalen Stamm- und Vorläuferzellen (MSPCs) und beeinträchtigt die Hämatopoese und die Integrität des Skelettsystems erheblich.

Unabhängig von der Art der Aktivierung - ob durch Zellstress in einem stressanfälligen Mausmodell ($O5A^{\Delta/\Delta}$) unter Verwendung des Chemotherapeutikums 5-FU oder durch letale Bestrahlung von Wildtyp-Mäusen mit anschließender hämatopoetischer Stammzelltransplantation (HSCT) - führte eine Überaktivierung von CDC42 durchweg zu einer defekten F-Aktin-Faserbildung in MSPC. Diese Störung des Zytoskeletts führte zu unregelmäßigen oder völlig desorganisierten F-Aktin-Fasern, die wiederum wichtige zelluläre Erhaltungsprozesse wie die Autophagie beeinträchtigten, was sich auf das Verhalten der HSZ auswirkte.

Diese Forschungsarbeit zeigt, dass die pharmakologische *in-vivo*-Hemmung von CDC42 mit CASIN in Mäusen die erhöhte CDC42-Aktivierung abschwächt, eine defekte Aktin-verankerte Autophagie in MSPCs verhindert und vor tödlicher Zytopenie unter Stress sowie vor Skelettdegeneration nach HSCT schützt. Dies macht CDC42 zu einem vielversprechenden therapeutischen Ziel, insbesondere in Szenarien, in denen Stress, Alterung oder Behandlungen wie die HSCT die Funktion des Zytoskeletts und der HSC beeinträchtigen.

INTRODUCTION

Hematopoietic stem cells and their BM niche

Hematopoietic stem cell hierarchy

Blood cell formation (hematopoiesis) is a complex biological process that primarily occurs in the bone marrow (BM) in vertebrates. In mammalian species, blood cells are mainly produced by a heterogeneous small number of quiescent cells, called hematopoietic stem cells (HSCs) [1]. HSCs are characterized by their ability to self-renew and produce daughter stem cells, as well as to differentiate into various multipotent and restricted progenitors that form all blood cell types [1,2]. Quiescence serves as a protective mechanism to preserve the stem cell pool over time, as DNA damage misrepair can be passed to progeny [3]. Upon exposure to stress, these cells are reactivated and enter the cell cycle. A delicate balance must be maintained to prevent exhaustion and transformation of the stem cell pool while ensuring their ability to maintain homeostasis and respond to injury when necessary [4]. In mice, the most potent self-renewing HSC subset are experimentally defined as long-term-HSCs (LT-HSCs; $CD34^-$ $CD150^+$ $CD48^-$ $Lineage^-$ $SCA\text{-}1^+$ KIT^+ cells) [5]. LT-HSCs have been shown to divide and mature into different progenitor cell subsets, initially becoming positive for the surface markers CD34, Flk2, and CD48, and after several further differentiation steps, they form the two basic mature blood cell types: myeloid and lymphoid cells (Figure 1A [6]) [5,7,8].

The traditional hematopoietic hierarchy describes hematopoiesis as a classical *stepwise process* in which multipotent, oligopotent, and unipotent progenitors progressively differentiate into mature blood cells. Previously, this process was understood to be driven mainly by distinct populations of transiently amplifying committed progenitor cells, such as multipotent progenitors (MPPs) developing into common myeloid progenitors (CMPs) and common lymphoid progenitors (CLPs) [1,2]. In contrast to conventional population-based analyses, single cell genomics, particularly scRNA-seq, provides deeper insights into hematopoiesis, revealing the previously unrecognized heterogeneity of HSCs. The heterogeneity of HSCs is reflected in the different molecular signatures, cellular fates and functional outcomes observed in individual HSCs [6]. Recent studies further suggest that hematopoiesis is a *continuous*

differentiation process. The surprising discovery that multipotent lymphoid progenitors, which typically develop into cells of the lymphatic system, can differentiate into granulocyte-monocyte progenitors suggests that the classical model of hematopoiesis may not be as rigid as once believed and progenitor cells might deviate from their intended differentiation pathways under specific circumstances [6,9]. Furthermore, for instance in the differentiation of megakaryocytes (cells responsible for the formation of blood platelets), some intermediate stages can be bypassed, which indicates a greater flexibility of this process (Figure 1B [6]) [10,11].

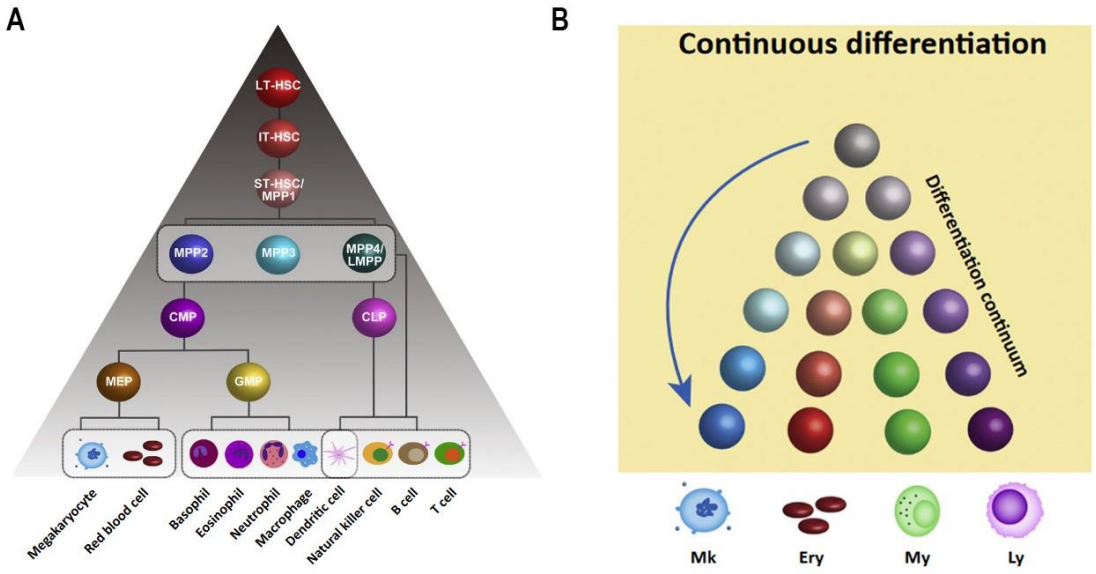

Figure 1: A) Revised roadmaps of hematopoietic hierarchy. B) Continuous differentiation landscapes. Adapted from Zhang et al., 2018.

The differentiation of hematopoietic stem cells ultimately leads to the formation of red blood cells (erythrocytes), platelets, and various types of white blood cells (leukocytes). Leukocytes are essential for immune defense, playing roles in both the innate (nonspecific) and adaptive (specific) immune responses [12,13]. The innate immune system includes monocytes, which become macrophages, and granulocytes (eosinophils, basophils, neutrophils), forming the first line of defense against pathogens and abnormal cells from birth [12-14]. These cells relay information to the adaptive immune response, the lymphocytes (B and T cells), to coordinate a more targeted response [12]. B cells differentiate in the bone marrow, while T cells mature in the thymus and are trained in the spleen and lymph nodes [9,15,16]. Leukocytes have the

unique ability to migrate into the bloodstream and surrounding tissues where they defend against pathogens and foreign substances. They migrate to areas of injury or infection through a process called “diapedesis” guided by molecules from pathogen-associated molecular patterns (PAMPs) and damage-associated molecular patterns (DAMPs) [17]. Innate immune cells like mast cells recognize PAMPs and DAMPs, releasing cytokines to direct leukocytes out of the bloodstream. Compounds such as histamine and heparin from mast cells, along with endothelial cell markers, facilitate leukocyte movement into tissues [17].

The development of the hematopoietic stem cell niche

Functional HSCs are rare cells (<0.01% of total BM cells). As such, HSCs are surrounded by a complex molecular and cellular environment. This environment controls all aspects of HSC behavior, particularly self-renewal and differentiation, both important to maintain and regulate hematopoiesis by expression of surface molecules and secretion of soluble factors [5,18-20]. Collectively, the stem cell regulatory factors and cells surrounding the stem cells are called the *microenvironment* or *niche*.

A fundamental understanding of the role of the hematopoietic niche requires an understanding of how this microenvironment evolves from the embryonic stage to adulthood and how the niche adapts its regulatory mechanisms depending on the changing needs of the organism [21,22]. The differentiation pathways of HSCs during embryonic development are far more complex than previously assumed. The application of scRNA-seq has significantly deepened our understanding of hematopoietic stem cell development. These analyses have confirmed that HSCs originate in different embryonic niches and that their development is highly dependent on the specific microenvironment and prevailing signaling mechanisms [23]. During embryogenesis, HSCs are first identified in the aorta-gonad-mesonephros (AGM) region, where they originate through endothelial-to-hematopoietic transition (EHT) [24-27]. These HSCs migrate to the fetal liver, the primary embryonic niche, where they rapidly proliferate, supported by stromal cells like Nestin+ NG2+ pericytes [28-30]. Through co-culture studies with HSCs, these mesenchymal stromal cells (MSCs) have been identified as the cornerstone for hematopoietic support, as they are expressing vital growth factors such as SCF (stem cell factor), Angptl3 (angiopoietin-like 3), IGF2 (insulin-like growth factor 2), and TPO (thrombopoietin), which drive HSC proliferation

and survival in the fetal liver [21]. Nestin+ NG2+ pericytes further promote HSC expansion by associating with portal vessels in this niche [21]. The fetal liver acts as a temporary but essential hematopoietic niche that promotes the rapid proliferation of HSCs and their differentiation into various blood cells before they finally translocate and settle in the BM. In adulthood, the BM becomes the **primary and permanent hematopoietic niche** in which HSCs reside, self-renew and differentiate into mature blood cells. However, if there is hematopoietic stress, the niche may shift to extramedullary areas such as spleen or liver [24,31].

The adult hematopoietic stem cell niche architecture and cell types

This dynamic evolution demonstrates the adaptability of the niche and the complex interplay of signaling pathways and cellular interactions. This doctoral thesis focuses in particular on the adult hematopoietic stem cell niche and its interaction with HSCs (Figure 2 [21]).

Recently, single-cell analyses have played a crucial role in revealing the composition of the niche as an ecosystem of various interdependent cell types. These analyses, which focused on deciphering the composition of the murine BM niche, have identified more than twenty different subpopulations of cells [32]. Among these, the adult hematopoietic niche primarily comprises non-hematopoietic endothelial cells (ECs), mesenchymal stem and progenitor cells (MSPCs), and osteoblasts (OBCs), all of which play critical roles in maintaining and regulating HSCs [32,33]. Nakamura et al. [34] analyzed bone lining cells that were negative for the cell surface markers CD45, PECAM-1 (platelet endothelial cell adhesion molecule), CD31, and TER-119 (glycoprotein A). They divided this fraction into subgroups based on their expression of ALCAM (activated leukocyte cell adhesion molecule) and SCA-1 (stem cell antigen 1) to determine their impact on HSC maintenance. $ALCAM^{-/low}$ $SCA\text{-}1^{+}$ cells were identified as immature MSPCs, while $ALCAM^{+}$ $SCA\text{-}1^{-}$ subpopulations were considered as OBCs. Additionally, ECs were considered as $CD31^{+}$ $SCA\text{-}1^{+}$ cells [34].

In addition to these core components, the hematopoietic niche also includes chondrocytes, fibroblasts, pericytes, smooth muscle cells, and Schwann cells [32,33]. In addition to non-hematopoietic cells, hematopoietic cells like monocytes and

macrophages also support the maintenance of HSCs and are considered an essential part of the niche [35,36].

HSCs are generally located near the endosteum, the interface between bone and BM, and close to sinusoidal blood vessels [37]. It is believed that there are two distinct locations for HSCs within the niche: the endosteal niche, which likely houses dormant HSCs and supports their maintenance, and the perivascular niche, which supports HSC proliferation and differentiation [38]. The perivascular niche typically contains cells that produce high levels of the chemokine CXCL12 (CAR cells), stromal cells with leptin receptors (LEPR+ cells), and nestin+ MSPCs [39-41]. Nestin+ MSPCs are also found in the endosteal niche, but to a lesser extent [41].

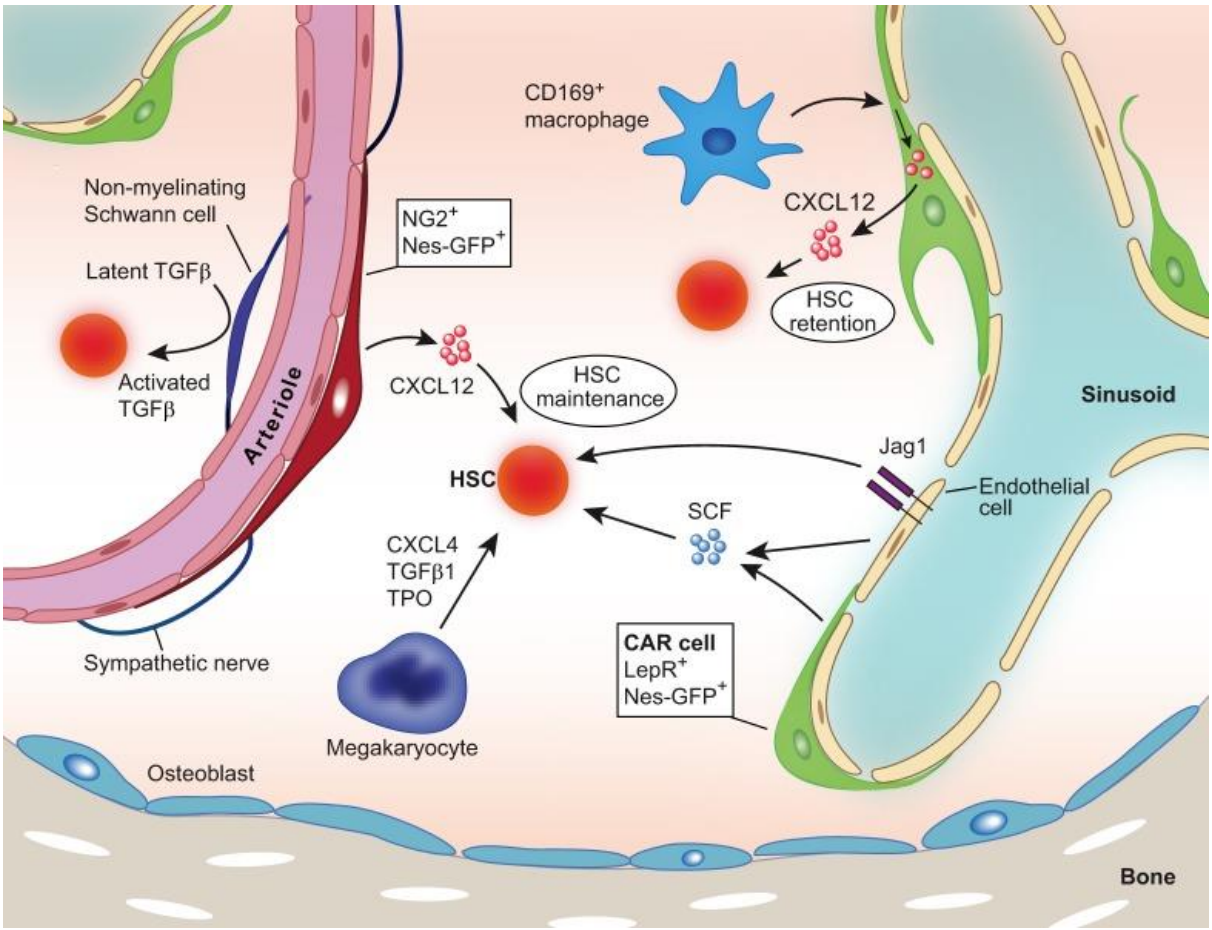

Figure 2: HSC niche players in the adult BM. Model from Gao et al., 2018.

The role of MSPCs in osteogenic differentiation and bone formation

MSPCs have been noted for their capacity to differentiate into fibroblast-like colonies and into various cell types, including adipocytes (fat cells), chondrocytes (cartilage cells), and osteogenic lineages *in vitro* [42,43]. The osteogenic lineages include osteoblasts (bone-forming cells), which are responsible for building bone structure, and osteocytes (mature bone cells), which arise from osteoblasts when they are integrated into the bone matrix. The balance between the differentiation of MSPCs into adipocytes and osteoblasts plays a critical role in determining whether fat or bone tissue is formed, with various signaling pathways such as Wnt and TGFβ/BMP being key regulators in this process [44,45]. Disruption in this balance can lead to pathological conditions where increased adipogenesis at the expense of osteogenesis contributes to bone loss and increased marrow fat, as seen in osteoporosis [44].

Osteoblasts produce the bone matrix by secreting collagen and ground substance to form the initial, non-mineralized bone (osteoid). This osteoid undergoes primary mineralization through the secretion of matrix vesicles by osteoblasts, and subsequently, calcium phosphate crystals are deposited during secondary mineralization, gradually increasing bone mineral density and forming the rigid structure of the bone [46,47]**.** This process is vital not only for initial bone formation but also for ongoing bone remodeling and repair. During bone remodeling and repair, MSPCs are recruited to injury sites where they proliferate and differentiate into osteoblasts, contributing to bone regeneration [46,47]. This process is crucial for maintaining bone density and healing fractures. The differentiation of MSPCs into distinct lineages, including osteogenic pathways, involves a two-phase process: initial lineage commitment followed by maturation into specialized cell types [46,47]. Several key signaling pathways, including the transforming growth factor-beta (TGFβ)/bone morphogenetic protein (BMP) pathway, the Wnt signaling pathway, Hedgehog (Hh) signaling, Notch signaling, and fibroblast growth factor (FGF) pathways, are crucial in guiding MSPCs toward osteogenic differentiation, ensuring proper bone formation and maintenance [48]. Each pathway plays a vital role in guiding MSPCs towards osteogenic differentiation, ensuring proper bone formation and maintenance (Figure 3 [48]):

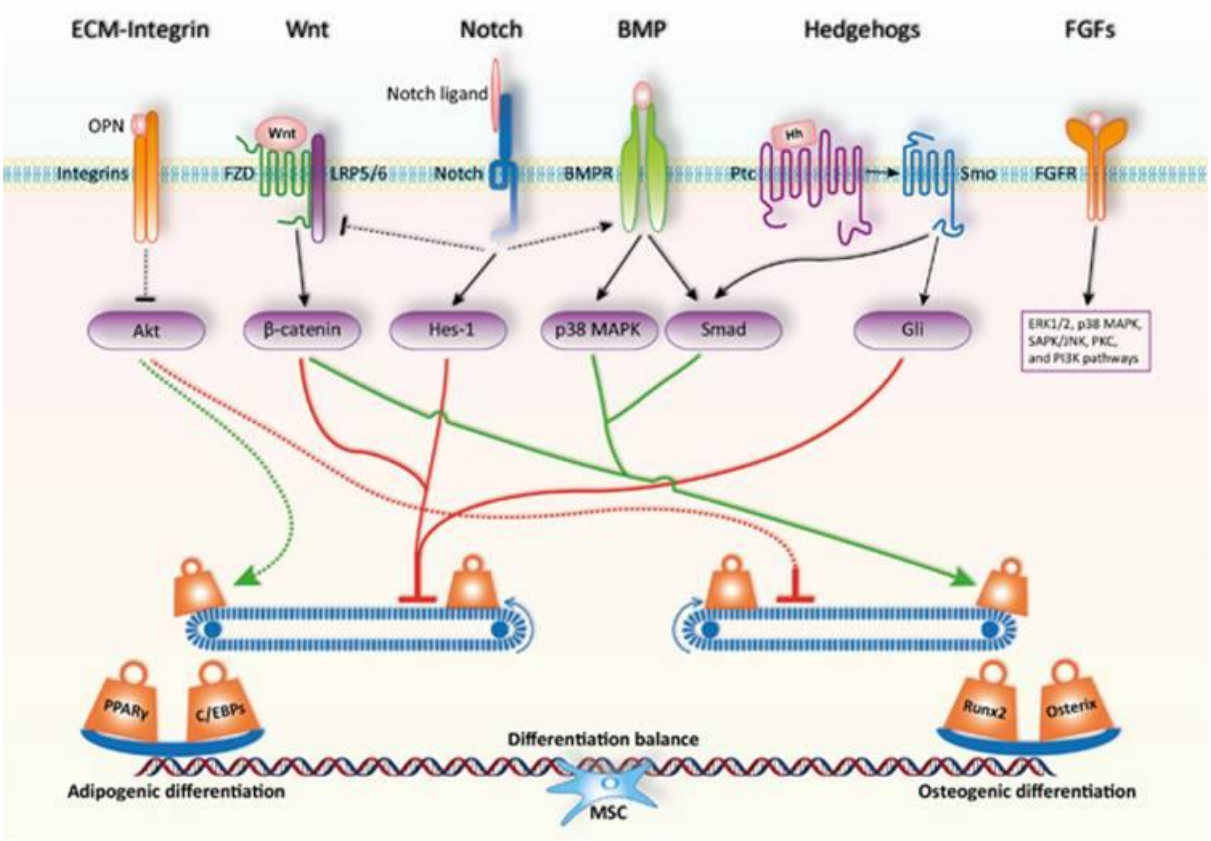

Figure 3: Fate decision of mesenchymal stem cells regulated by signaling pathways and key transcription factors. Model from Chen et al., 2016.

The TGFβ/BMP pathway helps MSPCs decide whether to become bone cells. For example, BMP2 and BMP4 within this pathway promote the differentiation of MSPCs into osteoblasts, thereby facilitating bone formation [45,49,50].

the Wnt signaling pathwayplays a crucial role in MSPC differentiation, promoting osteogenic differentiation and inhibiting adipogenic differentiation [51]. For instance, Wnt3a and Wnt5a are specific proteins in this pathway that help in the creation and strengthening of bone [52,53].

The Notch signaling pathway, involving Notch receptors and ligands, regulates MSPC differentiation through cell-cell communication, playing both an inhibitory and an essential role in adipogenic differentiation [48]. Notch suppresses osteogenesis by inhibiting Wnt/β-catenin signaling but can also promote osteogenesis through interactions with BMP2 [50,54].

The Hedgehog pathway is active in the early stages of bone formation and helps MSPCs become osteoblasts, often working together with the BMP pathway [55,56].

Moreover, FGFs regulate both adipogenesis and osteogenesis, highlighting the intricate network of signaling pathways that govern MSPC differentiation [57]. This clearly demonstrates that the signaling pathways involved in MSPC differentiation do not function in isolation but interact within a network influenced by the microenvironment.

Regulation of the hematopoietic stem cell niche

The regulation of the HSC niche and the HSCs themselves is mediated by a complex network of signaling pathways involving a wealth of secreted factors from stromal cells, endothelial cells, and MSPCs (Figure 2 [21]) [58]. These signaling pathways not only collaborate to fine-tune the niche environment but also directly influence HSCs [33,58]. Additionally, nutrient sensors within niche cells, such as those involved in mTOR (mammalian target of rapamycin) signaling, respond to fluctuations in nutrient availability by altering their metabolic state. This metabolic shift can lead to changes in the secretion of growth factors and cytokines, which in turn modify the composition and structure of the bone marrow microenvironment, thereby directly influencing HSCs' behavior and function [59-61].

The extracellular matrix (ECM) and adhesion molecules, such as integrins and selectins, are essential in structuring and regulating the HSC niche [62-64]. The ECM provides a physical scaffold that maintains the spatial organization of cells, crucial for a functional niche, while also acting as a reservoir and active presenter of growth factors and cytokines [64]. This dual role allows the ECM to modulate signaling pathways by delivering specific signals to HSCs [64].

During the transition from extracellular components to the intracellular environment, the cytoskeletal components F-actin and tubulin stabilise the cellular dynamics of the niche. The cytoskeleton not only supports cell architecture and movement, but also facilitates responses to extracellular signals [65,66]. Both F-actin, along with its associated assembly factors, and tubulin, which forms microtubules, have been shown to be essential for the effective functioning of HSCs and in the BM [65,67]. However, although cytoskeletal components are known to be critical for maintaining cellular architecture and differentiation of niche cells, the role of the cytoskeleton in niche support of HSCs has been underinvestigated.

Dynamic interplay between HSCs and their niche

The dynamic interactions between niche cells and ECM allows HSCs to respond and adapt to changes in their microenvironment, which is essential for the maintenance of homeostasis and regeneration of the hematopoietic system under normal and pathological conditions [19,24,68]. However, the dynamic interplay between HSCs and the niche is not unidirectional. HSCs and their progeny also influence and remodel their microenvironment.

HSCs secrete factors such as angiopoietin-1 (Angpt1), which acts primarily on MSPCs by binding to the Tie2 receptor on niche cells, promoting HSC quiescence and preventing exhaustion due to excessive division, thus ensuring long-term stem cell maintenance [69]. While Angpt1 is not expressed by osteoblasts, it is found in other niche components, such as c-kit+ progenitor cells and LepR+ stromal cells [69]. Although deletion of Angpt1 has no effect on steady-state hematopoiesis or maintenance of HSCs, it accelerates vascular and hematopoietic recovery after irradiation by increasing vascular leakage [69]. This emphasises the role of Angpt1 in regulating the regeneration and stability of niches. Consequently, HSCs contribute directly to their own maintenance and to the overall health of the bone marrow niche by influencing MSPC and other niche components.

Furthermore, bone marrow megakaryocytes, primarily located along sinusoidal vessels, regulate HSC quiescence through the secretion of CXCL4, thrombopoietin (TPO), and TGFβ. In doing so, they influence not only the HSC niche but also the overall maintenance of HSCs, highlighting the complexity of this interplay [21,70-72].

Dysfunctional hematopoiesis

In the previous chapters, I described in detail the characteristics and dynamics of a healthy niche and the interplay between HSCs and their niche as well as the cellular and molecular mechanisms that ensure the stability and functionality of the HSC niche in a steady state. This chapter focuses on the pathologies that occur when the hematopoietic niche is disrupted. It discusses how factors such as inflammation and aging can impair niche function and lead to the development of disease.

The HSC niche is influenced by various external and internal factors, resulting in continuous homeostatic remodeling and re-balancing [73]. A critical de-stabilizing influence of homeostasis is the impact of acute and chronic inflammation on the HSC niche. Understanding the impact of inflammation is critical, as it occurs regularly during the organisms life-time, and it has been shown to be a common hallmark of many pathological conditions (Figure 4 [73]). Even minor disturbances within the niche, triggered by sterile or infection-related inflammatory stimuli have been found to induce dormant HSCs to proliferate, impair their self-renewal capacity and potentially increase the chance of malignant transformation [74-78]. In addition to inflammation, environmental factors, lifestyle, and exposure to toxic or therapeutic substances or radiation further influence homeostasis [79]. Together, these factors may trigger systemic diseases, leading to conditions such as anemia or leukemia, which are characterized by defective responses to infections, impaired oxygen distribution, or bleeding disorders [79,80].

Accelerated aging as a result of continuous stress challenges

The inability to maintain homeostatic remodeling and re-balancing during chronic inflammatory processes has severe disruptive effects on both the niche and HSCs, leading to premature aging [33,79]. Aging, a natural process characterized by the slow but progressive deterioration of cells and tissues, is the primary risk factor for the decline in the functionality of HSCs, immune system defects, and increased hematological abnormalities [33,79,81,82]. The interdependent cellular and molecular interactions between aging and inflammation confound the search for possible therapeutic interventions, as the aged niche shows different responses to inflammatory stimuli than the naïve, young and healthy niche. In the young niche, the niche rapidly releases proinflammatory cytokines such as Interferon alpha (IFN-α), which, in turn, equally rapidly recruit dormant HSCs into the cell cycle and stimulates BM ECs to remodel the vascular niche [76,83]. Interestingly, imaging of aged BM reveals remodeling of both arteriolar and sinusoidal vessels, in which sinusoidal areas protect the most potent repopulating HSCs [84]. These sinusoidal niches are preserved with age in terms of shape, morphology and number. This clearly demonstrates that aging is not restricted to HSCs, but also affects their microenvironment [84].

Given the lifelong homeostatic remodeling and re-balancing in response to inflammatory stimuli, aging could be understood as a 'chronic stress model'. To investigate the effects of naturally occurring stressors on stem cells and their niche and

to stimulate the regeneration of the hematopoietic system after injury, polyinosinic:polycytidylic acid (pI:pC) treatment is often used, as it triggers a defined short inflammatory impulse, similar to that observed in a viral infection [74]. In line with the idea that multiple minor inflammatory events would stimulate aging-like degeneration, multiple low-dose pI:pC stimulation leads to a cumulative inhibitory effect on the ability of HSCs to engraft [74]. Similarly, chronic exposure to low-dose lipopolysaccharide (LPS), a component of the outer membrane of gram-negative bacteria, triggers inflammatory stress. Acute LPS challenge induces proliferation of quiescent HSCs *in vivo* and impairs HSC self-renewal and competitive repopulation activity [85-87].

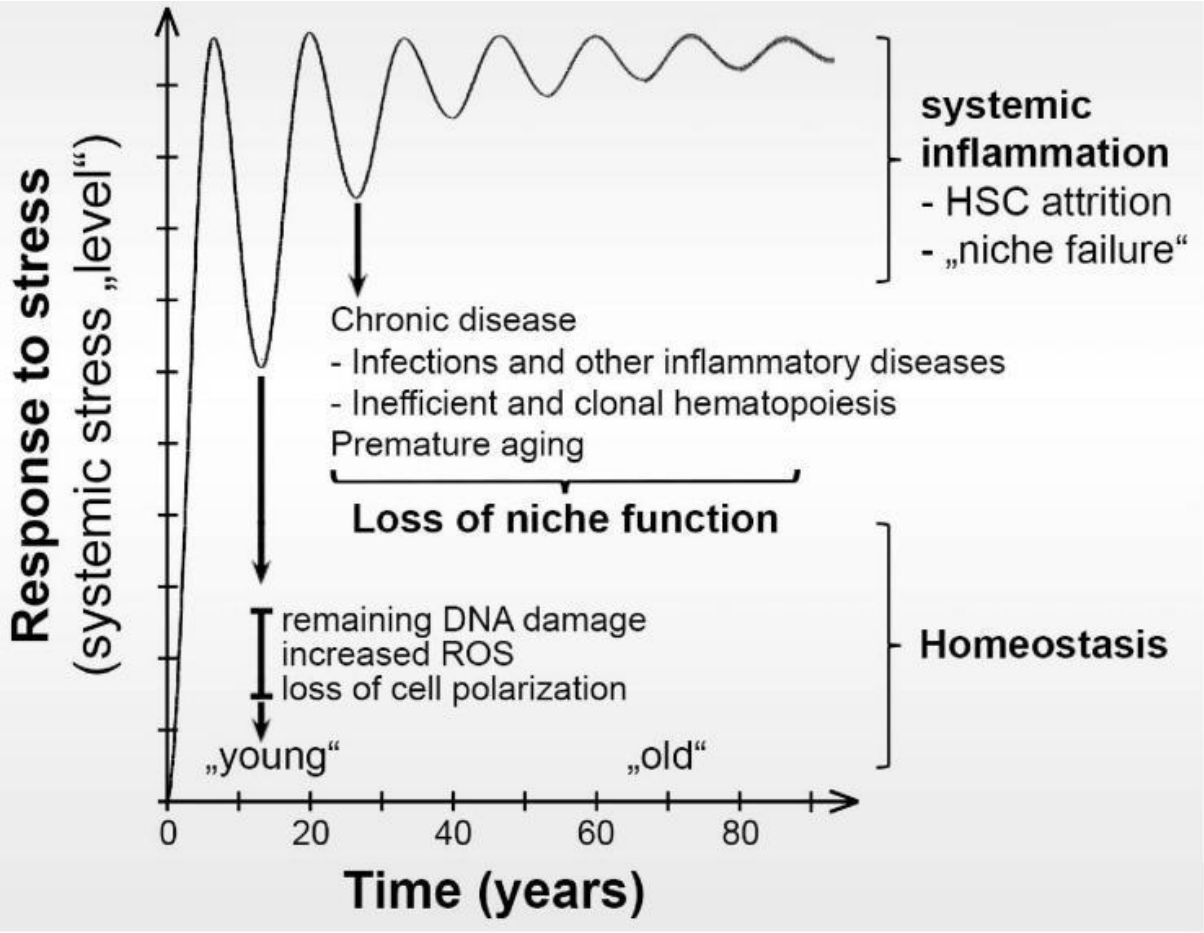

Figure 4: The Hematopoietic BM Niche Ecosystem: Impact of repeated stress on BM niche cells; Model from Fröbel, Landspersky, et al., 2021.

Another well-established stress model is the treatment with the anti-proliferative chemotherapeutic agent 5-fluorouracil (5-FU). It targets cells in S-phase, the phase of the cell cycle where DNA is replicated, and rapidly recruits dormant HSCs into the cell

cycle [88]. Although dormant HSCs are resistant to 5-FU, HSCs pre-treated with IFN-α and thus induced to proliferate are efficiently eliminated by 5-FU treatment *in vivo* [76]. In addition, although a single treatment of mice with 150 mg/kg 5-FU is not lethal, multiple weekly exposures severely reduce HSC engraftment ability and can even be lethal after 2 to 3 treatments [89,90].

In sum, repeated stress can progressively alter the fitness of HSCs and its BM niche cells. Under steady-state conditions, the niche protects HSCs from overstimulation and aging, but as the niche degenerates, this protective effect is progressively diminished (Figure 4 [73]). Over time, accumulating minor changes affect the transcriptional, proteomic, and ecological landscapes of the cellular composition of the BM niche. Ultimately, aging-like changes in the BM niche lead to the loss of functional HSCs, systemic inflammation, and the development of chronic changes with the loss of niche support for healthy hematopoiesis in the BM. Instead, the altered niche supports the development of chronic diseases [33].

Aging phenotypes in HSCs and MSPCs

Age-related changes in HSCs and their niche can be identified through specific phenotypes, commonly referred to as “hallmarks of aging” (Figure 5 [91]) [79,91,92]. Aging phenotypes in HSCs and MSPCs include a reduced ability to renew and differentiate, a myeloid-biased differentiation potential, and increased ROS (Reactive Oxygen Species) production leading to oxidative stress and DNA damage, often recognisable by increased markers such as gamma-H2AX, an indicator of DNA double-strand breaks [91].

Aged HSCs also exhibit decreased cellular polarity, impairing their division and function. In young and healthy HSCs, polarity is a characteristic feature in which the cellular components are asymmetrically distributed, contributing to efficient division and function of these cells. However, in aged HSCs, this polarity decreases, resulting in a more apolar organisation where the asymmetric distribution of cellular components is lost [93]. This loss of polarity impairs the ability of cells to orientate and divide properly, contributing to reduced regenerative capacity [93]. Therefore, with increasing age, the ratio of quiescent HSCs decreases, leading to more HSCs entering an active state, which results in increased cell division. This can lead to a depletion of the stem cell reserve and exhaustion or even cellular senescence. Cellular senescence,

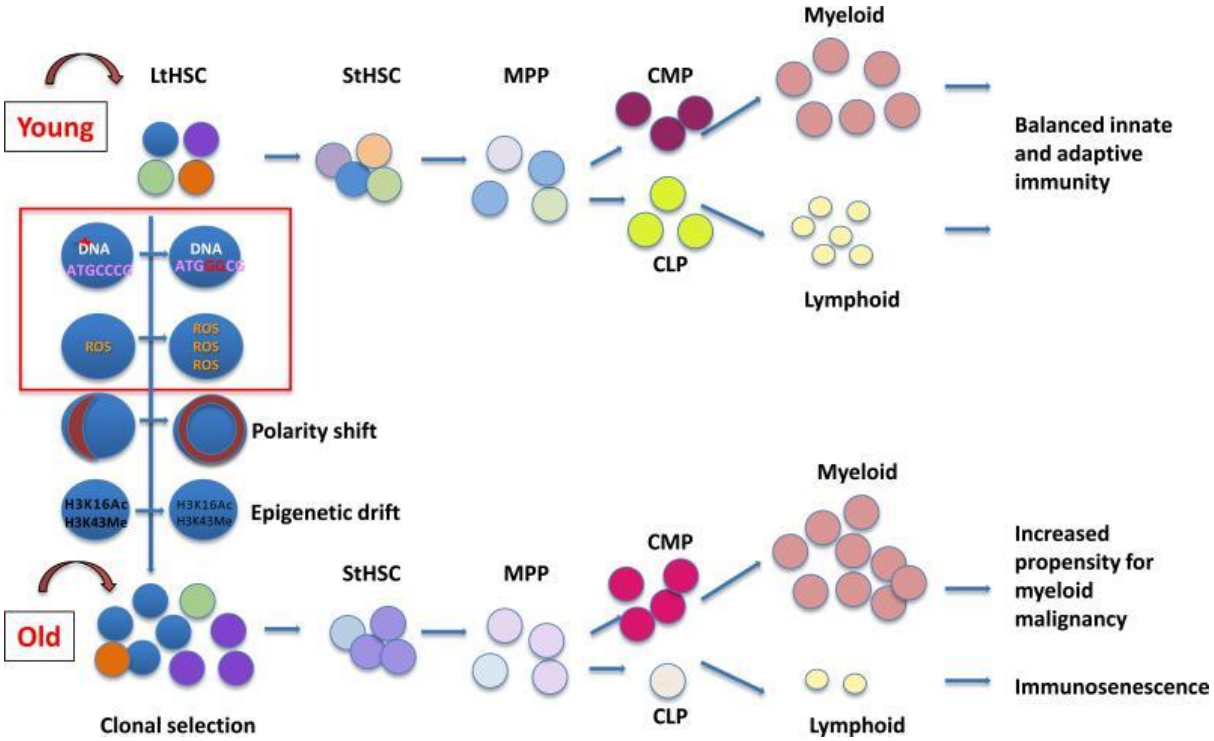

Figure 5: Model from Akunuru and Geiger, 2016.

characterized by stable cell cycle arrest and often caused by oxidative stress-induced DNA damage or telomere shortening, further contributes to a decline in HSC functionality [79,94].

Senescence is also a hallmark of aging in MSPCs, involving genetic material damage, loss of proteostasis, and mitochondrial dysfunction [95]. Various signaling pathways such as AMPK, sirtuins, Nrf2, and Hedgehog have anti-senescent effects, while others like mTOR, ROS, IGF1, and NF-κB promote senescence (Figure 6 [95]) [95,96]. Aging leads to chronic remodeling of the BM niche, characterized by an increase in adipogenic cells, a decline in osteogenic cells, stromal senescence, loss of endomucin-positive vessels, and altered innervation [97-100]. These changes contribute to niche remodeling, which is often associated with chronic malignancies and the progression to aggressive myeloid leukemias. Malignant cells further disrupt normal hematopoiesis by creating an environment that does not support efficient hematopoiesis. The potential effects of HSC aging on the BM include various abnormalities, such as altered vasculature, increased adipogenesis, reduced osteogenesis, altered secretion of extrinsic factors from niche cells (increased secretion of CCL5 and decreased osteopontin (OPN) levels), and reduced adhesion between HSCs and supportive niche cells (Figure 7 [21]) [21]. Moreover, the aged niche directly impacts young HSCs. According to the work of

Florian et al. (2013), aged niche cells can induce a switch from canonical to non-canonical Wnt signaling in young HSCs, leading to their premature aging [93]. This reciprocal influence highlights the dynamic interplay between HSCs and their niche during aging. Therefore, there is a need to consider both cell-intrinsic and extrinsic factors in understanding HSC and niche aging.

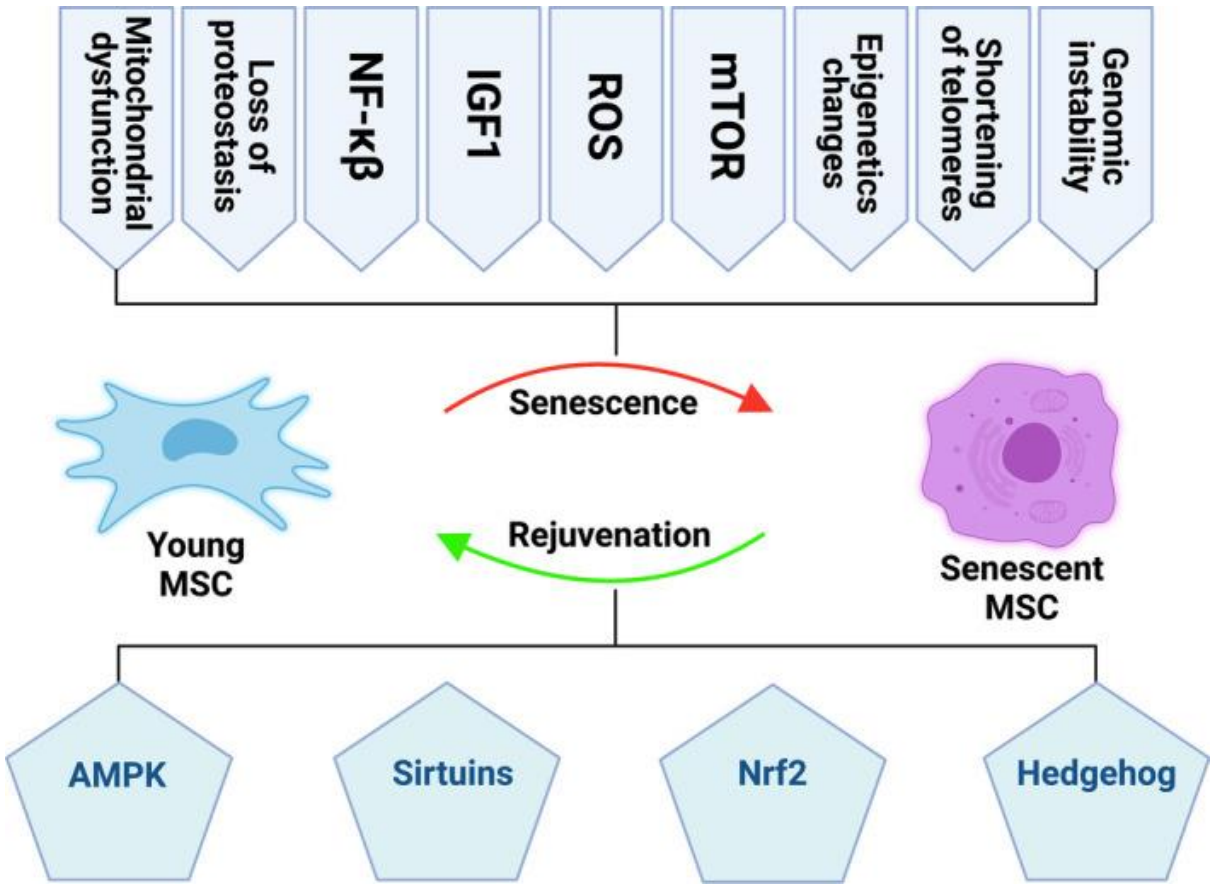

Figure 6: MSPC senescence homeostasis; Model from Al-Azab et al., 2022.

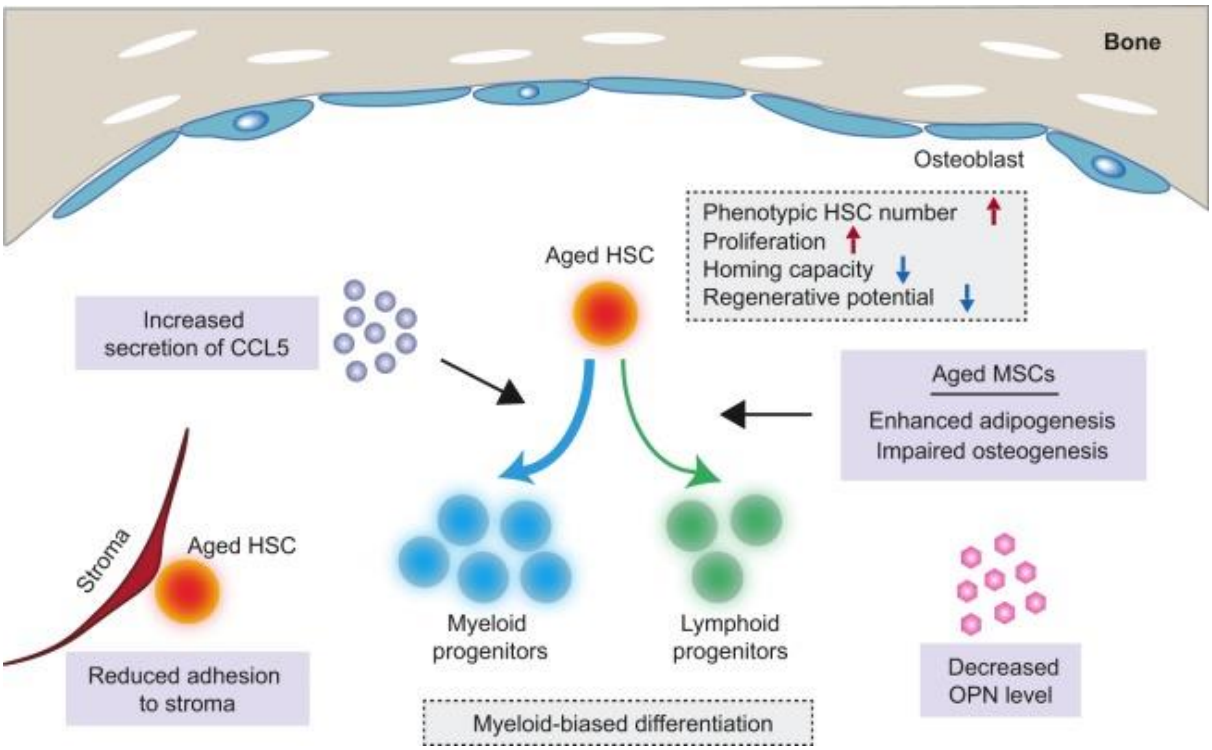

Figure 7: Schematic of the aging HSC niche and its associated alterations. Model from Gao et al., 2018.

In summary, the hallmarks of aging, as described by López-Otín et al. (2013; 2022), identify several main characteristics of aging, including genomic instability, telomere shortening, epigenetic changes, and loss of proteostasis [79,92]. These primary hallmarks cause damage, while antagonistic hallmarks like deregulated nutrient sensing, mitochondrial dysfunction, and cellular senescence respond to damage. Integrative hallmarks, such as chronic inflammation, stem cell exhaustion and altered intercellular communication, result from these processes (Figure 8 [92]) [79,92]. The authors additionally propose “hallmarks of health”, which include features such as spatial compartmentalization, maintenance of homeostasis over time, and effective responses to disturbances [92,101]. Aging is associated with the gradual deterioration of these health hallmarks, leading to the loss of barrier integrity, disrupted homeostasis, and reduced ability to respond to stress through repair and regeneration. This decline affects all levels of biological organization, from molecules to organ systems. The 'hallmarks of aging' are interconnected with these “health hallmarks”, creating a complex network that may explain aspects of the aging process [79,92,101].

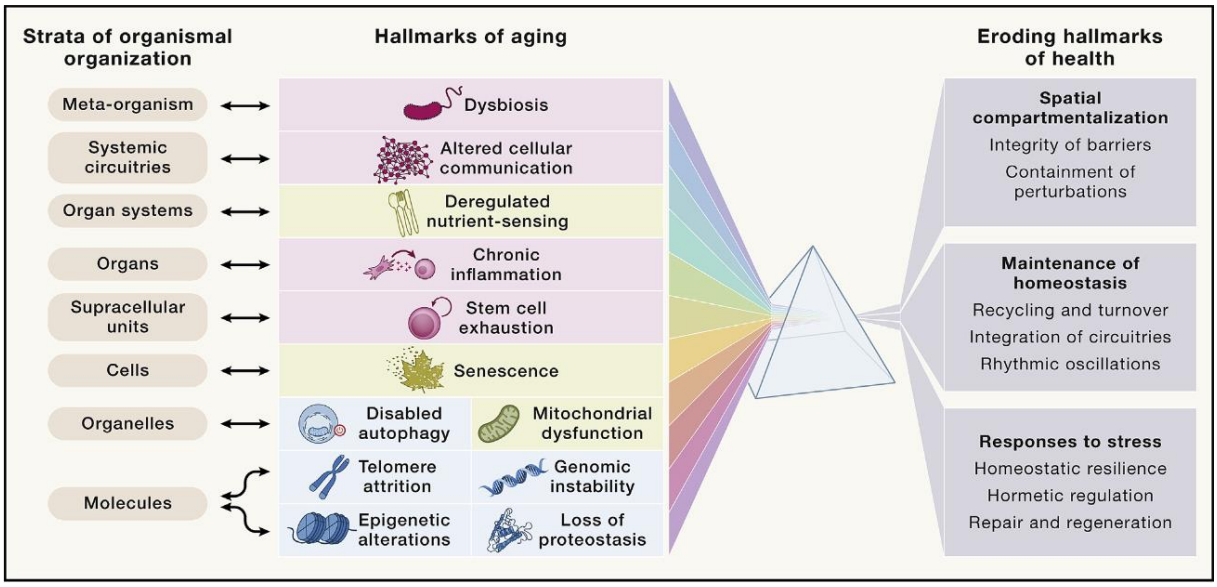

Figure 8: Hallmarks of aging; Model from López-Otín et al., 2022.

Wnt5a as an early indicator of aging

After discussing the hallmarks of aging and health, I will now focus on the specific molecular mechanisms driving these cellular changes. A deeper understanding of the molecules involved in aging, such as signaling proteins, transcription factors and structural components, is crucial to unravel the complex biological processes behind the decline of cellular and tissue function. In particular, the changes in signaling pathways and the involvement of specific molecules offer insights into the underlying causes of age-related dysfunction and open up possible approaches for therapeutic interventions. Therefore, many researchers have contributed to defining specific markers associated with aging, often linked to shifts in key signaling pathways.

One such significant shift involves the transition from β-catenin-associated (canonical) Wnt signaling to non-canonical Wnt signaling with aging [93]. Thus, there appears to be a change in the association of Frizzled receptors with downstream G proteins and Disheveled that leads to interactions with both the canonical β-, γ- or δ-catenin-dependent pathways and with non-canonical Wnt signaling pathways that are dependent on calcium or small GTPases. For proper HSC function, catenin-dependent Wnt signaling must be finely tuned since the precise level of β-catenin activation determines different cell fates: low levels of catenin activation favor self-renewal, while higher levels lead to differentiation [102].

Non-canonical Wnt signaling encompasses various pathways of cellular activation, including Ca2+-dependent signaling, phospholipids, inflammation, and non-Frizzled Wnt receptors. Particularly, **the non-canonical Wnt factor WNT5A** (Wingless-type MMTV integration site family member *Wnt5a*), has been found to play an important role in aging (Figure 9 [103]) [93,103]. *Wnt5a* expression is essential for embryonic development, since a complete *Wnt5a* knockout in mice is lethal, leading to death before birth [104]. Interestingly, *Wnt5a* expression is minimal in HSCs from young mice, but it increases considerably with aging [102]. Other Wnt family proteins, such as WNT1, WNT3A, WNT5B, and WNT10B, do not show this differential expression in aged HSCs [93]. The increase in *Wnt5a* expression with aging is most interesting because it is a driver of the switch from canonical to the non-canonical Wnt signaling in aged HSCs [93]. The non-canonical Wnt pathway actively downregulates canonical β-catenin signaling and activates more diverse signaling pathways from calcium-, NFAT, planar polarity, ROR, to PTK7 receptors [105,106]. Upon WNT5A binding to its FZD and non-FZD receptors, various intracellular signaling pathways are activated, depending on which WNT5A receptors are being expressed by the target cells. These targets include the activation of small GTPases like Ras homologue (Rho), Rac, and Cell Division Control protein 42 (CDC42). These small GTPases regulate various cellular processes, many of which depend on the actin and tubulin cytoskeleton, and calcium-dependent signaling through CAMKII and p21-activated kinases (PAK) [105,107,108].

Given its significant role in driving the switch from canonical to non-canonical Wnt signaling in aged HSCs, *Wnt5a* serves as an early biomarker for detecting age-related cellular changes and potential dysfunctions.

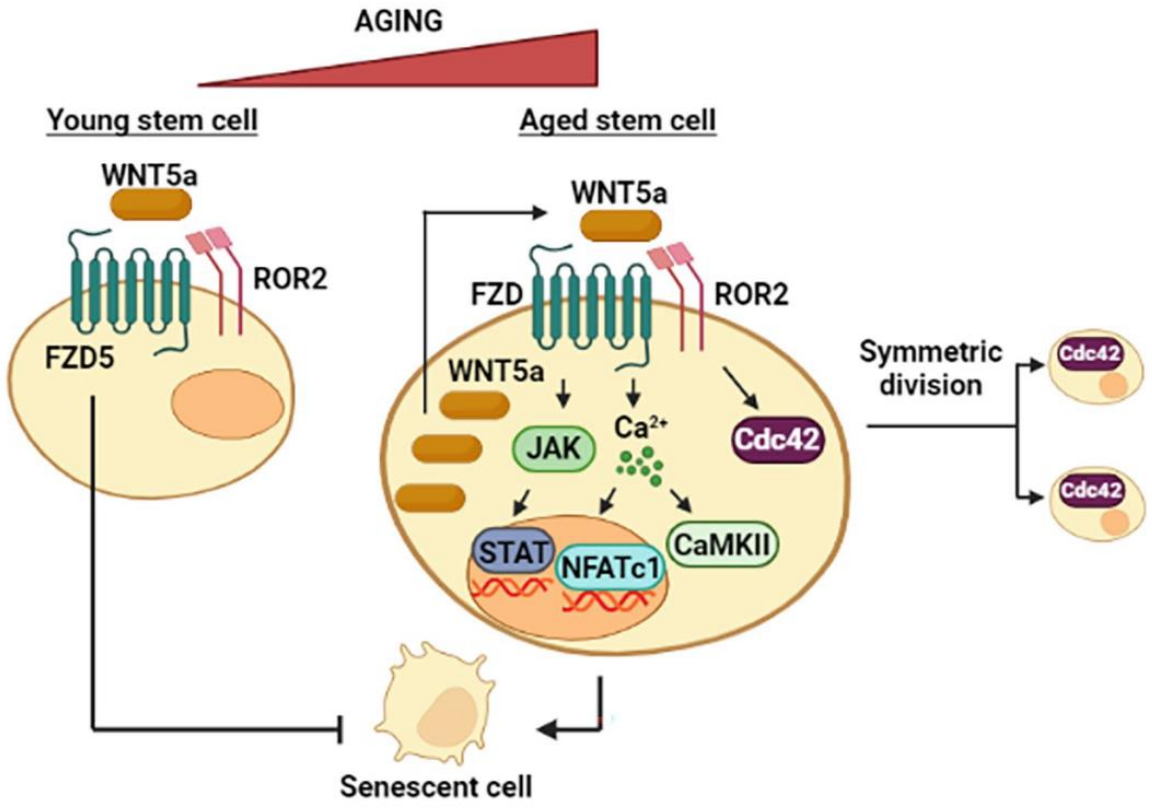

Figure 9: Wnt5a's Role in Aging: Wnt5a has a dual role in aging. It helps prevent cells from entering senescence, with the FZD5 receptor playing a key role. However, in cells that have already aged, Wnt5a levels are high. In these aged cells, Wnt5a activates the JAK/STAT and Calcium/CaMKII/NFATc1 pathways. Additionally, CDC42, which responds to Wnt5a, influences how cells divide, particularly in ensuring symmetric divisions in aging cells. Model from Sarabia-Sánchez and Robles-Flores, 2024.

CDC42 as key node for balancing homeostasis

A large part of this thesis focuses on the influence of the small Rho GTPase CDC42 and the associated intracellular changes it triggers (Figure 10 [109]). Like all GTPases (short for guanosine triphosphatase), CDC42 functions as a molecular switch, alternating between an inactive GDP-bound state and an active GTP-bound state. CDC42 is regulated by GEFs (Guanine Nucleotide Exchange Factors), which catalyze the exchange of GDP for GTP, and by RhoGDI (Rho GDP Dissociation Inhibitor), which stabilizes the inactive GDP-bound form and can sequester CDC42 in the cytoplasm [109-111]. The binding of GTP to CDC42 induces a conformational change, marking the active state of CDC42 (CDC42-GTP). In this state, CDC42 can interact with and activate its downstream effector proteins. The inactivation of CDC42-GTP occurs through the hydrolytic cleavage of GTP to GDP, a process that is accelerated by GTPase-activating proteins (GAPs). After GTP hydrolysis, CDC42 returns to its

inactive GDP-bound state. This dynamic of GTP/GDP binding and hydrolysis allows CDC42 to function as a regulatable switch controlling intracellular signaling pathways. These pathways are mainly regulated through effectors with a CDC42/Rac1-interactive binding (CRIB) or transducer of Cdc42-dependent actin assembly (TOCA) domain [112]. Through these effectors, CDC42 regulates the assembly of actin filaments, which is crucial not only for cell shaping and dynamic processes such as cell movement, cell-cell interactions, and cell division [113] but also for DNA repair [114]. In processes such as wound healing and embryonic development, CDC42 controls cell migration by restructuring the cytoskeleton and directing the cell in specific directions [115]. Additionally, CDC42 is involved in the regulation of endocytosis, a process in which cells absorb material from their extracellular space or from interacting cells, and plays a role in the transport of vesicles within the cell [115].

Through the age-related upregulation of non-canonical Wnt signaling, CDC42-directed signaling cascades have a significant impact on HSC quality and quantity [93]. Furthermore, treatment of young HSCs with WNT5A induced a CDC42-GTP-induced aging-like redistribution of the cytoskeleton (cell polarity), associated with reduced regenerative ability and an aging-like myeloid/lymphoid differentiation defect in HSCs [93,116]. However, aging-like changes are not restricted to hematopoiesis and they also

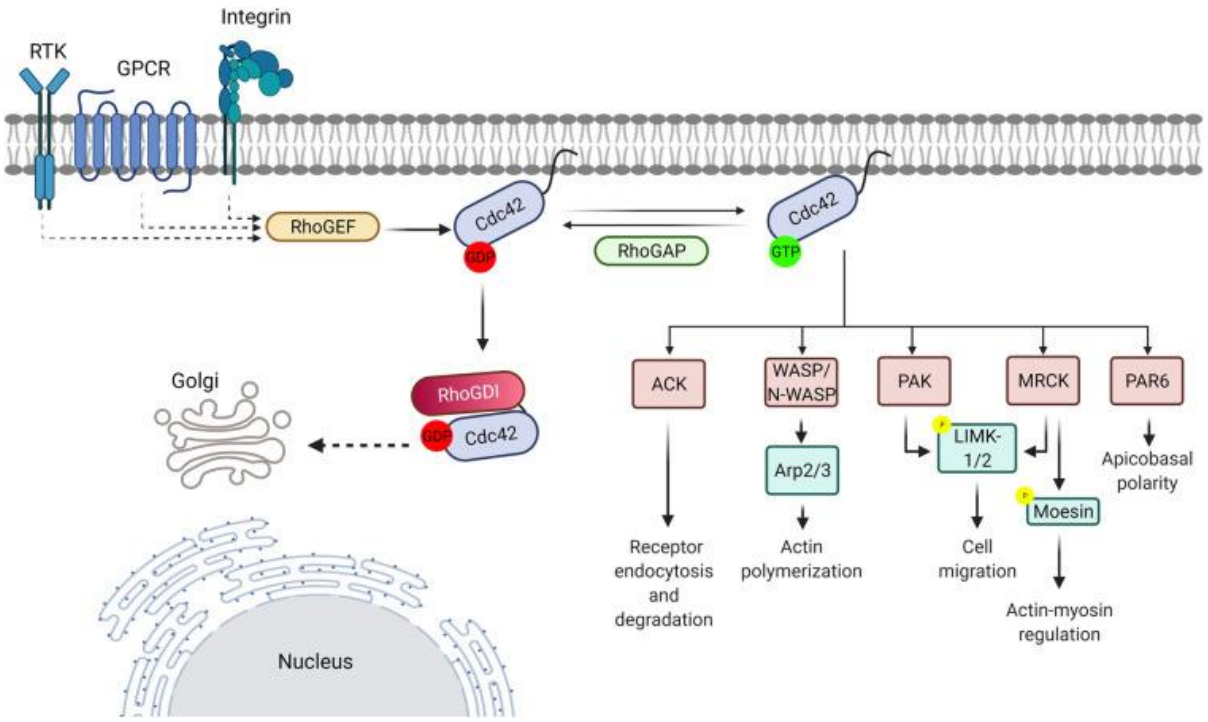

Figure 10: Cdc42 Regulation: Receptors activate Cdc42 via GEF proteins, converting it to its active form (Cdc42·GTP). GAP proteins inactivate it, while RhoGDI proteins stabilize or transport Cdc42. Cdc42 controls actin dynamics, vesicle trafficking, and cell motility. Model from Murphy et al., 2021.

occur in most other tissues. Therefore, it is relevant to examine the influence of aging-like changes in the microenvironment on HSC function. Indeed, when HSCs from young mice are transplanted into old mice (with an “old niche”), the donor HSCs showed significantly reduced repopulation function with increased WNT5A and CDC42-GTP levels [93]. This suggests that the old niche has a negative impact on the performance and regenerative capacity of HSCs. Conversely, when HSCs from old mice were transplanted into young recipients (with a “young niche”), it was found that the old donor HSCs show a highly improved repopulating function with decrease in WNT5A and CDC42-GTP levels [93]. These data suggest that WNT5A expression in the microenvironment strongly impacts HSC quality by modulating the exchange of GDP for GTP on CDC42.

Niche WNT5A regulates the actin cytoskeleton in HSCs

As the aging environment influences the HSC quality and quantity, it was interesting to investigate whether extrinsic WNT5A expression from the niche could be responsible for this preaged phenotype. In the manuscript 'Niche WNT5A regulates the actin cytoskeleton during regeneration of hematopoietic stem cells,' where I am a **co-author**, we analyzed the impact of heterozygous *Wnt5a* deletion in mice (*Wnt5a+/−*) [65]. Indeed, when wildtype HSCs are transplanted into a *Wnt5a*-haploinsufficient microenvironment, they lose their qualitative and quantitative functionality and are no longer capable of secondary engraftment. Interestingly, the *Wnt5a*-haploinsufficient niche triggered an increase in WNT5A as well as an increase of CDC42-GTP expression and its apolar distribution in HSCs, suggesting the promotion of an aging-like HSC phenotype. In agreement with this view was the observation that cytoskeletal F-actin, was distributed in an apolar manner, similar to that found in dysfunctional aged HSCs [65]. In summary, the maintenance of HSC function depends on Wnt5a expression in their environment, which also regulates the engraftment of donor HSCs [65].

Role of WNT5A in cytoskeletal integrity and autophagy regulation in MSPCs

In my **first lead authorship**, we further investigated the influence of *Wnt5a* selectively deleted in Osx+ osteoblast precursors ($O5A^{\Delta/\Delta}$), which means a *Wnt5a* deletion in MSPCs and OBCs [89]. The remaining cells and tissues express *Wnt5a* at wildtype

levels. And indeed, the niche lacking *Wnt5a* exhibits defective F-actin stress fiber orientation due to elevated CDC42 activity. The integrity of the cytoskeleton is closely linked to crucial cellular processes, including autophagy, which maintains cellular homeostasis by degrading and recycling cellular components [117].

The F-actin fibers play a central role in the formation of autophagosomes and their fusion with lysosomes to form autophagolysosomes. Specifically, autophagosomes, marked by LC3, encapsulate proteins or organelles and prepare them for degradation [118,119]. Lysosomes, which contain proteases and other enzymes necessary for breaking down cellular material, are marked by LAMP1 [120]. The fusion of autophagosomes with lysosomes, facilitated by the cytoskeleton, initiates the degradation and recycling process [120]. However, when the cytoskeleton is defective, this fusion process is impaired, leading to a significant increase in the size of mitochondria and lysosomes, both of which indicate defective autophagy [78].

Mitophagy is a specialized form of autophagy that specifically degrades mitochondria (Figure 11 A). It has been described, that mitophagy specifically targets damaged or dysfunctional mitochondria. Hence, mitophagy is a major player in mitochondria quality control. Mitochondrial damage results in the accumulation of PINK1 at the mitochondria and the subsequent recruitment of the E3 ubiquitin ligase Parkin [121]. PINK1 phosphorylates and activates Parkin, which then ubiquitinates proteins located on the outer mitochondrial membrane, such as the Ras Homolog Family Member T1 (Rhot-1/ Miro1). Interestingly, the Parkin activated upon mitochondrial damage is derived from a small pool of Parkin which is already bound to Miro1, prior to activation of PINK1 and independent of Miro ubiquitination [122]. The Miro1/Parkin complex serves as a sensor of mitochondrial damage. The ubiquitinated proteins, including the Rho GTPase Miro1, are targeted for proteasomal degradation, effectively disconnecting the mitochondria from the cytoskeleton to stop their transport [123]. These isolated mitochondria are then primed for uptake by autophagosomes [121,124]. Rhot1/Miro1 is also forming a complex with the motor proteins dynein, kinesin, and myosin and thereby allowing mitochondrial movement along the cytoskeleton [124]. The motor protein myosin 6 (MYO6) plays a central role in detecting and isolating defective mitochondria [125]. MYO6 forms a complex with Parkin and Tax1 Binding Protein 1 (TAX1BP1), which is a crucial selective autophagy cargo receptor. Parkin-mediated ubiquitination links TAX1BP1 to LC3, as well as recruits MYO6, linking the damaged mitochondria to the

ubiquitination system. On the mitochondrial surface, MYO6 recruits and initiates the formation of F-actin cages (Figure 11 B [125]). These cages serve as a quality control mechanism to isolate defective mitochondria and prevent their fusion with neighbouring healthy mitochondria. MYO6 also plays a role in the later stages of the mitophagy pathway by binding endosomes to actin filaments, facilitating the maturation of mitophagosomes and the fusion of autophagosomes with lysosomes [126]. These processes are particularly important in the context of HSCs and MSPCs, where maintaining mitochondrial integrity is crucial for cell function [127].

In summary, the crucial role of the actin cytoskeleton in auto- and mitophagy implies that defects in F-actin formation lead to defects in autophagic processes. Considering the strong regulatory activity of CDC42 activation on F-actin assembly, highlights the importance of WNT5A and CDC42 from the niche in connecting cytoskeletal remodeling, including cytoskeletal polarization, with auto-/ mitophagy in HSCs and MSPCs [128].

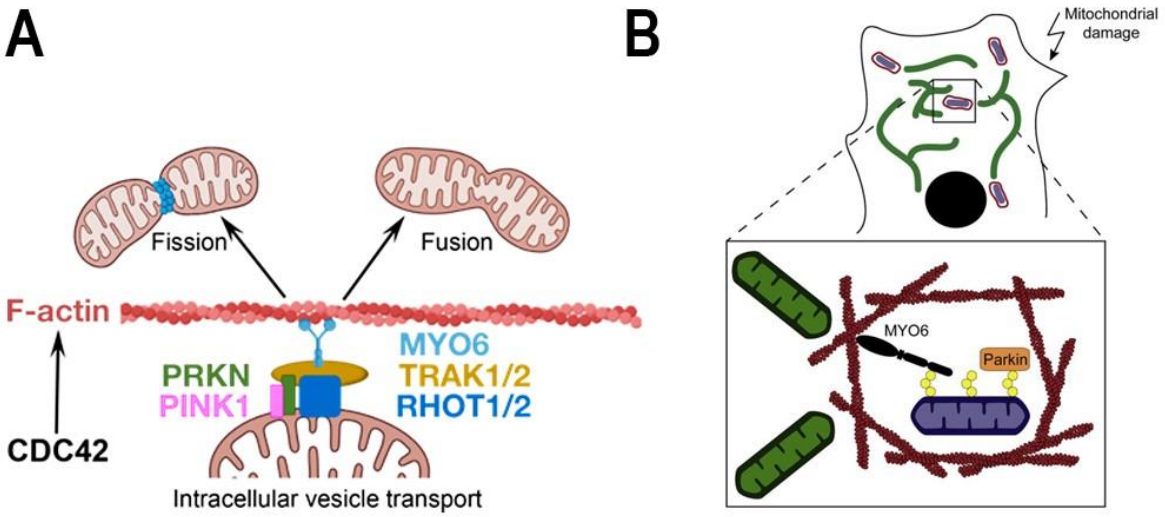

Figure 11: A) Intracellular CDC42-related vesicle transport, Simplified Model from Robert A.J. Oostendorp. B) Actin cages surround damaged mitochondria marked with Myo6; Model from Kruppa et al., 2018

Autophagy in bone homeostasis and in the development of osteoporosis

In mammals, bone serves multiple vital functions including protecting organs, providing muscle attachment points, acting as a site for blood cell synthesis, storing minerals, and secreting hormones [129]. The skeletal system is constantly remodeled through a balance between bone formation and degradation: Bone formation involves MSPC-derived osteoblasts, which synthesize and secrete the bone matrix [47]. As these osteoblasts become embedded in the matrix, they differentiate into osteocytes, which form a mechanosensing network within the bone as previously mentioned [48].

Proper autophagy in MSPCs is essential for their differentiation into osteoblasts [130]. Reduced autophagy is accompanied by a decreased expression of selective autophagy receptors, such as Optineurin (OPTN), TAX1BP1, or Sequestosome 1 (SQSTM1/p62) [131,132]. These changes lead to reduced osteogenesis through reduced degradation of adipogenic factors, such as FABP3, which increases adipogenesis [100,133]. In turn, increased myelopoiesis of aged HSCs leads to enhanced formation of bone degrading osteoclasts, and thus to diseases characterized by a reduction in bone density and structure, making the bones weaker and more susceptible to fractures at later ages [100,133]. Osteoclasts degrade and resorb the surrounding bone matrix, ensuring the continuous renewal and remodeling of bone tissue.

A dynamic balance between osteoblast and osteoclast activity maintains healthy bone mass and structure. Disruptions in this balance can lead to pathological conditions such as osteopetrosis and osteopenia, or even worse, osteoporosis [130]. Osteopetrosis is characterized by excessive bone formation, leading to overmineralization and increased bone mass whereas in osteoporosis, bone formation is reduced compared to bone degradation, which leads to decreased bone mass, weakened bone structure, and increased fracture vulnerability [130]. Osteoporosis is often preceded by osteopenia, a condition marked by slightly reduced bone density, though not as severe as in osteoporosis [134,135]. Importantly, individuals with osteopenia have an increased risk of developing osteoporosis later. Osteoporosis leads to an increased risk of fractures, particularly in the hip, spine, and distal forearm [136].

Osteopenia and osteoporosis are often the result of a combination of genetic factors, aging, hormonal changes, insufficient calcium and vitamin D intake, and lack of

physical activity [135,137]. Women are particularly at risk after the menopause, as a lack of estrogen leads to accelerated bone loss. Additionally, osteoporosis can also be induced by clinically necessary procedures. In the human system, osteoporosis is a frequently documented long-term complication after allogeneic hematopoietic stem cell transplantation (alloHSCT) [138,139]. Ten years after successful alloHSCT, osteoporosis is diagnosed in about 50% of HSCT recipients, regardless of the previous conditioning regime or the age of the patients [140,141]. However, myeloablative treatment of patients with chemotherapy and/or irradiation is still necessary for the engraftment of donor stem cells, the regeneration of hematopoiesis, and ultimately for the healing of the patient.

My **first publication** in this cumulative doctoral thesis examines the role of *Wnt5a* in Osterix+ MSPCs in maintaining the homeostasis of the hematopoietic niche and supporting hematopoiesis under stress conditions, particularly following treatment with 5-FU [80]. It specifically examines how WNT5A expression in osteoprogenitors influences MSPC stress responses, its downstream effects on CDC42-GTP levels, and the subsequent cytoskeletal defects that arise from this dysregulation. Understanding the molecular interactions between CDC42 activation and cytoskeletal regulation in stress responses provides valuable insights into the underlying mechanisms of stress- and age-related cellular dysfunction and how this dysregulation leads to defective autophagy processes. As proper autophagy in MSPCs is controlled by functional cytoskeleton which decreases in induced stress conditions and during aging.

My **second publication** [120] explores the role of CDC42 and cytoskeletal deregulation in skeletal degeneration during normal aging after hematopoietic stem cell transplantation, focusing on mitophagy in MSPCs isolated at late time points post-transplantation.

Possible strategies to restore cytoskeletal functions by reducing overactivation of CDC42

All skeletal defects identified during my dissertation were associated with an overactivation of CDC42 in MSPCs. As previously mentioned, CDC42 is responsible not only for cytoskeleton remodeling but also for initiating a variety of cellular responses such as cell polarity, proliferation, migration, cellular transformation, filopodia and invadopodia formation, invasion, enzyme activity, adhesion, membrane trafficking, and transportation [109,142]. I primarily investigated whether modulating CDC42 signaling pathways could treat cytoskeletal defects in MSPCs to prevent autophagy failures. CDC42 affects various downstream CRIB-domain-containing effectors like PAK, ACK (product of the *Tnk* genes), MRCK (products of the *Cdc42bp* gene family), MLKs (products of the *Map3k9*, *-10*, or *-11* genes), and WASP (products of the *Was*, *Wasl*, *Wasf*, or *Wash* Wiskott-Aldrich syndrome genes) family proteins [109,143] (Figure 10 [109]).

Thus, modulating CDC42 affects all of these processes. Inhibitors have been developed to regulate CDC42, either by affecting its CDC42-GDP/RhoGDI membrane

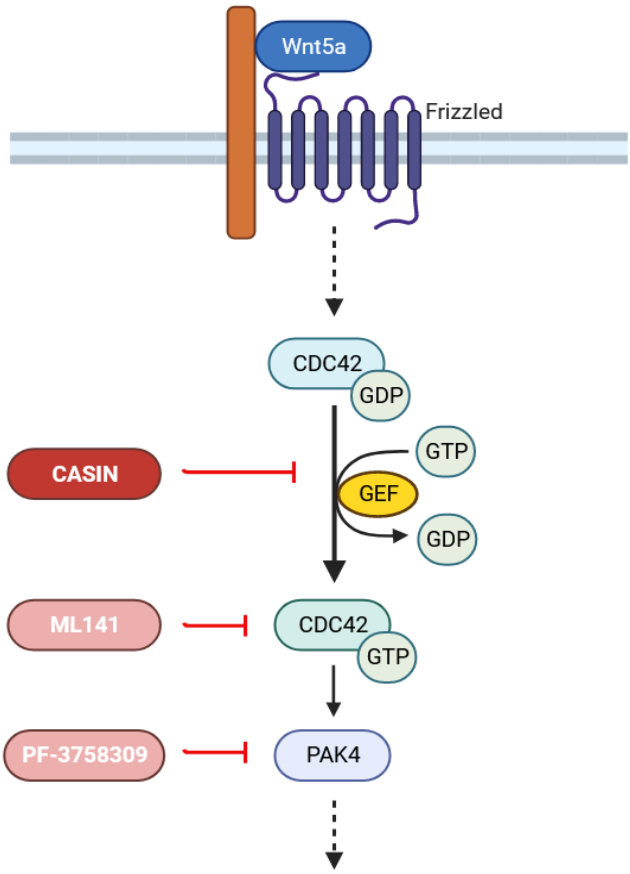

Figure 12: Non-canonical Wnt5a pathway with specific inhibitors; simplified for a better overview, Model from Theresa Landspersky

translocation (CASIN), GDP-GTP exchange (ZCL278), competitive inhibition of GTP binding (ML141), or inhibition of downstream kinase effectors such as PAK4 (PF-3758309) (Figure 12)**.**

CASIN (CDC42 Activity-Specific Inhibitor) directly inhibits the activation of Cdc42/RhoGDI [110,144]. It inhibits the activity of CDC42 in a concentration-dependent manner by inhibiting the GEFs that normally catalyze the exchange of GDP to GTP on CDC42 (Figure 12). It selectively binds to the CDC42-GDP/RhoGDI complex without affecting other similar proteins such as Rac1 or RhoA [144,145]. Additionally, CASIN inhibits actin reorganization by directly binding to the Arp2/3 complex, and it also affects platelet secretion, aggregation, and thrombus formation *in vivo* [144,145]. HSCs from aged mice or humans show overactivity of CDC42 [146-148]. When treated *ex vivo* with CASIN, these HSCs rejuvenate to a phenotype with a polar distribution of CDC42 and F-actin and repopulating activity after transplantation into young recipients similar to HSCs from young mice [93]. Florian et al. (2013) and Guidi et al. (2021) describe CDC42 as a potential therapeutic target to rejuvenate old stem cells, thereby improving both their quality and quantity [93,149].

ML141 is a selective and reversible inhibitor of the small GTPase CDC42 (Figure 12) [150,151]. However, while both inhibitors target CDC42, their mechanisms of action are different. ML141 belongs to the second generation of CDC42 inhibitors and is highly selective for CDC42-GTP. ML141 acts as a competitive inhibitor of GTP binding to CDC42, directly preventing the transfer and binding of GTP to CDC42 and thus maintaining CDC42 in its inactive GDP-bound state [152]. Unlike CASIN, ML141 does not prevent the membrane translocation of CDC42 but instead blocks its activation by inhibiting GTP binding. Due to its selective inhibition, ML141 provides an excellent tool to reduce the overactivation of CDC42, offering insights into the specific roles of GTP-bound CDC42 in cellular functions. Although ML141 alone had a modest effect on HSPC mobilization [151], when combined with Granulocyte-Colony Stimulating Factor (G-CSF), a growth factor that stimulates the production and release of white blood cells from the BM, it significantly increased HSPC counts and colony-forming units in peripheral blood compared to G-CSF alone [151]. G-CSF increased GTP-bound CDC42 levels without changing its overall expression [151]. These results indicate that CDC42-GTP is a negative regulator of G-CSF-mediated HSPC mobilization, and reducing CDC42-GTP with ML141 treatment enhances mobilization efficiency [151]. The authors

suggest, that therapy with the G-CSF/ ML-141 combination could improve HSPC mobilization, especially in patients unresponsive to G-CSF alone [151]. Another study showed, that inhibiting CDC42 with ML141 significantly enhances hepatocyte differentiation from human adipose-derived mesenchymal stem cells (hADSCs) derived from aged donors (women, 57.6 ± 0.9 years old) [153]. ML141 reversed age-related declines in cell functions, improved hepatic gene expression, cytochrome activity, urea and albumin production, LDL uptake, and glycogen storage [153]. These findings indicate that CDC42 inhibition by ML141 can effectively improve hepatocyte stem cell function and promote their differentiation in aged cells[153].

While ML141 offers a promising approach to modulate CDC42 activity and improve various stem cell functions, another strategy to address CDC42 overactivation involves targeting downstream effectors, such as p21-activated kinase 4 (PAK4). As previously mentioned, the PAK family comprises several effectors regulated by CDC42, with PAK1, PAK2, and PAK3 classified as group I PAKs, which have the CDC42/RAC interactive binding (CRIB) domain, while PAK4, PAK5, and PAK6, classified as group II PAKs, lack this domain [152,154]. The CRIB domain is a specific protein sequence that allows certain kinases to interact with the small GTPases CDC42 and RAC1. This domain enables the binding and activation of these GTPases, thereby facilitating downstream signaling pathways. Next to the PAKs, there are several proteins that have a CRIB domain and interact with CDC42 and RAC1 like as mentioned above MRCK that binds to CDC42 and influences the cytoskeleton and cell movement (Figure 10 [109]) [143]. Additionally, LIMK (LIM kinase) affects the cytoskeleton by controlling a protein called cofilin, which alters the structure of cell filaments, as well as MLKs and ACK, which are involved in regulating cell growth [143]. PAK4 is a member of the PAK family that plays a role in signal transduction within cells. Although PAK4 having no CRIB domain, the activity of Pak4 kinase and its interaction with activated CDC42 are essential for the induction of cytoskeletal reorganisation [154]. PAK4 inhibitors work by inhibiting the kinase activity of PAK4, thus preventing PAK4-mediated phosphorylation [152]. This phosphorylation is a critical step in many cellular processes, including cell growth, cell movement, and cell survival. CDC42 can act as an upstream regulator of PAK4, allowing the inhibition of PAK4 to indirectly dampen CDC42 activity [155]. When CDC42 is activated, it can directly interact with PAK4 and stimulate its kinase activity. This activation of PAK4 leads to the phosphorylation of various substrates involved in the regulation of cell growth, cell shape, and other important cellular functions [155]. This

plays a significant role in cell morphogenesis and movement. In cancer, the dysregulated activity of CDC42 and PAK4 can lead to uncontrolled cell growth and metastasis [155]. Understanding this interaction and developing inhibitors targeting these proteins is a significant area in cancer research. Recently, numerous PAK4 inhibitors have been reported, including PF-3758309, the first PAK4 inhibitor to enter clinical trials (Figure 12) [156]. Although developed for PAK4, it showed high efficacy for other PAK1 isoforms [157], and the allosteric inhibitor KPT-9274, which is tested in Phase I clinical trials for solid tumors, non-Hodgkin's lymphomas, and acute myeloid leukemia [156]. It inhibits cancer cell proliferation and shows promising results in preclinical studies by suppressing tumor growth and inhibiting the formation of cancer stem cells [156].

In summary, within my PhD work, I tested CASIN and ML141, two inhibitors that specifically target CDC42 but through different mechanisms. CASIN prevents the membrane tethering of the CDC42/RhoGDI complex, thus inhibiting the conversion of GDP to GTP and keeping CDC42 inactive. In contrast, ML141 acts as a competitive inhibitor, directly preventing GTP binding to CDC42, thereby also maintaining it in its inactive state. My goal was to determine which of these mechanisms most effectively restores cellular function by reducing CDC42-GTP levels after stress (e.g., 5-FU, irradiation, HSCT) and/or aging, to normal (= young) levels, and preventing the disorientation and elongation of F-actin fibers

Research question no. 1 and methodical approach

The *Wnt5a* knockout niche under stress conditions

In **my first lead authorship**, my co-authors and I aimed to investigate how the deletion of *Wnt5a* in MSPCs influences HSC function, particularly in the context of extrinsic WNT5A expression. For this purpose, we used a mouse model with the floxed *Wnt5a* gene selectively deleted in Osterix^{+} (Osx; product of the *Sp7* gene) osteoblast precursors (O5A$^{\Delta/\Delta}$), resulting in *Wnt5a* deletion in MSPCs and OBCs [80,158,159]. However, Wnt5a was still expressed by CD31+ ECs and other cell types. Unlike the homozygous knockout, which is embryonically lethal, the O5A$^{\Delta/\Delta}$ mice only showed mild dwarfism at birth, but were otherwise healthy. To assess the impact of *Wnt5a* deletion in osteoprogenitors on stress responses, we treated O5A$^{\Delta/\Delta}$ and wildtype mice with 5-FU and analyzed them eight days post-injection.

This model allowed us to investigate how intact stress response mechanisms, such as autophagy and DNA repair response, function in MSPCs in O5A$^{\Delta/\Delta}$ compared to wildtype mice, and to further examine their impact on HSCs. We conducted a detailed analysis of stress-induced niche remodeling using whole mount staining and Fluorescence-Activated Cell Sorting (FACS). Key parameters such as F-actin fiber orientation, CDC42 levels, mitochondrial function and morphology, and autophagic vesicle delivery in MSPCs were evaluated using immunofluorescence microscopy (IF), FACS (Cyto-ID levels), and Seahorse assay. In addition, secondary effects on repopulating ability of LT-HSCs were studied using a transplantation assay.

Impaired niche health in aging and malignancies is associated with ineffective hematopoiesis and dysfunctional HSCs, leading to cytopenias and progressive bone marrow hypocellularity [89]. To translate our findings to human conditions with hypocellular marrow failure, we further examined the WNT5A-CDC42 induced cytoskeleton and autophagic defect in human bone-derived MSPCs from Shwachman Diamond Syndrome (SDS) patients using IF.

In the introduction, we presented multiple stress challenges as an aging model to characterize the gradual changes in tissue and cell function associated with aging (Figure 5) [73]. To address effects of multiple stress challenges in O5A$^{\Delta/\Delta}$ mice, we treated the mice twice with 5-FU eight days apart. The effect of attenuation of CDC42

activity was then studied by injection of CASIN for four consecutive days (days 5 to 8) after the first 5-FU treatment. This approach was used to investigate whether CASIN could dampen the negative effects of 5-FU-induced stress on MSPCs, and more outspoken in O5A$^{\Delta/\Delta}$ MSPCs, and restore their function under these conditions. By combining 5-FU with CASIN treatment, we aimed to evaluate the potential protective effects of CDC42 inhibition on tissue (niche), cellular (HSC), and molecular (mitophagy, F-actin orientation) levels during the 5-FU-induced stress response.

Research question no. 2 and methodical approach

Replicative and regenerative stress after hematopoietic stem cell transplantation

My first study demonstrated that CDC42 activation plays a crucial role in resolving stress responses by regulating F-actin and autophagy. In my **second lead authorship** on the role of CDC42 during stress scenarios (HSCT, regenerative stress, bone biology), I focused more on the niche and specifically on the bone remodeling function of MSPCs [120]. In this study, the HSCT stress model combined three factors: cytostatic conditioning (irradiation), HSC transplantation, and post-transplantation aging [120]. We compared HSCT mice to normally aged mice with the idea to filter out HSCT-specific changes in MSPC behaviour [120]. As one main function of MSPCs is the maintenance of bone formation. Thus, I was particularly interested to find out whether CDC42 inhibition would reduce the commonly observed complications of HSCT: osteopenia and osteoporosis.

To answer this question, I transplanted whole BM from wildtype mice into young lethally irradiated wildtype recipients and treated them afterwards *in vivo* with either CASIN or a vehicle for four consecutive days (days 5 to 8 after HSCT), similar to the approach used in my first study. To compare their phenotype to “normal aging”, two additional groups were included without myeloablative treatment (irradiation) and HSCT but with either CASIN or vehicle treatment as age-matched controls as well as a group of young control mice. This experimental setup allowed us to differentiate between replicative stress (aging) and regenerative stress following HSCT, as well as to evaluate the protective effects of early CASIN treatment after HSCT. The mice were analysed ten months post HSCT with in total 13 months. First, an RNA-seq analysis was performed

on 13-month-old sorted MSPCs (CD45- TER119- CD31- SCA-1+ Alcam$^{-/low}$) to identify age-related changes in gene expression. Additionally, the niche was analysed via FACS and the MSPCs afterwards cultured out of the bones and their function analysed with CFU-F assay, for DNA damage response and senescence markers. Further we investigated the F-actin cytoskeleton and CDC42-GTP levels in MSPCs with IF as well as their mitochondrial potential by Seahorse assay, IF and FACS (ROS and TMRM staining). Macroscopic effects of HSCT and/or CASIN treatments on skeletal function were assessed using µCT.

To extend the relevance of our findings from the mouse model to human (allo)HSCT, we analyzed CT data (T- and Z-Scores) from patients post-HSCT (Acute Lymphoblastic Leukemia (ALL) and Acute Myeloid Leukemia (AML)) over time, along with microscopic single-cell data from their bone-derived MSPCs, focusing on F-actin fibers and CDC42-GTP levels using IF.

Summary Paper #1

“Autophagy in mesenchymal progenitors protects mice against BM failure after severe intermittent stress”

In my first lead authorship study, we identified WNT5A in Osterix+ MSPCs as a key regulator of niche-dependent hematopoiesis under stress conditions. Our research demonstrated that mice lacking Wnt5a in MSPCs suffer from stress-related bone marrow failure and increased mortality, which we attributed to defective F-actin fiber orientation. This defect, driven by elevated activity of the small GTPase CDC42 in niche cells lacking WNT5A, led to improper positioning of autophagosomes and lysosomes, reduced autophagy, and increased oxidative stress. We also observed similar defects in MSPCs from patients with bone marrow failure syndromes such as Shwachman Diamond Syndrome (SDS), including misaligned F-actin fibers, impaired autophagosome-lysosome colocalization, and heightened CDC42 activation. Importantly, we demonstrated that short-term pharmacological inhibition of CDC42 in mice can prevent these autophagic defects in MSPCs, thereby rescuing hematopoiesis and protecting against lethal cytopenia under stress.

My responsibilities in this project included conducting a range of *in vivo* mouse experiments, such as handling, bleeding, irradiation, hematopoietic stem cell transplantation (HSCT), and administering 5-FU/CASIN treatments. I also performed extensive *in vitro* analyses, examining various cell types and tissues such as bone marrow, blood, bones, and spleen using advanced techniques like FACS. I cultured MSPCs from mouse and human tissues, assessed their stem cell potential through assays like CFU-F, differentiation, and senescence assays, and analyzed protein expression using IF microscopy. I also assessed mitochondrial quality in MSPCs using the Seahorse assay and collaborated with the Hartmut Geiger group in Ulm to prepare mouse bones for whole-mount imaging analysis. As the lead author, I played a significant role in experimental design and was deeply involved in writing and editing the manuscript to ensure that our findings were clearly and accurately communicated to the scientific community.

Appendix 1: “Autophagy in mesenchymal progenitors protects mice against BM failure after severe intermittent stress”, Landspersky et al., 2021, Blood.

Summary Paper #2

“Targeting CDC42 reduces skeletal degeneration after hematopoietic stem cell transplantation”

In my second lead authorship study, we addressed osteoporosis and osteopenia as significant long-term complications following allogeneic hematopoietic stem cell transplantation (alloHSCT). Although myeloablative treatments like chemotherapy or irradiation are essential for donor stem cell engraftment, they frequently result in substantial bone density loss that persists for years post-transplantation. In a comparable mouse model, we identified key cellular and molecular changes in MSPCs, including oxidative stress, reduced autophagy, and elevated CDC42 activity, which were linked to significant bone density decline observed one-year post-HSCT.

Importantly, treating damaged MSPCs with CASIN *in vitro* restored mitochondrial quality control and the F-actin cytoskeleton. *In vivo*, CASIN treatment post-HSCT improved bone volume and trabecular thickness, suggesting that CDC42 inhibition can prevent or reverse HSCT-induced osteoporotic changes. We confirmed these findings in human MSPCs from leukemia patients post-HSCT, observing similar disruptions in CDC42 activity and F-actin organization.

In summary, our study supports targeting CDC42 activity with CASIN to restore MSPC function and bone integrity, providing a potential therapeutic strategy to manage and prevent bone loss in HSCT patients. My responsibilities included conducting in vivo mouse experiments, such as handling, bleeding, irradiation, HSCT, and CASIN/vehicle injections. I also analyzed various cell types and tissues, including bone marrow, blood, and bones, using advanced techniques like FACS. Additionally, I cultured mouse and human MSPCs, assessing their stem cell potential through *in vitro* assays such as CFU-F, senescence staining, and DNA repair mechanisms. I further analyzed protein expression in MSPCs using IF and confocal microscopy. I evaluated mitochondrial quality in MSPCs with Seahorse assays and FACS-based ROS and TMRM staining. In collaboration with research teams in Ulm, I prepared mouse bones for micro-CT imaging. As the lead author, I was deeply involved in planning experiments and played a key role in writing and editing the manuscript to ensure our findings were clearly and accurately communicated.

Appendix 2: “Targeting CDC42 reduces skeletal degeneration after hematopoietic stem cell transplantation”, Landspersky et al., Blood advances 2024

DISCUSSION

In this doctoral thesis, I identify CDC42 as a key regulator in cytostatic stress responses in hematopoiesis and the skeletal system. The key finding of both studies is that overactivation of CDC42 (CDC42-GTP) plays a central role in the functional defects observed in both HSCs and MSPCs, significantly impacting hematopoiesis and skeletal integrity. Firstly, I induced the activation of CDC42 by cell stress in a stress-susceptible mouse model (O5A$^{\Delta/\Delta}$) using 5-FU [89], and secondly by lethal irradiation of wildtype mice followed by HSCT [120]. These methods enabled me to observe the consequences of CDC42 overactivation in various contexts of stress and damage. Furthermore, I found evidence for the involvement of CDC42 activation in physiological aging processes of MSPCs.

To study aging-like effects in stress models, we created a scenario in which *Wnt5a* was specifically deleted in osterix positive MSPCs (O5A$^{\Delta/\Delta}$), while other cells, including HSCs and ECs, retained normal (= wildtype) *Wnt5a* expression [89]. *Wnt5a* is not expressed in young mice under steady state conditions [65,160].

In line with this, we found that in this mouse model, CDC42-GTP was not increased in O5A$^{\Delta/\Delta}$ LT-HSCs nor was CDC42 apolar distributed under steady-state conditions. Previous studies have shown that in *ex vivo* culture systems in the absence of niche cells, extrinsic WNT5A is crucial to maintain HSC repopulating activity [161,162]. Since the lack of microenvironmental feedback in culture systems can be regarded as a stressor, we expected functional changes in different cell types of our O5A$^{\Delta/\Delta}$ mice after stress induction. Indeed, after mice were recovered from 5-FU cytostatic stress, CDC42-GTP levels were increased in LT-HSCs, and CDC42 was found in an apolar distribution, both indicative of molecular aging-like changes in LT-HSCs. Importantly, LT-HSCs from 5-FU-treated O5A$^{\Delta/\Delta}$ mice showed reduced repopulation activity. These findings demonstrate that while other cell types are still capable of secreting WNT5A, it is only osteoprogenitor-derived WNT5A that is crucial for recovery from stress-induced, aging-like alterations in CDC42 activation and for preventing the stress-induced functional decline of LT-HSCs.

One possible explanation for our findings is that, along with the functional decline of LT-HSCs, we observed prolonged stress-induced CDC42 activation and defective F-actin fiber organization in the MSPCs of the O5A$^{\Delta/\Delta}$ mice. The cytoskeleton of the

MSPCs lost the regular structure typical of wildtype cells, with F-actin fibers becoming irregularly arranged or, in some cases, entirely disrupted. This disruption in cytoskeletal structure is significant because the cytoskeleton plays a crucial role in cellular maintenance processes such as autophagy, where it enables the transport of lysosomes and autophagosomes important for their fusion into autophagolysosomes for the removal and recycling of cell debris, surplus protein (aggregates) and organelles. It is likely that the defective cytoskeletal infrastructure in the MSPCs is involved in the secondary functional decline of the HSCs, ultimately contributing to BM failure. Our results suggest that osteoprogenitor-derived WNT5A regulates cellular maintenance processes in an autocrine manner. The defective cell maintenance likely explains why the O5A$^{\Delta/\Delta}$ niche could no longer support stem cells, whereas wildtype MSPCs, with intact CDC42 responsiveness, F-actin structure, and autophagy processes, were still able to maintain stem cell support.

The results presented in this paper do not provide direct evidence that impaired cellular maintenance in MSPCs directly causes defective functional maintenance of LT-HSCs. Although it is well-established that autophagy plays a direct role in maintaining the repopulation activity of adult LT-HSCs [163], it remains uncertain whether autophagy in the MSPCs of the niche is essential for their regulation of LT-HSCs. Future studies in mice with MSPC-specific defects in F-actin assembly (downstream of CDC42 and/or CRIB effectors), or direct MSPC-specific disruption of autophagy, should answer whether such defects in MSPCs cause aging-like secondary functional decline of LT-HSCs.

Whereas, my first study focused mainly on the secondary functional decline of LT-HSC in O5A$^{\Delta/\Delta}$ mice, the second study focused on the MSPCs in a model of lethal radiotherapy-induced damage and HSCT. The mouse model used in this study simulated the premise that human recipients usually undergo severe myeloablative treatment prior to clinical HSCT, which may include not only chemotherapy but also total body irradiation or local radiotherapy. The aim of these clinical regimens is to prevent rejection of the graft by suppressing the body's immune system, the elimination of any remaining malignant HSCs, and to ensure optimal engraftment of donor HSCs in the recipients [164]. A common late complication found in HSCT recipients is osteoporosis [138,140], suggesting that in HSCT recipients, the MSPCs might not contribute sufficiently to bone remodelling. To study this, we isolated MSPCs from mice

that were lethally irradiated and subsequently underwent HSCT. We found similar defective MSPC function as observed in our O5A$^{\Delta/\Delta}$ mice from the previous study: Even ten months after transplantation and prior irradiation, an increase in CDC42-GTP in the MSPCs, a disrupted F-actin cytoskeleton, and reduced autophagic clearance of damaged mitochondria were observable in HSCT-MSPCs. This persistent defect suggests that the effects of CDC42 overactivation are long-lasting and continue to impact stem cell function well beyond the initial stress event.

Regardless of how the overactivation of this small Rho GTPase occurred, the outcomes were strikingly similar and the consistent overactivation of CDC42 observed in both studies highlights its potential role as a therapeutic target to prevent or mitigate defects in LT-HSCs and MSPCs, including BM failure. Indeed, a short pharmacological intervention with CASIN, a CDC42-specific activation inhibitor, administered on the fifth day after the first 5-FU injection into O5A$^{\Delta/\Delta}$ mice, reduced the elevated CDC42 activation *in vivo*, prevented defective actin-anchored autophagy in MSPCs, rescued hematopoiesis, and protected the mice from lethal cytopenia. This intervention demonstrates that targeting CDC42 activity could be a viable therapeutic strategy for preserving hematopoietic function under severe stress conditions.

The significance of the second study is further highlighted by the fact that CASIN treatment reversed skeletal changes in old, transplanted mice, restoring bone volume to levels comparable to younger mice. This finding is particularly important because it suggests that CASIN could address well-known long-term complications of HSCT, such as osteoporotic bone changes.

Since osteoporosis is primarily related to aging or stress-induced aging-like degeneration, this study addresses another very important aspect by allowing us to distinguish between *aging-like changes*, which occurs due to the collaboration between responses to severe stress and post-stress regeneration, and *aging*, caused by repeated minor stressors leading to natural aging. This distinction was achieved by comparing our HSCT mice (13 months; *both* aging *and* aging-like changes) with young (three months, unchanged) and age-matched control mice (13 months; only aging). Both the HSCT mice and the age-matched controls show elevated CDC42-GTP levels as well as cytoskeletal defects, but we observed additional CDC42-dependent defects in the HSCT-MSPCs distinct from those caused by aging-like changes. Interestingly,

CASIN treatment showed effects in both *in vivo* models, even in the absence of HSCT or myeloablative therapy in the age-matched 13-months-old mice.

Myeloablative treatment remains the preferred method before patients receive a stem cell transplant. The observation that elevated CDC42-GTP levels in MSPCs, seen in both cytostatic models (5-FU and irradiation), can be reduced by a short CASIN treatment is of significant interest for cancer therapy. In particular, in tissue regeneration post anti-cancer treatments, healthy cells are brought into a disturbed environment, which does not necessarily support optimal regeneration of healthy tissue cells, such as HSCs [5,165]. Furthermore, transplanted HSCs should home to the correct niches (migrate towards, settle, proliferate, self-renew, and differentiate into mature tissue cells). That the niche is not yet regenerated at this point and what negative effects this has for the HSCs could be a reason for the many proven long-term defects after surviving transplantation [166-168]. A proposed strategy to mitigate these negative effects is to allow the periosteal niche to expand before the stem cells are transplanted [169].

Chemotherapeutics or radiation are not only used in leukemia models but also for the curative treatment of other cancers such as brain tumors, lung cancer, breast cancer, prostate cancer, colorectal cancer, lymphomas, sarcomas and many more [164]. Here, they play an important role in neoadjuvant and adjuvant therapy, to reduce tumor size before surgery or to eliminate remaining cancer cells after surgery. Additionally, chemotherapeutics and radiation are used in advanced stages of cancer to alleviate symptoms and improve quality of life [170]. Considering that the level of active CDC42-GTP is elevated after cytostatic treatment, CASIN treatment holds promise for cancer therapies, as it may improve or even restore the cell cytoskeleton and autophagy processes of healthy cells post cytostatic treatment. This restoration allows cells to maintain cellular health properly or, if the cytostatic damage is too severe, trigger apoptosis. A crucial aspect is that many different cancer cells are selected to bypass apoptosis by enhancing the anti-apoptotic machinery and downregulating the pro-apoptotic program [171]. Therefore, inducing programmed cell death in defective cells by inhibiting CDC42-GTP with CASIN could be a promising approach when the damage is too extensive for the cells to be repaired through treatment. However, initial experiments suggest that CASIN promotes cell survival by suppressing apoptotic processes [172]. This mechanism must therefore be investigated much more deeply

before any therapeutic application, as its suppression could be potentially dangerous, especially given CASIN's significant potential in cancer therapies, which requires further assessment of its effects on malignant cells. For instance, since CASIN adds to mobilization of stem cells [173], there is a chance that CASIN promotes cell metastasis. Since Cdc42 plays a crucial role in cytoskeletal dynamics, manipulating this process could inadvertently enhance metastatic potential. In addition, little is known about CDC42 activation in cancer cells. Since many cancers show molecular changes in cellular maintenance processes allowing their survival instead of triggering cell death, inhibition of CDC42 could, in theory, also improve cellular maintenance of cancer cells. Therefore, thorough preclinical studies are necessary to assess these risks before advancing CASIN as a therapeutic option.

As the small Rho GTPase CDC42 plays a significant role in aging, CASIN could also be of interest in treating aging-associated degenerative neuronal diseases such as Alzheimer [174] and Parkinson [175], as well as in addressing chronic inflammatory reactions, particularly in connection with age-related autoimmune diseases like Rheumatoid Arthritis[176,177]. The extent of research on the role of CDC42 in these diseases varies. In Alzheimer, CDC42 has been linked to the regulation of neuronal signaling and synaptic function, which are critical in disease progression [174]. In Parkinson disease, research has begun to uncover the involvement of CDC42 in neuronal survival and dopaminergic signaling [175]. However, the precise mechanisms and therapeutic potential of targeting CDC42 in Parkinson are still areas of active research. For autoimmune diseases like Rheumatoid Arthritis, CDC42 has been implicated in inflammatory cell migration and joint inflammation, but more research is needed to fully understand its role and therapeutic potential in these conditions [176,177].

As my studies show, using a CDC42 inhibitor could also be beneficial for osteoporosis patients. This approach may prevent, or slow down osteoporosis caused not only therapy induced by chemotherapy or radiation but also age-related osteoporosis, particularly in postmenopausal women [166-168]. Indeed, hsa-miR-133a-3p, a microRNA involved in gene regulation, particularly affecting the actin cytoskeleton through CDC42, has been identified as a critical pathway in a meta-analysis of postmenopausal osteoporosis [178]. In clinical practice, proteasome inhibitors are being used to enhance osteoblast functions, the cells responsible for bone formation [179,180]. Enhancing their function can slow down or reverse the bone degradation seen in osteoporosis. A

common prescribed medication for osteoporosis is bisphosphonates, which act by inhibiting bone resorption by osteoclasts. Although bisphosphonates can affect CDC42 activity by inhibiting prenylation, their effects on HSCs and the hematopoietic niche are controversial [181-184]. Unlike bisphosphonates, CASIN targets the CDC42 pathway directly and may therefore offer a more targeted approach to the treatment of osteoporosis. As CDC42 plays a key role in cytoskeleton dynamics and cellular maintenance processes such as autophagy, the use of CASIN could offer two benefits: it not only helps in reducing the overactivity of CDC42 but also helps in maintaining cellular integrity, which is crucial for bone health. In contrast to other common drugs, influencing these processes with CASIN could not only prevent or alleviate osteoporosis, but also contribute to better bone health.

In summary, modulating CDC42 activity in MSPCs through substances like CASIN could be important for improving BM homeostasis and hematopoietic functions. My findings strongly suggest that targeted down-regulation of CDC42 activity is a promising therapeutic approach for restoring hematopoietic functions after severe stress and might benefit treatment of BM diseases, especially in the context of niche-disrupting therapies such as chemotherapy or radiotherapy. But, as CDC42 has diverse roles in various cancers, inflammatory processes, immune responses, and osteoporosis, modulating its activity could also be a key addition in the treatments of a range of additional diseases. Future research should focus on exploring the role of CDC42 in different disease models and finding ways to effectively modulate its activity to develop and optimize individualized treatment methods in clinical practice.

LIST OF FIGURES

PUBLICATIONS LANDSPERSKY/SIPPENAUER

A. **Landspersky, T.** et al. *Autophagy in mesenchymal progenitors protects mice against BM failure after severe intermittent stress*. **Blood** 139, 690-703.

B. **Landspersky, T.** et al. *Targeting CDC42 reduces skeletal degeneration after hematopoietic stem cell transplantation.* **Blood Adv** (2024).

C. Schreck, C…**Sippenauer, T.** … et al. *Niche WNT5A regulates the actin cytoskeleton during regeneration of hematopoietic stem cells.* **J Exp Med** 214, 165-181,

D. Fröbel, J., **Landspersky, T.** ... et al. *The Hematopoietic BM Niche Ecosystem.* **Front Cell Dev Biol** 9, 705410.

E. Hettler, F. … **Landspersky, T.** … et al. *Osteoprogenitor SFRP1 prevents exhaustion of hematopoietic stem cells via PP2A-PR72/130-mediated regulation of p300.* **Haematologica** 108, 490-501,

F. Romero Marquez, S. … **Landspersky, T.** … et al. *Secreted factors from mouse embryonic fibroblasts maintain repopulating function of single cultured hematopoietic stem cells.* **Haematologica** 106, 2633-2640.

G. Redondo Monte, E. … **Landspersky, T.** … et al. *Specific effects of somatic GATA2 zinc finger mutations on erythroid differentiation.* **Exp Hematol** 108, 26-35,

REFERENCES

1 Sawai, C. M. *et al.* Hematopoietic Stem Cells Are the Major Source of Multilineage Hematopoiesis in Adult Animals. *Immunity* **45**, 597-609 (2016). https://doi.org/10.1016/j.immuni.2016.08.007

2 Sun, J. *et al.* Clonal dynamics of native haematopoiesis. *Nature* **514**, 322-327 (2014). https://doi.org/10.1038/nature13824

3 Cheshier, S. H., Morrison, S. J., Liao, X. & Weissman, I. L. In vivo proliferation and cell cycle kinetics of long-term self-renewing hematopoietic stem cells. *Proc Natl Acad Sci U S A* **96**, 3120-3125 (1999). https://doi.org/10.1073/pnas.96.6.3120

4 Blanpain, C., Mohrin, M., Sotiropoulou, P. A. & Passegué, E. DNA-damage response in tissue-specific and cancer stem cells. *Cell Stem Cell* **8**, 16-29 (2011). https://doi.org/10.1016/j.stem.2010.12.012

5 Renström, J., Kroger, M., Peschel, C. & Oostendorp, R. A. How the niche regulates hematopoietic stem cells. *Chem Biol Interact* **184**, 7-15 (2010). https://doi.org/10.1016/j.cbi.2009.11.012

6 Zhang, Y., Gao, S., Xia, J. & Liu, F. Hematopoietic Hierarchy - An Updated Roadmap. *Trends Cell Biol* **28**, 976-986 (2018). https://doi.org/10.1016/j.tcb.2018.06.001

7 Säwen, P. *et al.* Murine HSCs contribute actively to native hematopoiesis but with reduced differentiation capacity upon aging. *Elife* **7** (2018). https://doi.org/10.7554/eLife.41258

8 Laurenti, E. & Göttgens, B. From haematopoietic stem cells to complex differentiation landscapes. *Nature* **553**, 418-426 (2018). https://doi.org/10.1038/nature25022

9 Bast, L. *et al.* Computational modeling of stem and progenitor cell kinetics identifies plausible hematopoietic lineage hierarchies. *iScience* **24**, 102120 (2021). https://doi.org/10.1016/j.isci.2021.102120

10 Notta, F. *et al.* Distinct routes of lineage development reshape the human blood hierarchy across ontogeny. *Science* **351**, aab2116 (2016). https://doi.org/10.1126/science.aab2116

11 Carrelha, J. *et al.* Hierarchically related lineage-restricted fates of multipotent haematopoietic stem cells. *Nature* **554**, 106-111 (2018). https://doi.org/10.1038/nature25455

12 Yatim, K. M. & Lakkis, F. G. A brief journey through the immune system. *Clin J Am Soc Nephrol* **10**, 1274-1281 (2015). https://doi.org/10.2215/cjn.10031014

13 Hillion, S. *et al.* The Innate Part of the Adaptive Immune System. *Clin Rev Allergy Immunol* **58**, 151-154 (2020). https://doi.org/10.1007/s12016-019-08740-1

14 Comazzetto, S., Shen, B. & Morrison, S. J. Niches that regulate stem cells and hematopoiesis in adult bone marrow. *Dev Cell* **56**, 1848-1860 (2021). https://doi.org/10.1016/j.devcel.2021.05.018

15 Cheng, H., Zheng, Z. & Cheng, T. New paradigms on hematopoietic stem cell differentiation. *Protein Cell* **11**, 34-44 (2020). https://doi.org/10.1007/s13238-019-0633-0

16 Bast, L. *et al.* Computational modeling of stem and progenitor cell kinetics identifies plausible hematopoietic lineage hierarchies. *iScience* **24**, 102120 (2021). https://doi.org/10.1016/j.isci.2021.102120

17 Zindel, J. & Kubes, P. DAMPs, PAMPs, and LAMPs in Immunity and Sterile Inflammation. *Annu Rev Pathol* **15**, 493-518 (2020). https://doi.org/10.1146/annurev-pathmechdis-012419-032847

18 Groarke, E. M. & Young, N. S. Aging and Hematopoiesis. *Clin Geriatr Med* **35**, 285-293 (2019). https://doi.org/10.1016/j.cger.2019.03.001

19 Pinho, S. & Frenette, P. S. Haematopoietic stem cell activity and interactions with the niche. *Nat Rev Mol Cell Biol* **20**, 303-320 (2019). https://doi.org/10.1038/s41580-019-0103-9

20 Istvanffy, R. *et al.* Stromal pleiotrophin regulates repopulation behavior of hematopoietic stem cells. *Blood* **118**, 2712-2722 (2011). https://doi.org/10.1182/blood-2010-05-287235

21 Gao, X., Xu, C., Asada, N. & Frenette, P. S. The hematopoietic stem cell niche: from embryo to adult. *Development* **145** (2018). https://doi.org/10.1242/dev.139691

22 Orkin, S. H. & Zon, L. I. Hematopoiesis: an evolving paradigm for stem cell biology. *Cell* **132**, 631-644 (2008). https://doi.org/10.1016/j.cell.2008.01.025

23 Vink, C. S., Mariani, S. A. & Dzierzak, E. Embryonic Origins of the Hematopoietic System: Hierarchies and Heterogeneity. *Hemasphere* **6**, e737 (2022). https://doi.org/10.1097/hs9.0000000000000737

24 Morrison, S. J. & Scadden, D. T. The bone marrow niche for haematopoietic stem cells. *Nature* **505**, 327-334 (2014). https://doi.org/10.1038/nature12984

25 Karlsson, G., Sommarin, M. N. E. & Böiers, C. Defining the Emerging Blood System During Development at Single-Cell Resolution. *Front Cell Dev Biol* **9**, 660350 (2021). https://doi.org/10.3389/fcell.2021.660350

26 de Bruijn, M. F., Speck, N. A., Peeters, M. C. & Dzierzak, E. Definitive hematopoietic stem cells first develop within the major arterial regions of the mouse embryo. *Embo j* **19**, 2465-2474 (2000). https://doi.org/10.1093/emboj/19.11.2465

27 Oostendorp, R. A. *et al.* Stromal cell lines from mouse aorta-gonads-mesonephros subregions are potent supporters of hematopoietic stem cell activity. *Blood* **99**, 1183-1189 (2002). https://doi.org/10.1182/blood.v99.4.1183

28 Bowie, M. B. *et al.* Identification of a new intrinsically timed developmental checkpoint that reprograms key hematopoietic stem cell properties. *Proc Natl Acad Sci U S A* **104**, 5878-5882 (2007). https://doi.org/10.1073/pnas.0700460104

29 Morrison, S. J., Hemmati, H. D., Wandycz, A. M. & Weissman, I. L. The purification and characterization of fetal liver hematopoietic stem cells. *Proc Natl Acad Sci U S A* **92**, 10302-10306 (1995). https://doi.org/10.1073/pnas.92.22.10302

30 Ema, H. & Nakauchi, H. Expansion of hematopoietic stem cells in the developing liver of a mouse embryo. *Blood* **95**, 2284-2288 (2000).

31 Trumpp, A., Essers, M. & Wilson, A. Awakening dormant haematopoietic stem cells. *Nat Rev Immunol* **10**, 201-209 (2010). https://doi.org/10.1038/nri2726

32 Dolgalev, I. & Tikhonova, A. N. Connecting the Dots: Resolving the Bone Marrow Niche Heterogeneity. *Front Cell Dev Biol* **9**, 622519 (2021). https://doi.org/10.3389/fcell.2021.622519

33 Frobel, J. *et al.* The Hematopoietic Bone Marrow Niche Ecosystem. *Front Cell Dev Biol* **9**, 705410 (2021). https://doi.org/10.3389/fcell.2021.705410

34 Nakamura, Y. *et al.* Isolation and characterization of endosteal niche cell populations that regulate hematopoietic stem cells. *Blood* **116**, 1422-1432 (2010). https://doi.org/10.1182/blood-2009-08-239194

35 Chow, A. *et al.* Bone marrow CD169+ macrophages promote the retention of hematopoietic stem and progenitor cells in the mesenchymal stem cell niche. *J Exp Med* **208**, 261-271 (2011). https://doi.org/10.1084/jem.20101688

36 Winkler, I. G. *et al.* Bone marrow macrophages maintain hematopoietic stem cell (HSC) niches and their depletion mobilizes HSCs. *Blood* **116**, 4815-4828 (2010). https://doi.org/10.1182/blood-2009-11-253534

37 Kiel, M. J. *et al.* SLAM family receptors distinguish hematopoietic stem and progenitor cells and reveal endothelial niches for stem cells. *Cell* **121**, 1109-1121 (2005). https://doi.org/10.1016/j.cell.2005.05.026

38 Kiel, M. J. & Morrison, S. J. Uncertainty in the niches that maintain haematopoietic stem cells. *Nat Rev Immunol* **8**, 290-301 (2008). https://doi.org/10.1038/nri2279

39 Sugiyama, T., Kohara, H., Noda, M. & Nagasawa, T. Maintenance of the hematopoietic stem cell pool by CXCL12-CXCR4 chemokine signaling in bone marrow stromal cell niches. *Immunity* **25**, 977-988 (2006). https://doi.org/10.1016/j.immuni.2006.10.016

40 Ding, L., Saunders, T. L., Enikolopov, G. & Morrison, S. J. Endothelial and perivascular cells maintain haematopoietic stem cells. *Nature* **481**, 457-462 (2012). https://doi.org/10.1038/nature10783

41 Méndez-Ferrer, S. *et al.* Mesenchymal and haematopoietic stem cells form a unique bone marrow niche. *Nature* **466**, 829-834 (2010). https://doi.org/10.1038/nature09262

42 Bianco, P., Robey, P. G. & Simmons, P. J. Mesenchymal stem cells: revisiting history, concepts, and assays. *Cell Stem Cell* **2**, 313-319 (2008). https://doi.org/10.1016/j.stem.2008.03.002

43 James, A. W. Review of Signaling Pathways Governing MSC Osteogenic and Adipogenic Differentiation. *Scientifica (Cairo)* **2013**, 684736 (2013). https://doi.org/10.1155/2013/684736

44 Kokabu, S., Lowery, J. W. & Jimi, E. Cell Fate and Differentiation of Bone Marrow Mesenchymal Stem Cells. *Stem Cells Int* **2016**, 3753581 (2016). https://doi.org/10.1155/2016/3753581

45 Massagué, J. TGFβ signalling in context. *Nat Rev Mol Cell Biol* **13**, 616-630 (2012). https://doi.org/10.1038/nrm3434

46 Hasegawa, T. *et al.* Matrix Vesicle-Mediated Mineralization and Osteocytic Regulation of Bone Mineralization. *Int J Mol Sci* **23** (2022). https://doi.org/10.3390/ijms23179941

47 Bonucci, E. Bone mineralization. *Front Biosci (Landmark Ed)* **17**, 100-128 (2012). https://doi.org/10.2741/3918

48 Chen, Q. *et al.* Fate decision of mesenchymal stem cells: adipocytes or osteoblasts? *Cell Death Differ* **23**, 1128-1139 (2016). https://doi.org/10.1038/cdd.2015.168

49 Kang, Q. *et al.* A comprehensive analysis of the dual roles of BMPs in regulating adipogenic and osteogenic differentiation of mesenchymal progenitor cells. *Stem Cells Dev* **18**, 545-559 (2009). https://doi.org/10.1089/scd.2008.0130

50 Deng, Z. L. *et al.* Regulation of osteogenic differentiation during skeletal development. *Front Biosci* **13**, 2001-2021 (2008). https://doi.org/10.2741/2819

51 Clevers, H., Loh, K. M. & Nusse, R. Stem cell signaling. An integral program for tissue renewal and regeneration: Wnt signaling and stem cell control. *Science* **346**, 1248012 (2014). https://doi.org/10.1126/science.1248012

52 Keller, K. C. *et al.* Wnt5a Supports Osteogenic Lineage Decisions in Embryonic Stem Cells. *Stem Cells Dev* **25**, 1020-1032 (2016). https://doi.org/10.1089/scd.2015.0367

53 He, X. *et al.* TLR4 Activation Promotes Bone Marrow MSC Proliferation and Osteogenic Differentiation via Wnt3a and Wnt5a Signaling. *PLoS One* **11**, e0149876 (2016). https://doi.org/10.1371/journal.pone.0149876

54 Shimizu, T. *et al.* Notch signaling pathway enhances bone morphogenetic protein 2 (BMP2) responsiveness of Msx2 gene to induce osteogenic differentiation and mineralization of vascular smooth muscle cells. *J Biol Chem* **286**, 19138-19148 (2011). https://doi.org/10.1074/jbc.M110.175786

55 Fontaine, C., Cousin, W., Plaisant, M., Dani, C. & Peraldi, P. Hedgehog signaling alters adipocyte maturation of human mesenchymal stem cells. *Stem Cells* **26**, 1037-1046 (2008). https://doi.org/10.1634/stemcells.2007-0974

56 Spinella-Jaegle, S. *et al.* Sonic hedgehog increases the commitment of pluripotent mesenchymal cells into the osteoblastic lineage and abolishes adipocytic differentiation. *J Cell Sci* **114**, 2085-2094 (2001). https://doi.org/10.1242/jcs.114.11.2085

57 Eswarakumar, V. P., Lax, I. & Schlessinger, J. Cellular signaling by fibroblast growth factor receptors. *Cytokine Growth Factor Rev* **16**, 139-149 (2005). https://doi.org/10.1016/j.cytogfr.2005.01.001

58 Baksh, D. & Tuan, R. S. Canonical and non-canonical Wnts differentially affect the development potential of primary isolate of human bone marrow mesenchymal stem cells. *J Cell Physiol* **212**, 817-826 (2007). https://doi.org/10.1002/jcp.21080

59 Zoncu, R., Efeyan, A. & Sabatini, D. M. mTOR: from growth signal integration to cancer, diabetes and ageing. *Nat Rev Mol Cell Biol* **12**, 21-35 (2011). https://doi.org/10.1038/nrm3025

60 Laplante, M. & Sabatini, D. M. mTOR signaling at a glance. *J Cell Sci* **122**, 3589-3594 (2009). https://doi.org/10.1242/jcs.051011

61 André, C. & Cota, D. Coupling nutrient sensing to metabolic homoeostasis: the role of the mammalian target of rapamycin complex 1 pathway. *Proc Nutr Soc* **71**, 502-510 (2012). https://doi.org/10.1017/s0029665112000754

62 Ellis, S. J. & Tanentzapf, G. Integrin-mediated adhesion and stem-cell-niche interactions. *Cell Tissue Res* **339**, 121-130 (2010). https://doi.org/10.1007/s00441-009-0828-4

63 Grenier, J. M. P., Testut, C., Fauriat, C., Mancini, S. J. C. & Aurrand-Lions, M. Adhesion Molecules Involved in Stem Cell Niche Retention During Normal Haematopoiesis and in Acute Myeloid Leukaemia. *Front Immunol* **12**, 756231 (2021). https://doi.org/10.3389/fimmu.2021.756231

64 Domingues, M. J., Cao, H., Heazlewood, S. Y., Cao, B. & Nilsson, S. K. Niche Extracellular Matrix Components and Their Influence on HSC. *J Cell Biochem* **118**, 1984-1993 (2017). https://doi.org/10.1002/jcb.25905

65 Schreck, C. *et al.* Niche WNT5A regulates the actin cytoskeleton during regeneration of hematopoietic stem cells. *J Exp Med* **214**, 165-181 (2017). https://doi.org/10.1084/jem.20151414

66 Fan, Y. L., Zhao, H. C., Li, B., Zhao, Z. L. & Feng, X. Q. Mechanical Roles of F-Actin in the Differentiation of Stem Cells: A Review. *ACS Biomater Sci Eng* **5**, 3788-3801 (2019). https://doi.org/10.1021/acsbiomaterials.9b00126

67 Garcin, C. & Straube, A. Microtubules in cell migration. *Essays Biochem* **63**, 509-520 (2019). https://doi.org/10.1042/ebc20190016

68 Yu, V. W. & Scadden, D. T. Hematopoietic Stem Cell and Its Bone Marrow Niche. *Curr Top Dev Biol* **118**, 21-44 (2016). https://doi.org/10.1016/bs.ctdb.2016.01.009

69 Zhou, B. O., Ding, L. & Morrison, S. J. Hematopoietic stem and progenitor cells regulate the regeneration of their niche by secreting Angiopoietin-1. *Elife* **4**, e05521 (2015). https://doi.org/10.7554/eLife.05521

70 Bruns, I. *et al.* Megakaryocytes regulate hematopoietic stem cell quiescence through CXCL4 secretion. *Nat Med* **20**, 1315-1320 (2014). https://doi.org/10.1038/nm.3707

71 Smith, B. W. & Murphy, G. J. Stem cells, megakaryocytes, and platelets. *Curr Opin Hematol* **21**, 430-437 (2014). https://doi.org/10.1097/moh.0000000000000064

72 Olson, T. S. *et al.* Megakaryocytes promote murine osteoblastic HSC niche expansion and stem cell engraftment after radioablative conditioning. *Blood* **121**, 5238-5249 (2013). https://doi.org/10.1182/blood-2012-10-463414

73 Fröbel, J. *et al.* The Hematopoietic Bone Marrow Niche Ecosystem. *Front Cell Dev Biol* **9**, 705410 (2021). https://doi.org/10.3389/fcell.2021.705410

74 Bogeska, R. *et al.* Inflammatory exposure drives long-lived impairment of hematopoietic stem cell self-renewal activity and accelerated aging. *Cell Stem Cell* **29**, 1273-1284.e1278 (2022). https://doi.org/10.1016/j.stem.2022.06.012

75 Baldridge, M. T., King, K. Y., Boles, N. C., Weksberg, D. C. & Goodell, M. A. Quiescent haematopoietic stem cells are activated by IFN-gamma in response to chronic infection. *Nature* **465**, 793-797 (2010). https://doi.org/10.1038/nature09135

76 Essers, M. A. *et al.* IFNalpha activates dormant haematopoietic stem cells in vivo. *Nature* **458**, 904-908 (2009). https://doi.org/10.1038/nature07815

77 Raaijmakers, M. H. *et al.* Bone progenitor dysfunction induces myelodysplasia and secondary leukaemia. *Nature* **464**, 852-857 (2010). https://doi.org/10.1038/nature08851

78 Rizo, A., Vellenga, E., de Haan, G. & Schuringa, J. J. Signaling pathways in self-renewing hematopoietic and leukemic stem cells: do all stem cells need a niche? *Hum Mol Genet* **15 Spec No 2**, R210-219 (2006). https://doi.org/10.1093/hmg/ddl175

79 López-Otín, C., Blasco, M. A., Partridge, L., Serrano, M. & Kroemer, G. The hallmarks of aging. *Cell* **153**, 1194-1217 (2013). https://doi.org/10.1016/j.cell.2013.05.039

80 Landspersky, T. *et al.* Autophagy in mesenchymal progenitors protects mice against bone marrow failure after severe intermittent stress. *Blood* **139**, 690-703 (2022). https://doi.org/10.1182/blood.2021011775

81 Yamashita, M. & Iwama, A. Aging and Clonal Behavior of Hematopoietic Stem Cells. *Int J Mol Sci* **23** (2022). https://doi.org/10.3390/ijms23041948

82 Kowalczyk, M. S. *et al.* Single-cell RNA-seq reveals changes in cell cycle and differentiation programs upon aging of hematopoietic stem cells. *Genome Res* **25**, 1860-1872 (2015). https://doi.org/10.1101/gr.192237.115

83 Prendergast Á, M. *et al.* IFNα-mediated remodeling of endothelial cells in the bone marrow niche. *Haematologica* **102**, 445-453 (2017). https://doi.org/10.3324/haematol.2016.151209

84 Saçma, M. *et al.* Haematopoietic stem cells in perisinusoidal niches are protected from ageing. *Nat Cell Biol* **21**, 1309-1320 (2019). https://doi.org/10.1038/s41556-019-0418-y

85 Demel, U. M. *et al.* A complex proinflammatory cascade mediates the activation of HSCs upon LPS exposure in vivo. *Blood Adv* **6**, 3513-3528 (2022). https://doi.org/10.1182/bloodadvances.2021006088

86 Takizawa, H. *et al.* Pathogen-Induced TLR4-TRIF Innate Immune Signaling in Hematopoietic Stem Cells Promotes Proliferation but Reduces Competitive Fitness. *Cell Stem Cell* **21**, 225-240.e225 (2017). https://doi.org/10.1016/j.stem.2017.06.013

87 Esplin, B. L. *et al.* Chronic exposure to a TLR ligand injures hematopoietic stem cells. *J Immunol* **186**, 5367-5375 (2011). https://doi.org/10.4049/jimmunol.1003438

88 Venezia, T. A. *et al.* Molecular signatures of proliferation and quiescence in hematopoietic stem cells. *PLoS Biol* **2**, e301 (2004). https://doi.org/10.1371/journal.pbio.0020301

89 Landspersky, T. *et al.* Autophagy in mesenchymal progenitors protects mice against bone marrow failure after severe intermittent stress. *Blood* **139**, 690-703 (2022). https://doi.org/10.1182/blood.2021011775

90 Oravecz-Wilson, K. I. *et al.* Huntingtin Interacting Protein 1 mutations lead to abnormal hematopoiesis, spinal defects and cataracts. *Hum Mol Genet* **13**, 851-867 (2004). https://doi.org/10.1093/hmg/ddh102

91 Akunuru, S. & Geiger, H. Aging, Clonality, and Rejuvenation of Hematopoietic Stem Cells. *Trends Mol Med* **22**, 701-712 (2016). https://doi.org/10.1016/j.molmed.2016.06.003

92 López-Otín, C., Blasco, M. A., Partridge, L., Serrano, M. & Kroemer, G. Hallmarks of aging: An expanding universe. *Cell* **186**, 243-278 (2023). https://doi.org/10.1016/j.cell.2022.11.001

93 Florian, M. C. *et al.* A canonical to non-canonical Wnt signalling switch in haematopoietic stem-cell ageing. *Nature* **503**, 392-396 (2013). https://doi.org/10.1038/nature12631

94 Wu, Y. *et al.* Identification of key genes and transcription factors in aging mesenchymal stem cells by DNA microarray data. *Gene* **692**, 79-87 (2019). https://doi.org/10.1016/j.gene.2018.12.063

95 Al-Azab, M., Safi, M., Idiiatullina, E., Al-Shaebi, F. & Zaky, M. Y. Aging of mesenchymal stem cell: machinery, markers, and strategies of fighting. *Cell Mol Biol Lett* **27**, 69 (2022). https://doi.org/10.1186/s11658-022-00366-0

96 Templeman, N. M. & Murphy, C. T. Regulation of reproduction and longevity by nutrient-sensing pathways. *J Cell Biol* **217**, 93-106 (2018). https://doi.org/10.1083/jcb.201707168

97 Sánchez-Aguilera, A. *et al.* Estrogen signaling selectively induces apoptosis of hematopoietic progenitors and myeloid neoplasms without harming steady-state hematopoiesis. *Cell Stem Cell* **15**, 791-804 (2014). https://doi.org/10.1016/j.stem.2014.11.002

98 Kusumbe, A. P., Ramasamy, S. K. & Adams, R. H. Coupling of angiogenesis and osteogenesis by a specific vessel subtype in bone. *Nature* **507**, 323-328 (2014). https://doi.org/10.1038/nature13145

99 Maryanovich, M. *et al.* Adrenergic nerve degeneration in bone marrow drives aging of the hematopoietic stem cell niche. *Nat Med* **24**, 782-791 (2018). https://doi.org/10.1038/s41591-018-0030-x

100 Chan, G. K. & Duque, G. Age-related bone loss: old bone, new facts. *Gerontology* **48**, 62-71 (2002). https://doi.org/10.1159/000048929

101 López-Otín, C. & Kroemer, G. Hallmarks of Health. *Cell* **184**, 33-63 (2021). https://doi.org/10.1016/j.cell.2020.11.034

102 Luis, T. C. *et al.* Canonical wnt signaling regulates hematopoiesis in a dosage-dependent fashion. *Cell Stem Cell* **9**, 345-356 (2011). https://doi.org/10.1016/j.stem.2011.07.017

103 Sarabia-Sánchez, M. A. & Robles-Flores, M. WNT Signaling in Stem Cells: A Look into the Non-Canonical Pathway. *Stem Cell Rev Rep* **20**, 52-66 (2024). https://doi.org/10.1007/s12015-023-10610-5

104 Yamaguchi, T. P., Bradley, A., McMahon, A. P. & Jones, S. A Wnt5a pathway underlies outgrowth of multiple structures in the vertebrate embryo. *Development* **126**, 1211-1223 (1999). https://doi.org/10.1242/dev.126.6.1211

105 Qin, K. *et al.* Canonical and noncanonical Wnt signaling: Multilayered mediators, signaling mechanisms and major signaling crosstalk. *Genes Dis* **11**, 103-134 (2024). https://doi.org/10.1016/j.gendis.2023.01.030

106 Kumawat, K. & Gosens, R. WNT-5A: signaling and functions in health and disease. *Cell Mol Life Sci* **73**, 567-587 (2016). https://doi.org/10.1007/s00018-015-2076-y

107 Mezzacappa, C., Komiya, Y. & Habas, R. Activation and function of small GTPases Rho, Rac, and Cdc42 during gastrulation. *Methods Mol Biol* **839**, 119-131 (2012). https://doi.org/10.1007/978-1-61779-510-7_10

108 Ha, B. H. & Boggon, T. J. CDC42 binds PAK4 via an extended GTPase-effector interface. *Proc Natl Acad Sci U S A* **115**, 531-536 (2018). https://doi.org/10.1073/pnas.1717437115

109 Murphy, N. P., Binti Ahmad Mokhtar, A. M., Mott, H. R. & Owen, D. Molecular subversion of Cdc42 signalling in cancer. *Biochem Soc Trans* **49**, 1425-1442 (2021). https://doi.org/10.1042/bst20200557

110 Murphy, N. P., Mott, H. R. & Owen, D. Progress in the therapeutic inhibition of Cdc42 signalling. *Biochem Soc Trans* **49**, 1443-1456 (2021). https://doi.org/10.1042/bst20210112

111 Arias-Romero, L. E. & Chernoff, J. Targeting Cdc42 in cancer. *Expert Opin Ther Targets* **17**, 1263-1273 (2013). https://doi.org/10.1517/14728222.2013.828037

112 Watson, J. R., Owen, D. & Mott, H. R. Cdc42 in actin dynamics: An ordered pathway governed by complex equilibria and directional effector handover. *Small GTPases* **8**, 237-244 (2017). https://doi.org/10.1080/21541248.2016.1215657

113 Fu, J. *et al.* The role of cell division control protein 42 in tumor and non-tumor diseases: A systematic review. *J Cancer* **13**, 800-814 (2022). https://doi.org/10.7150/jca.65415

114 Magalhaes, Y. T., Farias, J. O., Silva, L. E. & Forti, F. L. GTPases, genome, actin: A hidden story in DNA damage response and repair mechanisms. *DNA Repair (Amst)* **100**, 103070 (2021). https://doi.org/10.1016/j.dnarep.2021.103070

115 Harris, K. P. & Tepass, U. Cdc42 and vesicle trafficking in polarized cells. *Traffic* **11**, 1272-1279 (2010). https://doi.org/10.1111/j.1600-0854.2010.01102.x

116 Florian, M. C. *et al.* Aging alters the epigenetic asymmetry of HSC division. *PLoS Biol* **16**, e2003389 (2018). https://doi.org/10.1371/journal.pbio.2003389

117 Wang, J. *et al.* The role of autophagy in bone metabolism and clinical significance. *Autophagy* **19**, 2409-2427 (2023). https://doi.org/10.1080/15548627.2023.2186112

118 Kast, D. J. & Dominguez, R. The Cytoskeleton-Autophagy Connection. *Curr Biol* **27**, R318-r326 (2017). https://doi.org/10.1016/j.cub.2017.02.061

119 Moore, A. S., Wong, Y. C., Simpson, C. L. & Holzbaur, E. L. Dynamic actin cycling through mitochondrial subpopulations locally regulates the fission-fusion balance within mitochondrial networks. *Nat Commun* **7**, 12886 (2016). https://doi.org/10.1038/ncomms12886

120 Landspersky, T. *et al.* Targeting CDC42 reduces skeletal degeneration after hematopoietic stem cell transplantation. *Blood Adv* (2024). https://doi.org/10.1182/bloodadvances.2024012879

121 Wang, X. *et al.* PINK1 and Parkin target Miro for phosphorylation and degradation to arrest mitochondrial motility. *Cell* **147**, 893-906 (2011). https://doi.org/10.1016/j.cell.2011.10.018

122 Safiulina, D. *et al.* Miro proteins prime mitochondria for Parkin translocation and mitophagy. *Embo j* **38** (2019). https://doi.org/10.15252/embj.201899384

123 Connelly, E. M., Frankel, K. S. & Shaw, G. S. Parkin and mitochondrial signalling. *Cell Signal* **106**, 110631 (2023). https://doi.org/10.1016/j.cellsig.2023.110631

124 Grossmann, D., Berenguer-Escuder, C., Chemla, A., Arena, G. & Krüger, R. The Emerging Role of RHOT1/Miro1 in the Pathogenesis of Parkinson's Disease. *Front Neurol* **11**, 587 (2020). https://doi.org/10.3389/fneur.2020.00587

125 Kruppa, A. J. *et al.* Myosin VI-Dependent Actin Cages Encapsulate Parkin-Positive Damaged Mitochondria. *Dev Cell* **44**, 484-499.e486 (2018). https://doi.org/10.1016/j.devcel.2018.01.007

126 Kruppa, A. J. & Buss, F. Actin cages isolate damaged mitochondria during mitophagy. *Autophagy* **14**, 1644-1645 (2018). https://doi.org/10.1080/15548627.2018.1486152

127 Joshi, A. & Kundu, M. Mitophagy in hematopoietic stem cells: the case for exploration. *Autophagy* **9**, 1737-1749 (2013). https://doi.org/10.4161/auto.26681

128 Stergiou, I. E. & Kapsogeorgou, E. K. Autophagy and Metabolism in Normal and Malignant Hematopoiesis. *Int J Mol Sci* **22** (2021). https://doi.org/10.3390/ijms22168540

129 Palmiter, R. D. Physiology: Bone-derived hormone suppresses appetite. *Nature* **543**, 320-322 (2017). https://doi.org/10.1038/nature21501

130 Yin, X. *et al.* Autophagy in bone homeostasis and the onset of osteoporosis. *Bone Res* **7**, 28 (2019). https://doi.org/10.1038/s41413-019-0058-7

131 Gatica, D., Lahiri, V. & Klionsky, D. J. Cargo recognition and degradation by selective autophagy. *Nat Cell Biol* **20**, 233-242 (2018). https://doi.org/10.1038/s41556-018-0037-z

132 Liu, Z. *et al.* Ubiquitylation of autophagy receptor Optineurin by HACE1 activates selective autophagy for tumor suppression. *Cancer Cell* **26**, 106-120 (2014). https://doi.org/10.1016/j.ccr.2014.05.015

133 Liu, Z. Z. *et al.* Autophagy receptor OPTN (optineurin) regulates mesenchymal stem cell fate and bone-fat balance during aging by clearing FABP3. *Autophagy* **17**, 2766-2782 (2021). https://doi.org/10.1080/15548627.2020.1839286

134 Karaguzel, G. & Holick, M. F. Diagnosis and treatment of osteopenia. *Rev Endocr Metab Disord* **11**, 237-251 (2010). https://doi.org/10.1007/s11154-010-9154-0

135 Chen, L. R., Ko, N. Y. & Chen, K. H. Medical Treatment for Osteoporosis: From Molecular to Clinical Opinions. *Int J Mol Sci* **20** (2019). https://doi.org/10.3390/ijms20092213

136 Dennison, E. & Cooper, C. Epidemiology of osteoporotic fractures. *Horm Res* **54 Suppl 1**, 58-63 (2000). https://doi.org/10.1159/000063449

137 Rizzoli, R., Bonjour, J. P. & Ferrari, S. L. Osteoporosis, genetics and hormones. *J Mol Endocrinol* **26**, 79-94 (2001). https://doi.org/10.1677/jme.0.0260079

138 Inamoto, Y. & Lee, S. J. Late effects of blood and marrow transplantation. *Haematologica* **102**, 614-625 (2017). https://doi.org/10.3324/haematol.2016.150250

139 Schimmer, A. D. *et al.* Decreased bone mineral density is common after autologous blood or marrow transplantation. *Bone Marrow Transplant* **28**, 387-391 (2001). https://doi.org/10.1038/sj.bmt.1703149

140 Savani, B. N. *et al.* Increased risk of bone loss without fracture risk in long-term survivors after allogeneic stem cell transplantation. *Biol Blood Marrow Transplant* **13**, 517-520 (2007). https://doi.org/10.1016/j.bbmt.2007.01.085

141 Lane, N. E. Epidemiology, etiology, and diagnosis of osteoporosis. *Am J Obstet Gynecol* **194**, S3-11 (2006). https://doi.org/10.1016/j.ajog.2005.08.047

142 Qadir, M. I., Parveen, A. & Ali, M. Cdc42: Role in Cancer Management. *Chem Biol Drug Des* **86**, 432-439 (2015). https://doi.org/10.1111/cbdd.12556

143 Prudnikova, T. Y., Rawat, S. J. & Chernoff, J. Molecular pathways: targeting the kinase effectors of RHO-family GTPases. *Clin Cancer Res* **21**, 24-29 (2015). https://doi.org/10.1158/1078-0432.Ccr-14-0827

144 Peterson, J. R., Lebensohn, A. M., Pelish, H. E. & Kirschner, M. W. Biochemical suppression of small-molecule inhibitors: a strategy to identify inhibitor targets and signaling pathway components. *Chem Biol* **13**, 443-452 (2006). https://doi.org/10.1016/j.chembiol.2006.02.009

145 Duan, X. *et al.* Pharmacologic targeting of Cdc42 GTPase by a small molecule Cdc42 activity-specific inhibitor prevents platelet activation and thrombosis. *Sci Rep* **11**, 13170 (2021). https://doi.org/10.1038/s41598-021-92654-6

146 Florian, M. C. *et al.* Cdc42 activity regulates hematopoietic stem cell aging and rejuvenation. *Cell Stem Cell* **10**, 520-530 (2012). https://doi.org/10.1016/j.stem.2012.04.007

147 Amoah, A. *et al.* Aging of human hematopoietic stem cells is linked to changes in Cdc42 activity. *Haematologica* **107**, 393-402 (2022). https://doi.org/10.3324/haematol.2020.269670

148 Su, H. C. & Orange, J. S. The Growing Spectrum of Human Diseases Caused by Inherited CDC42 Mutations. *J Clin Immunol* **40**, 551-553 (2020). https://doi.org/10.1007/s10875-020-00785-8

149 Guidi, N. *et al.* An aged bone marrow niche restrains rejuvenated hematopoietic stem cells. *Stem Cells* **39**, 1101-1106 (2021). https://doi.org/10.1002/stem.3372

150 Hong, L. *et al.* Characterization of a Cdc42 protein inhibitor and its use as a molecular probe. *J Biol Chem* **288**, 8531-8543 (2013). https://doi.org/10.1074/jbc.M112.435941

151 Chen, C. *et al.* Cdc42 inhibitor ML141 enhances G-CSF-induced hematopoietic stem and progenitor cell mobilization. *Int J Hematol* **101**, 5-12 (2015). https://doi.org/10.1007/s12185-014-1690-z

152 Amirthalingam, M., Palanisamy, S. & Tawata, S. p21-Activated kinase 1 (PAK1) in aging and longevity: An overview. *Ageing Res Rev* **71**, 101443 (2021). https://doi.org/10.1016/j.arr.2021.101443

153 Chaker, D. *et al.* Inhibition of the RhoGTPase Cdc42 by ML141 enhances hepatocyte differentiation from human adipose-derived mesenchymal stem cells via the Wnt5a/PI3K/miR-122 pathway: impact of the age of the donor. *Stem Cell Res Ther* **9**, 167 (2018). https://doi.org/10.1186/s13287-018-0910-5

154 Arias-Romero, L. E. & Chernoff, J. A tale of two Paks. *Biol Cell* **100**, 97-108 (2008). https://doi.org/10.1042/bc20070109

155 Yuan, Y. *et al.* PAK4 in cancer development: Emerging player and therapeutic opportunities. *Cancer Lett* **545**, 215813 (2022). https://doi.org/10.1016/j.canlet.2022.215813

156 Li, Y., Lu, Q., Xie, C., Yu, Y. & Zhang, A. Recent advances on development of p21-activated kinase 4 inhibitors as anti-tumor agents. *Front Pharmacol* **13**, 956220 (2022). https://doi.org/10.3389/fphar.2022.956220

157 Murray, B. W. *et al.* Small-molecule p21-activated kinase inhibitor PF-3758309 is a potent inhibitor of oncogenic signaling and tumor growth. *Proc Natl Acad Sci U S A* **107**, 9446-9451 (2010). https://doi.org/10.1073/pnas.0911863107

158 Rodda, S. J. & McMahon, A. P. Distinct roles for Hedgehog and canonical Wnt signaling in specification, differentiation and maintenance of osteoblast progenitors. *Development* **133**, 3231-3244 (2006). https://doi.org/10.1242/dev.02480

159 Mizoguchi, T. *et al.* Osterix marks distinct waves of primitive and definitive stromal progenitors during bone marrow development. *Dev Cell* **29**, 340-349 (2014). https://doi.org/10.1016/j.devcel.2014.03.013

160 Florian, M. C. *et al.* A canonical to non-canonical Wnt signalling switch in haematopoietic stem-cell ageing. *Nature* **503**, 392-396 (2013). https://doi.org/10.1038/nature12631

161 Murdoch, B. *et al.* Wnt-5A augments repopulating capacity and primitive hematopoietic development of human blood stem cells in vivo. *Proc Natl Acad Sci U S A* **100**, 3422-3427 (2003). https://doi.org/10.1073/pnas.0130233100

162 Buckley, S. M. *et al.* Maintenance of HSC by Wnt5a secreting AGM-derived stromal cell line. *Exp Hematol* **39**, 114-123.e111-115 (2011). https://doi.org/10.1016/j.exphem.2010.09.010

163 Mortensen, M. *et al.* The autophagy protein Atg7 is essential for hematopoietic stem cell maintenance. *J Exp Med* **208**, 455-467 (2011). https://doi.org/10.1084/jem.20101145

164 Kaur, R., Bhardwaj, A. & Gupta, S. Cancer treatment therapies: traditional to modern approaches to combat cancers. *Mol Biol Rep* **50**, 9663-9676 (2023). https://doi.org/10.1007/s11033-023-08809-3

165 Schreck, C., Bock, F., Grziwok, S., Oostendorp, R. A. & Istvanffy, R. Regulation of hematopoiesis by activators and inhibitors of Wnt signaling from the niche. *Ann N Y Acad Sci* **1310**, 32-43 (2014). https://doi.org/10.1111/nyas.12384

166 Sahin, U., Toprak, S. K., Atilla, P. A., Atilla, E. & Demirer, T. An overview of infectious complications after allogeneic hematopoietic stem cell transplantation. *J Infect Chemother* **22**, 505-514 (2016). https://doi.org/10.1016/j.jiac.2016.05.006

167 Yang, Y. M. *et al.* Prevalence of osteoporosis among patients after stem cell transplantation: a systematic review and meta-analysis. *Bone Marrow Transplant* **59**, 785-794 (2024). https://doi.org/10.1038/s41409-024-02243-0

168 Chen, L., Wu, X. Y., Jin, Q., Chen, G. Y. & Ma, X. The correlation between osteoporotic vertebrae fracture risk and bone mineral density measured by quantitative computed tomography and dual energy X-ray absorptiometry: a systematic review and meta-analysis. *Eur Spine J* **32**, 3875-3884 (2023). https://doi.org/10.1007/s00586-023-07917-9

169 Marino, R. *et al.* Delayed marrow infusion in mice enhances hematopoietic and osteopoietic engraftment by facilitating transient expansion of the osteoblastic niche. *Biol Blood Marrow Transplant* **19**, 1566-1573 (2013). https://doi.org/10.1016/j.bbmt.2013.07.025

170 Williams, G. R., Manjunath, S. H., Butala, A. A. & Jones, J. A. Palliative Radiotherapy for Advanced Cancers: Indications and Outcomes. *Surg Oncol Clin N Am* **30**, 563-580 (2021). https://doi.org/10.1016/j.soc.2021.02.007

171 Fernald, K. & Kurokawa, M. Evading apoptosis in cancer. *Trends Cell Biol* **23**, 620-633 (2013). https://doi.org/10.1016/j.tcb.2013.07.006

172 Kalkan, B. M. *et al.* CASIN and AMD3100 enhance endothelial cell proliferation, tube formation and sprouting. *Microvasc Res* **130**, 104001 (2020). https://doi.org/10.1016/j.mvr.2020.104001

173 Liu, W. *et al.* Rational identification of a Cdc42 inhibitor presents a new regimen for long-term hematopoietic stem cell mobilization. *Leukemia* **33**, 749-761 (2019). https://doi.org/10.1038/s41375-018-0251-5

174 Zhang, Y. & Niu, C. Relation of CDC42, Th1, Th2, and Th17 cells with cognitive function decline in Alzheimer's disease. *Ann Clin Transl Neurol* **9**, 1428-1436 (2022). https://doi.org/10.1002/acn3.51643

175 Ying, L. *et al.* Regulation of Cdc42 signaling by the dopamine D2 receptor in a mouse model of Parkinson's disease. *Aging Cell* **21**, e13588 (2022). https://doi.org/10.1111/acel.13588

176 Li, Y., Yang, W. & Wang, F. The relationship of blood CDC42 level with Th1 cells, Th17 cells, inflammation markers, disease risk/activity, and treatment efficacy of rheumatoid arthritis. *Ir J Med Sci* **191**, 2155-2161 (2022). https://doi.org/10.1007/s11845-021-02858-y

177 Yang, Y., Wu, B., Tian, P. & Huang, L. Serum CDC42 is increased during tumor necrosis factor inhibitor treatment, and its elevation correlates with satisfactory treatment response in rheumatoid arthritis patients. *Int J Rheum Dis* **26**, 1521-1528 (2023). https://doi.org/10.1111/1756-185x.14778

178 Pala, E. & Denkçeken, T. Differentially expressed circulating miRNAs in postmenopausal osteoporosis: a meta-analysis. *Biosci Rep* **39** (2019). https://doi.org/10.1042/bsr20190667

179 Mukherjee, S. *et al.* Pharmacologic targeting of a stem/progenitor population in vivo is associated with enhanced bone regeneration in mice. *J Clin Invest* **118**, 491-504 (2008). https://doi.org/10.1172/jci33102

180 Chandra, A. *et al.* Proteasome inhibitor bortezomib is a novel therapeutic agent for focal radiation-induced osteoporosis. *Faseb j* **32**, 52-62 (2018). https://doi.org/10.1096/fj.201700375R

181 D'Souza, A. B., Grigg, A. P., Szer, J. & Ebeling, P. R. Zoledronic acid prevents bone loss after allogeneic haemopoietic stem cell transplantation. *Intern Med J* **36**, 600-603 (2006). https://doi.org/10.1111/j.1445-5994.2006.01154.x

182 Hari, P., DeFor, T. E., Vesole, D. H., Bredeson, C. N. & Burns, L. J. Intermittent zoledronic Acid prevents bone loss in adults after allogeneic hematopoietic cell transplantation. *Biol Blood Marrow Transplant* **19**, 1361-1367 (2013). https://doi.org/10.1016/j.bbmt.2013.06.015

183 Drake, M. T., Clarke, B. L. & Khosla, S. Bisphosphonates: mechanism of action and role in clinical practice. *Mayo Clin Proc* **83**, 1032-1045 (2008). https://doi.org/10.4065/83.9.1032

184 Dunford, J. E., Rogers, M. J., Ebetino, F. H., Phipps, R. J. & Coxon, F. P. Inhibition of protein prenylation by bisphosphonates causes sustained activation of Rac, Cdc42, and Rho GTPases. *J Bone Miner Res* **21**, 684-694 (2006). https://doi.org/10.1359/jbmr.060118

ACKNOWLEDGEMENTS

Zunächst möchte ich meinen tiefen Dank an Professor Dr. Robert Oostendorp aussprechen. Robert, danke für die Jahre voller Wissen und Unterstützung, für deine Menschlichkeit und für das Vertrauen in unsere Zusammenarbeit.

Ein ebenso herzlicher Dank gilt meiner Betreuerin und guten Freundin Dr. Christina Schreck, die einfach nur wunderbar ist. Christina, du hast mich so sehr inspiriert und bist mir in vielerlei Hinsicht ein großes Vorbild. Ich bin dir sehr dankbar für alles, und unsere Zusammenarbeit wird mir immer in bester Erinnerung bleiben.

Auch Prof. Dr. Ralph Kühn möchte ich besonders danken. Er hat mir beigebracht, wissenschaftlich zu denken und dass man „erst aussteigen kann, wenn man eingestiegen ist“.

In all den (vielen) Jahren, die ich in der Trogerstraße 32 verbracht habe, sind mir viele KollegInnen sehr ans Herz gewachsen, die nun zum Teil zu meinen engsten Freundinnen gehören. Danke an euch alle für die tolle Zeit! Michèle Buck, Judith Hecker, Marie Weickert, Emely Schönhals, Rouzanna Istvánffy, Franziska Hettler, Sandra Romero Marquez, Anna Scherger, Jennifer Rivière, Mark van der Garde, Anna Navarro, Gerrit Siegers, Markus Schick, Stefan Habringer, the T, the Panther.

Besonderer Dank gilt auch meinen Eltern und Schwiegereltern, allen voran aber meiner Mama, die mich mein ganzes Leben lang auf eine unglaubliche und selbstlose Art und Weise unterstützt hat, die ich ihr nie vergessen werde, sowie meinen Brüdern und FreundInnen, die nicht wissen, was ich eigentlich mache, es aber trotzdem irgendwie cool finden.

Und nicht zuletzt meinen beiden Kindern Romy und Kurt, die meine größte Schwäche und zugleich meine größte Stärke sind. Wie viel Zeit und Nerven habt ihr mir geraubt, die ich gerne in meine Arbeit investiert hätte, und wie sehr habt ihr mich gleichzeitig gelehrt, was im Leben wirklich wichtig ist.

Ein ganz besonderer Dank gilt schließlich meinem Mann Christian, der mich ausdauernd ermutigt hat, diese Arbeit anzufangen und nun auch endlich abzuschließen. Wie recht du doch hattest, mein Liebster – es ist ein wunderschönes Gefühl, nun diese letzten Zeilen zu schreiben…

APPENDICES

Appendix 1:

“Autophagy in mesenchymal progenitors protects mice against BM failure after severe intermittent stress”, Landspersky et al., 2021, Blood.

Appendix 2:

“Targeting CDC42 reduces skeletal degeneration after hematopoietic stem cell transplantation”, Landspersky et al., Blood advances 2024

blood®
Regular Article

HEMATOPOIESIS AND STEM CELLS

Autophagy in mesenchymal progenitors protects mice against bone marrow failure after severe intermittent stress

Theresa Landspersky,[1] Mehmet Saçma,[2] Jennifer Rivière,[1] Judith S. Hecker,[1] Franziska Hettler,[1] Erik Hameister,[3] Katharina Brandstetter,[4] Rouzanna Istvánffy,[1] Sandra Romero Marquez,[1] Romina Ludwig,[1] Marilena Götz,[1] Michèle Buck,[1] Martin Wolf,[5] Matthias Schiemann,[6] Jürgen Ruland,[3] Dirk Strunk,[5] Akiko Shimamura,[7] Kasiani Myers,[8] Terry P. Yamaguchi,[9] Matthias Kieslinger,[10] Heinrich Leonhardt,[4] Florian Bassermann,[1,11] Katharina S. Götze,[1,11] Hartmut Geiger,[2] Christina Schreck,[1,*] and Robert A. J. Oostendorp[1,*]

[1]Technical University of Munich (TUM), School of Medicine, Department of Internal Medicine III, Munich, Germany; [2]Institute of Molecular Medicine, Ulm University, Ulm, Germany; [3]TUM, School of Medicine, Clinical Chemistry and Pathobiochemistry, Munich, Germany; [4]Human Biology and BioImaging, Faculty of Biology, Ludwig-Maximilians-Universität München, Munich, Germany; [5]Institute of Experimental and Clinical Cell Therapy, Paracelsus University Salzburg, Salzburg, Austria; [6]TUM, Institute for Medical Microbiology, Immunology and Hygiene, CyTUM-MIH, Munich, Germany; [7]Bone Marrow Failure and MDS Program, Dana Farber and Boston Children's Hospital, Boston, MA; [8]Division of Bone Marrow Transplantation and Immune Deficiency, Cincinnati Children's Hospital Medical Center, Cincinnati, OH; [9]Cancer and Developmental Biology Laboratory, Center for Cancer Research, National Cancer Institute-Frederick, National Institutes of Health, Frederick, MD; [10]Department for Small Animals and Horses, University of Veterinary Medicine, Vienna, Austria; and [11]German Cancer Consortium (DKTK), Heidelberg, Germany

KEY POINTS

- **Defective autophagy in mesenchymal progenitors associates with BM hypocellularity and mortality after severe stress.**
- **A short 4-day pharmacological in vivo treatment of mice to attenuate CDC42 activation protects against cytopenia and improves survival.**

The cellular mechanisms required to ensure homeostasis of the hematopoietic niche and the ability of this niche to support hematopoiesis upon stress remain elusive. We here identify *Wnt5a* in Osterix$^+$ mesenchymal progenitor and stem cells (MSPCs) as a critical factor for niche-dependent hematopoiesis. Mice lacking *Wnt5a* in MSPCs suffer from stress-related bone marrow (BM) failure and increased mortality. Niche cells devoid of *Wnt5a* show defective actin stress fiber orientation due to an elevated activity of the small GTPase CDC42. This results in incorrect positioning of autophagosomes and lysosomes, thus reducing autophagy and increasing oxidative stress. In MSPCs from patients from BM failure states which share features of peripheral cytopenia and hypocellular BM, we find similar defects in actin stress fiber orientation, reduced and incorrect colocalization of autophagosomes and lysosomes, and CDC42 activation. Strikingly, a short pharmacological intervention to attenuate elevated CDC42 activation in vivo in mice prevents defective actin-anchored autophagy in MSPCs, salvages hematopoiesis and protects against lethal cytopenia upon stress. In summary, our study identifies *Wnt5a* as a restriction factor for niche homeostasis by affecting CDC42-regulated actin stress-fiber orientation and autophagy upon stress. Our data further imply a critical role for autophagy in MSPCs for adequate support of hematopoiesis by the niche upon stress and in human diseases characterized by peripheral cytopenias and hypocellular BM.

Introduction

Declining niche homeostasis is an underlying defect contributing to aging and the development of aging-related malignant hematopoietic diseases.[1] Functional changes in bone marrow (BM)-derived mesenchymal stem and progenitor cells (MSPCs) include deregulated osteogenic and adipogenic differentiation, bone loss, and osteoporosis.[1-3] Intriguingly, compromised niche health in aging and malignant disease is associated with ineffective hematopoiesis and dysfunctional hematopoietic stem cells (HSCs), resulting in cytopenias and progressive BM hypocellularity. Thus, it is important to understand the mechanisms governing cellular health of niche cells.

Efforts studying HSC dysfunction have shown that interconnected cellular maintenance mechanisms, such as mitochondrial quality control,[4] macroautophagy (autophagy),[5] and lysosomal lysis[6,7] are critical for safeguarding HSC division and function. Interestingly, dysfunctional HSCs further show altered noncanonical WNT5A-CDC42 signaling with a loss of polarized cytoskeletal components,[8-10] associated with activation of the small GTPase CDC42 in both stem cells[8,9] and mature cells.[10] Since the cytoskeleton guides autophagosome formation and lysosomal fusion,[11] as well as mitochondrial fission,[12] correct assembly and orientation of the cytoskeleton is pivotal for cellular maintenance.

In the present study, we wondered whether and how the hematopoiesis-supportive function of the niche depends on CDC42 activation and autophagy under intermittent stress conditions. For this purpose, we studied hematopoiesis and niche cells in mice lacking *Wnt5a* expression, specifically in MSPCs. In addition, we studied whether similar molecular events operate in MSPCs from human conditions characterized by hypocellular BM and ineffective hematopoiesis. Such features are shared by different hematologic diseases, such as Shwachman-Diamond syndrome (SDS), hypocellular myelodysplastic syndrome (hypocellular MDS), and severe aplastic anemia as well as therapeutically conditioned leukemia/lymphoma patients undergoing allogeneic hematopoietic stem cell transplantation (HSCT).

We show that BM MSPCs from murine *Wnt5a*-deficient animals poorly support hematopoiesis associated with CDC42 activation and defective autophagy. Furthermore, MSPCs from the human diseases studied show similar CDC42 activation with reduced WNT5A expression and ineffective autophagy. More importantly, we show that pharmacological attenuation of RhoGDI/CDC42 activation not only restores stromal F-actin organization orientation and autophagy in mice but also protects from accelerated cytopenia and mortality after repeated cytotoxic stress.

Methods

Mice

Wnt5a$^{fl/fl}$ mice[13] were crossed with Osx-GFP::Cre mice[14] (Osx-Cre; The Jackson Laboratory, Bar Harbor, ME). Osx-Cre mice express the CRE recombinase under the control of the Osterix (Sp7) promotor. Although *Sp7* is expressed in only a small subpopulation of osteoprogenitors, the numerous progenies of these cells include all major mesenchymal populations.[15] Litters of Osx-Cre;Wnt5a$^{fl/+}$ mice were crossed with Wnt5a$^{fl/fl}$ (5A$^{fl/fl}$) mice so that litters yielded controls (5A$^{fl/fl}$ and Osx-Cre [O5A$^{+/+}$]) as well as Wnt5a deleted mutants (O5A$^{\Delta/\Delta}$). In all experiments, the results from 5A$^{fl/fl}$ and O5A$^{+/+}$ mice were combined as controls since both express a functional *Wnt5a* gene. Details about mouse models are summarized in supplemental Table 1, available on the *Blood* Web site.

All animal experiments were approved by the Government of Upper Bavaria and performed in accordance with ethical guidelines and approved protocols (Vet_02-14-112, and -17-124). All animals were housed under specific pathogen-free conditions, according to the Federation of Laboratory Animal Science Associations and institutional recommendations. Mice used were 8 to 10 weeks old.

Human BM samples

Human BM samples were collected from 15 healthy individuals and 6 hip replacement patients after written informed consent. In the healthy samples aged over 60 years, the presence of clonal hematopoiesis was excluded by targeted sequencing of 68 genes recurrently mutated in hematologic malignancies.[16] Furthermore, BM samples were obtained from patients with different BM failure states, such as SDS, an inherited BM failure syndrome, hypocellular MDS, or severe aplastic anemia. We also included 3 samples from leukemia/lymphoma patients undergoing allogeneic HSCT, 2 of which had received total body irradiation as part of their conditioning regimen, which may contribute to niche damage, and the third patient showed incomplete BM reconstitution after transplant (likely due to extensive pretreatment) (supplemental Table 2). The studies TUM 538/16 (Klinikum rechts der Isar, Technical University Munich, Munich, Germany) and P00020466 (Boston Children's Hospital, Boston, MA) were approved by the respective institutional review boards in accordance with the Declaration of Helsinki. Characteristics of healthy individuals and patients used in this study are detailed in supplemental Table 2.

Flow cytometry analysis and cell sorting

Hematopoietic lineage$^-$ SCA1$^+$ KIT$^+$ (LSK) cells and their HSC-enriched CD34$^-$ CD48$^-$ CD150$^+$ subpopulations (LT-HSCs) were isolated and labeled as reported.[10,17] Stromal subpopulations were sorted or analyzed as nonhematopoietic (CD45$^-$ TER119$^-$) cells as described.[10,18] All antibodies used in this study are listed in supplemental Table 3, machines in supplemental Table 4, and sorting schemes are shown in supplemental Figure 1.

Peripheral blood (PB) was analyzed by Animal Blood Cell Counter (Scil Vet Abc).

In vivo transplantation assay

Competitive repopulation was performed using transplantation (Tx) of LT-HSCs into lethally irradiated 129Ly5.1 Wild-type (WT)-recipient mice, as described previously.[10] Peripheral engraftment of donor cells was analyzed at regular intervals (4, 8, 12, and 16 weeks posttransplant). Sixteen weeks after transplantation, recipient mice were sacrificed, and the hematopoietic organs were analyzed by flow cytometry.

In vivo treatment with pharmacological compounds

For induction of cytotoxic stress, 5-fluorouracil (5-FU) was administered intraperitoneal (IP, 150 mg/kg, Ribosepharm) on day 0 in a single dose or in 2 doses at days 0 and 8, after which mice were analyzed and MSPCs cultured. Animals were monitored twice daily. Surviving O5A$^{\Delta/\Delta}$ animals were sacrificed at or prior to day 14 due to severe stress.

In some in vivo experiments, the CDC42/RhoGDI inhibitor CASIN (2.4 mg/kg, TOCRIS)[19] was administered by IP every 24 hours for 4 consecutive days (days 5, 6, 7, and 8) post first 5-FU treatment on day 0.

Whole-mount immunofluorescence staining

This procedure was performed as described previously.[20] Antibodies are listed in supplemental Table 3. For evaluation, fluorescently labeled bone tissues were placed onto a μ-slide 4 well and covered in antifade or phosphate-buffered saline (PBS) to prevent tissue desiccation. The preparations were examined using a Leica TCS SP8 confocal microscope and analyzed with the image analysis software Volocity (v6.2; Perkin Elmer) and ImageJ. In addition, bone matrix and adipocytes were detected using the TLD mode of the microscope. In analyses, the term arteriole includes both arterial and arteriolar cells.

Stromal cell (MSPC) isolation and culture

Flushed long bones from mice were crushed and digested as described.[21] Sorted MSPCs or MSPCs from digested compact bone were cultured on 0.1% gelatin-coated plates in MEM α

(with ribosides and Glutamax, Invitrogen), supplemented with fetal calf serum (FCS, 10%; PAA), antibiotics and 0.1% β-mercapto-ethanol (Invitrogen).

Human MSPCs were isolated from BM samples of healthy and diseased individuals and cultured using pooled platelet lysate as described previously.[3]

Cocultures of HSC and stromal cells

MSPCs were grown to confluence and irradiated (15 Gy). Freshly sorted WT LT-HSCs were seeded to the stroma in long-term culture (LTC) medium (M5300; Stemcell Technologies, Vancouver, Canada) with 1 μM hydrocortisone and incubated (37°C, 5% CO2, >95% humidity). After 6 days, cultures were either reseeded at 60 input LT-HSCs equivalents in MethoCult M3434 (Stemcell Technologies) or analyzed by flow cytometry. Hematopoietic colonies were counted using standard criteria.

Immunofluorescence staining (IF, confocal IF)

Hematopoietic cells were prepared and stained as described.[10] For staining of stromal cells, either sorted cells were spotted, or cultured MSPCs were reseeded on 0.1% gelatin-coated Superfrost Plus™ slides (Thermo Fisher Scientific) and cultured overnight in MSPC medium. Cells were fixed with 4% PFA for 5 minutes and staining was performed[10] using the antibodies listed in supplemental Table 3.

Pictures were taken using a Leica DM RBE microscope with AxioVision software (Carl Zeiss) using standardized exposure and diaphragm settings for all samples. Thirty randomly captured cells per sample were imaged at a 100-fold magnification.

Confocal fluorescence microscopy and deconvolution of the fluorescent images were performed on a Leica SP8 confocal microscope as described earlier.[22] Assessment of different parameters is outlined in the supplemental Methods.

Assessment of mitochondrial function

To interrogate mitochondrial function, mitochondrial number and diameter, reactive oxygen species (ROS) production, glycolysis, and oxygen consumption were assessed. ROS was detected by culturing fresh BM cells for 20 minutes at 37°C with either CM-H2DCFDA or MitoTracker. Staining for the mitochondrial outer membrane receptor TOMM20 indicated the number of mitochondria. Analysis of fluorescence intensity was performed using ImageJ. The extracellular acidification rate (ECAR), a measure of glycolysis, and oxygen consumption rate (OCR) were determined using an XF96 Extracellular Flux Analyzer (Seahorse Bioscience) as described.[23]

Autophagic flux assessment using CytoID

To determine the autophagic flux, MSPCs were cultured at 80% semiconfluence with rapamycin (1 μM), chloroquine (10 μM), CASIN (5 μM), or the vehiculum 0.01% DMSO for 16 hours (37°C, 5% CO_2, >95% humidity). The next day, cells were treated with Cyto-ID Autophagy Detection Kit as described by the manufacturer (Enzo Life Science). Autophagic flux was determined as ΔMFI (= $MFI_{chloroquine} - MFI_{test}$) and measured using mean fluorescence intensity (MFI) on the CyAn ADP LxP8.

Statistics

The variance was similar between groups that were statistically compared. To test for differences between 2 groups, a paired Student's *t* test was used unless the data point distribution was not normally distributed. In that case, the nonparametric Mann-Whitney *U* test was used. All statistical analyses were performed with the Prism software package.

Data

For original data, please contact the corresponding authors.

Results

Lack of *Wnt5a* in MSPCs impairs HSC function upon cytotoxic myeloablation

Maintenance of HSC function depends on the expression of *Wnt5a* in the environment.[10] In mice, WNT5A protein expression is regulated by different stressors, particularly after 5-FU treatment of WT MSPCs (supplemental Figure 2A). To test whether *Wnt5a* expression in MSPCs is responsible for reduced support of HSC function, we took advantage of a mouse model in which the floxed *Wnt5a* gene[13] was selectively deleted in osteoprogenitors ($O5A^{\Delta/\Delta}$).

In $O5A^{\Delta/\Delta}$ mice, *Wnt5a* is deleted in MSPCs and osteoblastic cells (OBCs), but is still expressed by $CD31^+$ endothelial cells (ECs) (supplemental Figure 2B-C), and is even elevated in LT-HSCs (supplemental Figure 2D). Moreover, the number of ECs and MSPCs was unchanged, but a relative increase in OBCs was noted (supplemental Figure 2E). $O5A^{\Delta/\Delta}$ mice showed normal hematopoiesis in comparison with control littermates, except for a significant decrease in LT-HSCs numbers. These LT-HSCs demonstrated a normal repopulation activity (supplemental Figure 2F).

To determine how stress alters niche and HSC function in the absence of stromal *Wnt5a*, mice were treated with 5-FU (Figure 1A), which selectively recruits quiescent HSCs through the niche.[20] Prior to 5-FU treatment, CDC42 activation, F-actin expression, or CDC42-GTP polarization is unchanged in LT-HSCs (supplemental Figure 2G-H). Eight days after 5-FU treatment, the LT-HSC numbers remain similar in $O5A^{\Delta/\Delta}$ and control animals (supplemental Figure 2I-K). However, treatment with 5-FU in $O5A^{\Delta/\Delta}$ animals altered LT-HSCs to not only show an elevation of WNT5A but also decreased F-actin with increased levels of active and nonpolarized CDC42-GTP (Figure 1B; supplemental Figure 3A-C), suggestive of HSC dysfunction.[8]

In support of this observation, we found that LT-HSCs cocultured with *Wnt5a* deleted MSPCs show strongly reduced maintenance of colony-forming cells (Figure 1C). Furthermore, transplantation experiments demonstrated that LT-HSCs from 5-FU-treated $O5A^{\Delta/\Delta}$ animals show reduced engraftment of both mature and immature cell lineages compared with HSCs from control mice (Figure 1D; supplemental Figure S3D-G), confirming dysfunction of LT-HSCs from 5-FU-treated $O5A^{\Delta/\Delta}$ mice (Figure 1E; supplemental Figure 3F).

Stress-induced niche remodeling in $O5A^{\Delta/\Delta}$ mice

To determine whether poor LT-HSC function associates with remodeling of the BM in 5-FU-treated $O5A^{\Delta/\Delta}$ or control mice, we performed whole-mount BM staining 30 days after 5-FU

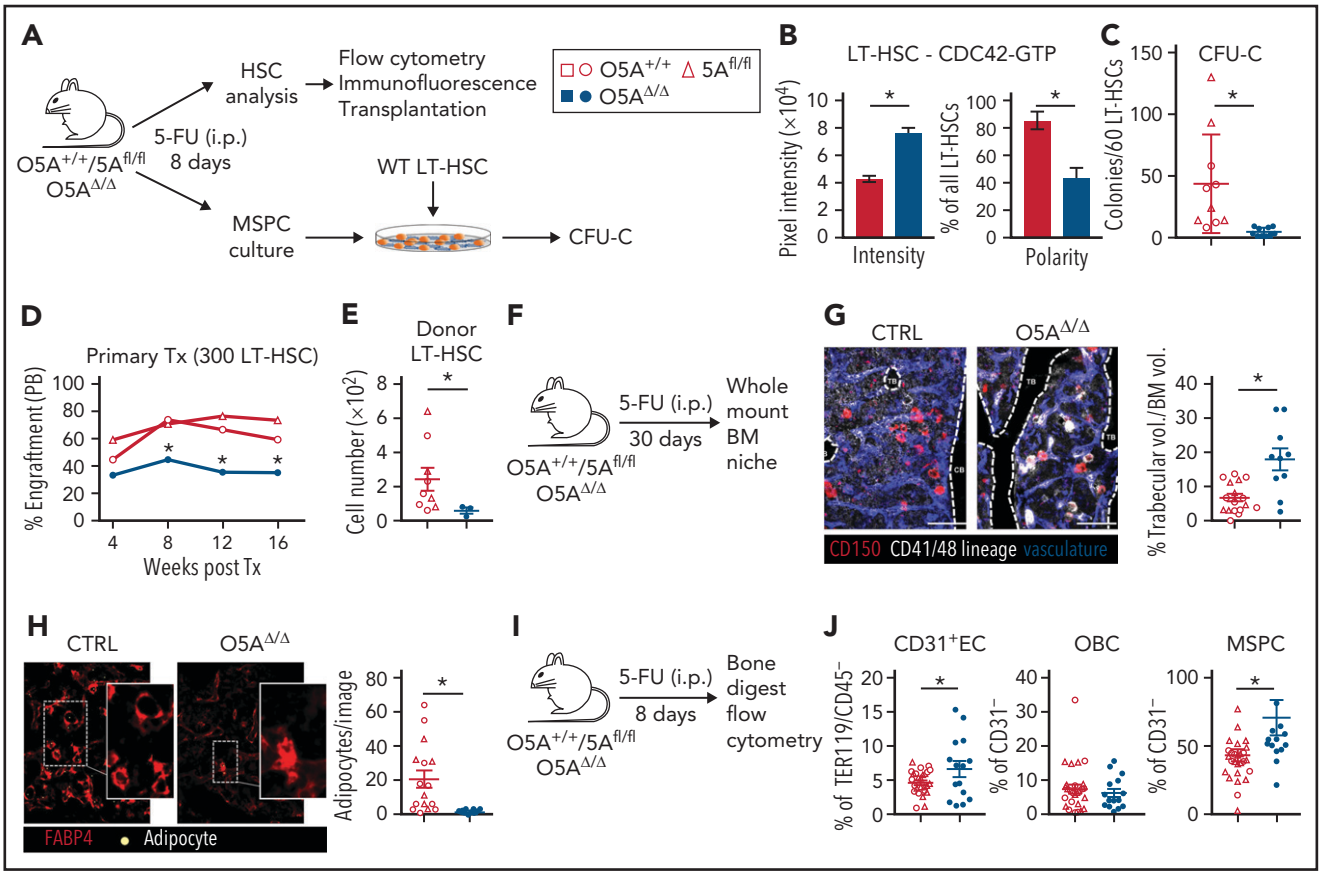

Figure 1. Stress-induced niche remodeling in O5A$^{\Delta/\Delta}$ mice. (A) Experimental design for IP injection of 5-Fluorouracil (5-FU) in coculture assay of MSPCs and LT-HSC. The following genotypes were analyzed by flow cytometry and IF 8 days after treatment: Control (CTRL): O5A$^{+/+}$, n = 5, 5A$^{fl/fl}$, n = 7 and O5A$^{\Delta/\Delta}$, n = 10. (B) Protein content and polarity of LT-HSCs stained for CDC42-GTP (n = 30), measured by ImageJ software. (C) Number of colonies from 60 LT-HSCs after coculture for 6 days on MSPCs isolated from 5-FU injected mice with the following genotype: (CTRL): O5A$^{+/+}$, n = 5, 5A$^{fl/fl}$, n = 5 and O5A$^{\Delta/\Delta}$, n = 10. (D) Primary transplantation (Tx) of 300 sorted LT-HSCs 8 days after 5-FU injection into lethally irradiated 129*Ly5.1 WT recipients. Experimental groups: CTRL: O5A$^{+/+}$, n = 5 and 5A$^{fl/fl}$, n = 4 and O5A$^{\Delta/\Delta}$, n = 7. Graph showing the donor engraftment in PB. (E) Absolute numbers of donor-type LT-HSCs in the BM, 16 weeks after Tx. For flow cytometry gating strategy, see supplemental Figure 1. (F) Experimental design for IP injection of 5-FU in 8- to 10-week-old mice of following genotypes: CTRL: O5A$^{+/+}$ n = 2, 5A$^{fl/fl}$ n = 2 and O5A$^{\Delta/\Delta}$, n = 2. BM analysis 30 days after treatment. (G) Stacked whole-mount images from epiphyseal/metaphyseal BM. FABP4^{+} vasculature is shown in blue. CD150 is shown in red, other hematopoietic markers (CD41, CD48, and lineage) are shown in gray. The dashed lines denote the endosteum. Scale bar, 100 µm; n = 10 images (n = 6 images 5A$^{fl/fl}$ PBS) from 2 mice each group. The results represent 2 independent experiments. The graph showing the % of trabecular volume per BM volume. (H) Stacked whole-mount images from epiphyseal/metaphyseal BM. FABP4^{+} adipocytes are shown in red. Adipocytes are additionally marked by a yellow circle. Extended focus projection images. Scale bar, 100 µm; n = 10 images from 2 mice each group, femora. The graph on the right shows the number of adipocytes per image. (I) Experimental design for analysis of bone-digested stromal cells, isolated from compact bones, 8 days post 5-FU treatment. (J) Relative numbers of CD31^{+} ECs, OBCs, and immature MSPCs; flow cytometry gating strategy in supplemental Figure 1. *$P < .05$ (nonparametric Mann-Whitney test: B-G,J). The results represent 2 to 3 independent experiments. Data are represented as dots per mouse or cell and the mean ± SEM. Symbol legends as shown in Figure 1A.

treatment, an endpoint for BM regeneration in WT mice[20] (Figure 1F; supplemental Figure 3H). Our analyses show similar localization of HSCs in O5A$^{\Delta/\Delta}$ and control BM to endosteal areas, megakaryocytes, or different types of vessels (supplemental Figure 3I-K). However, we found a striking BM remodeling associated with increased trabecular volume of the epiphysis/metaphysis of O5A$^{\Delta/\Delta}$ mice compared with controls (Figure 1G), a near loss of FABP4^{high} adipocytes with big fat droplets (Figure 1H), and a relative increase in both MSPCs and ECs in flow cytometry, but not in OBCs in the BM of O5A$^{\Delta/\Delta}$ mice (Figure 1I-J). Despite these changes in BM anatomy and niche cell numbers in vivo, the frequency of CFU-F and the osteo- and adipogenic potential in vitro was unchanged in both freshly isolated and cultured MSPCs from 5-FU-treated O5A$^{\Delta/\Delta}$ or control mice (supplemental Figure 4A-D).

Intermittent cytotoxic stress causes BM failure and mortality in O5A$^{\Delta/\Delta}$ mice

Repetitive 5-FU administration leads to HSC exhaustion and death by BM failure.[24] Considering impaired HSC function in 5-FU-treated O5A$^{\Delta/\Delta}$ mice (Figure 1D-E), we wondered whether an additional 5-FU treatment of O5A$^{\Delta/\Delta}$ mice would deplete HSCs (Figure 2A-B). Strikingly, whereas most control mice (13/18, 72%) survived 2 consecutive applications of 5-FU, few of the O5A$^{\Delta/\Delta}$ mice (1/11, 9%) survived this treatment until day 14 (Figure 2C). Diminished numbers of white and red blood cells (WBC and RBC) in PB and BM cells indicated a PB and BM cytopenia in surviving O5A$^{\Delta/\Delta}$ mice (Figure 2D-G; supplemental Figure 4E-F), with a strong decline in mature CD41^{+} CD42b^{+} megakaryocytes and LT-HSCs in the BM (Figure 2H; supplemental Figure 4G).

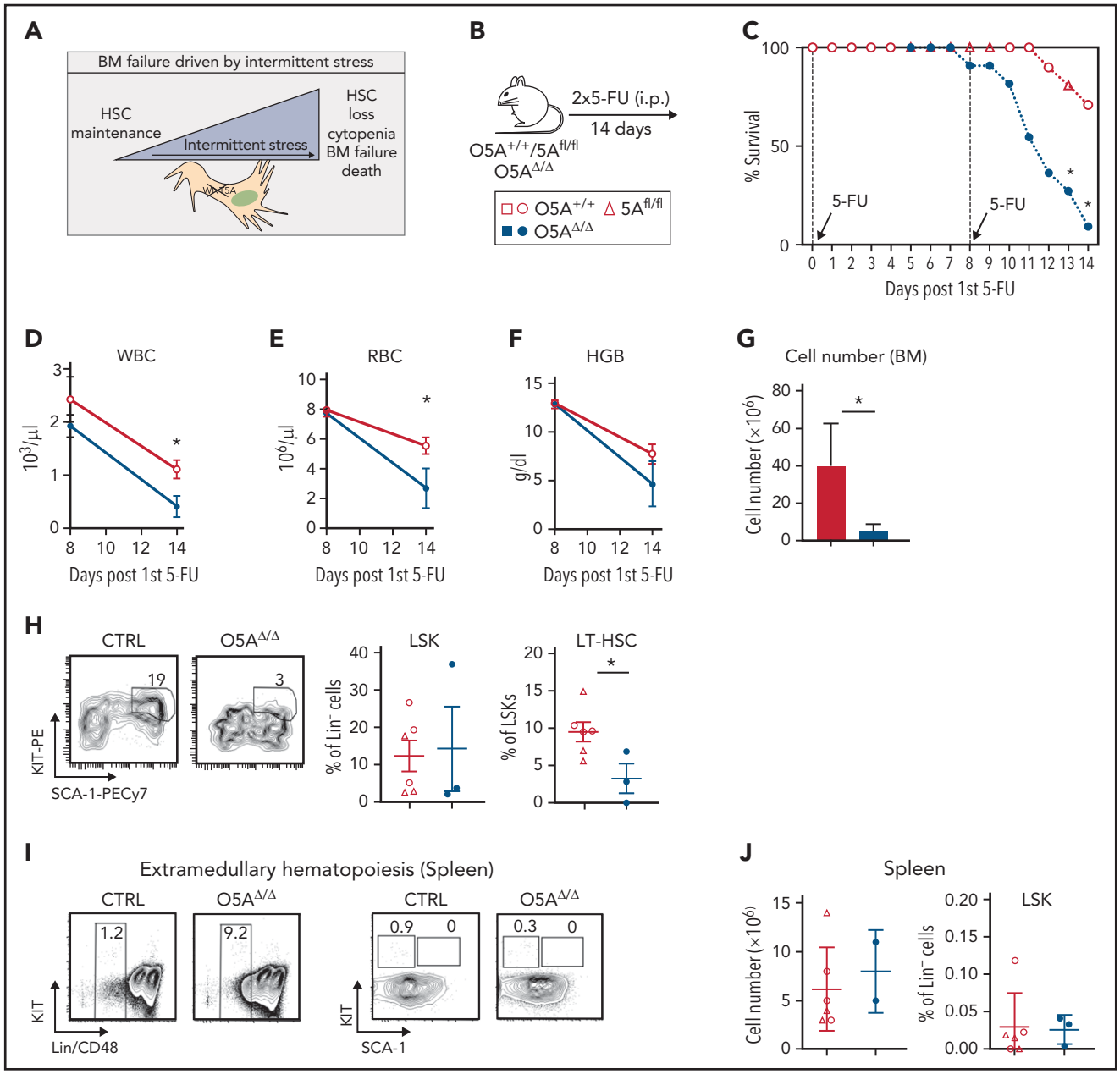

Figure 2. Peripheral and BM cytopenia in O5A$^{\Delta/\Delta}$ mice treated twice with 5-FU. (A) Graphical illustration of our hypothesis of how cytopenia is driven by declining niche homeostasis during consecutive periods of stress. (B) Experimental design for analysis of mice after 2 5-FU treatments (DAYS 0 AND 8). Control (CTRL): O5A$^{+/+}$, n = 7, 5A$^{fl/fl}$, n = 11 and O5A$^{\Delta/\Delta}$, n = 11. (C) Survival of WT (open symbols, combined results of 5A$^{fl/fl}$ and O5A$^{+/+}$ mice) and O5A$^{\Delta/\Delta}$ mice. (D-F) Graphs showing WBC, RBC, and hemoglobin (HGB) measured in PB, respectively, at DAYS 8 AND 14 from WT mice (open symbol, combined results of 5A$^{fl/fl}$ and O5A$^{+/+}$ mice) and O5A$^{\Delta/\Delta}$ mice (closed symbols). (G) Total BM cell number 14 days after the first 5-FU treatment in CTRL (n = 9) and O5A$^{\Delta/\Delta}$ (n = 5) mice. Analysis of BM from 4 flushed long bones. (H) Representative contour plots of the BM after 2 consecutive 5-FU treatments at day 14. Graphs showing the percentage of LSKs (left) and LT-HSCs (right) in CTRL and O5A$^{\Delta/\Delta}$ mice. (I) Representative contour plots of spleen cells from mice treated twice with 5-FU. (J) Graphs showing the absolute cell number of spleen cells (left) and relative number of LSK cells in spleen (right). *$P < .05$ (2-sided parametric Student's t test: [C-F]; Mann-Whitney test: [G-H]). The results represent 2 to 3 independent experiments. Data are represented as dots per mouse or cell and the mean ± SEM. Symbol legend shown in Figure 2B.

The loss of LT-HSC was, however, not caused by a relocation of LT-HSCs to other tissues, such as the spleens (Figure 2I-J).

Defects in autophagolysosome formation in MSPCs from O5A$^{\Delta/\Delta}$ mice

As it has been described that high WNT5A expression is associated with increased autophagy in melanoma[25] and pneumonia[26] and that, conversely, *Wnt5a*-deficient cells show decreased autophagy,[27] *Wnt5a* expression and autophagy might be linked in MSPCs. While defects in autophagy were shown to be harmful for HSCs,[5,28-30] the role of autophagy in maintaining MSPC niche function remains to be established.

Thus, we stained MSPCs and observed strongly increased levels of ATG7, LAMP1, LC3, and SQSTM1 in characteristic

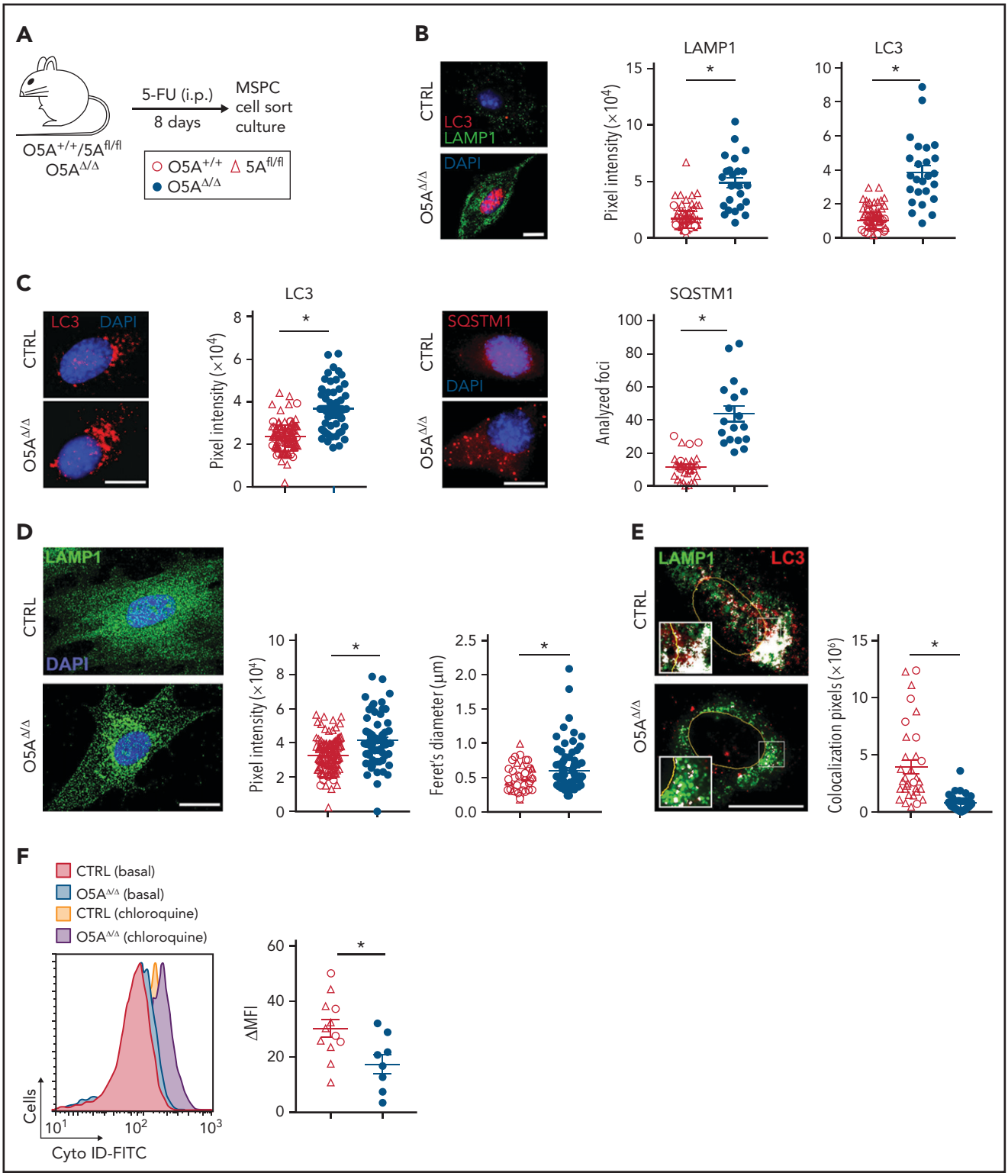

Figure 3. Defective autophagic vesicle delivery in MSPCs from O5A$^{\Delta/\Delta}$ mice. (A) Experimental design for IP injection of 5-FU in the following genotypes: CTRL: O5A$^{+/+}$, n = 5, 5A$^{fl/fl}$, n = 7 and O5A$^{\Delta/\Delta}$, n = 10. Analysis of autophagy relevant mechanisms in compact bone-derived MSPCs 8 days after in vivo treatment. All experiments were performed either with sorted ([B], o/n culture) or compact bone-derived MSPCs ([C-F], passage 4). (B) Fluorescent staining of LC3 (red) and LAMP1 (green) in sorted primary MSPCs from the BM of 5-FU-treated mice, cultured overnight on 0.1%-gelatin-coated coverslips. (C) Fluorescent microscopy images of LC3 (red/left), SQSTM1 (=p62; red/right) and DAPI (blue) staining in compact bone-derived MSPCs (p4). The left graph shows the perinuclear distribution of LC3 measured with ImageJ software. SQSTM1 foci were counted with ImageJ software (graph, right). (D) Confocal images of perinuclear LAMP1 (green) and DAPI (blue) staining. The graphs show the perinuclear distribution of LAMP1 and the diameter of the lysosomes designated as feret's diameter measured with ImageJ software. (E) Confocal images of perinuclear colocalization of LAMP1 (green) and LC3 (red) measured by ImageJ software. Colocalization was measured by ImageJ software (PLUGIN: colocalization) and visualized in white. (F) Representative flow cytometry histogram of basal autophagy and quantification of Cyto-ID dye levels (DMFI: Cyto-ID dye level chloroquine treated-Cyto-ID dye level WITHOUT treatment). Data were measured by ImageJ software. Scale bars, 10 µm. *$P < .05$ (nonparametric Mann-Whitney test: B-F). The results of each panel represent 2 to 3 independent experiments. Each dot represents the measurement of 1 cell. Data are represented as mean ± SEM. Symbol legends are shown in Figure 3A,F.

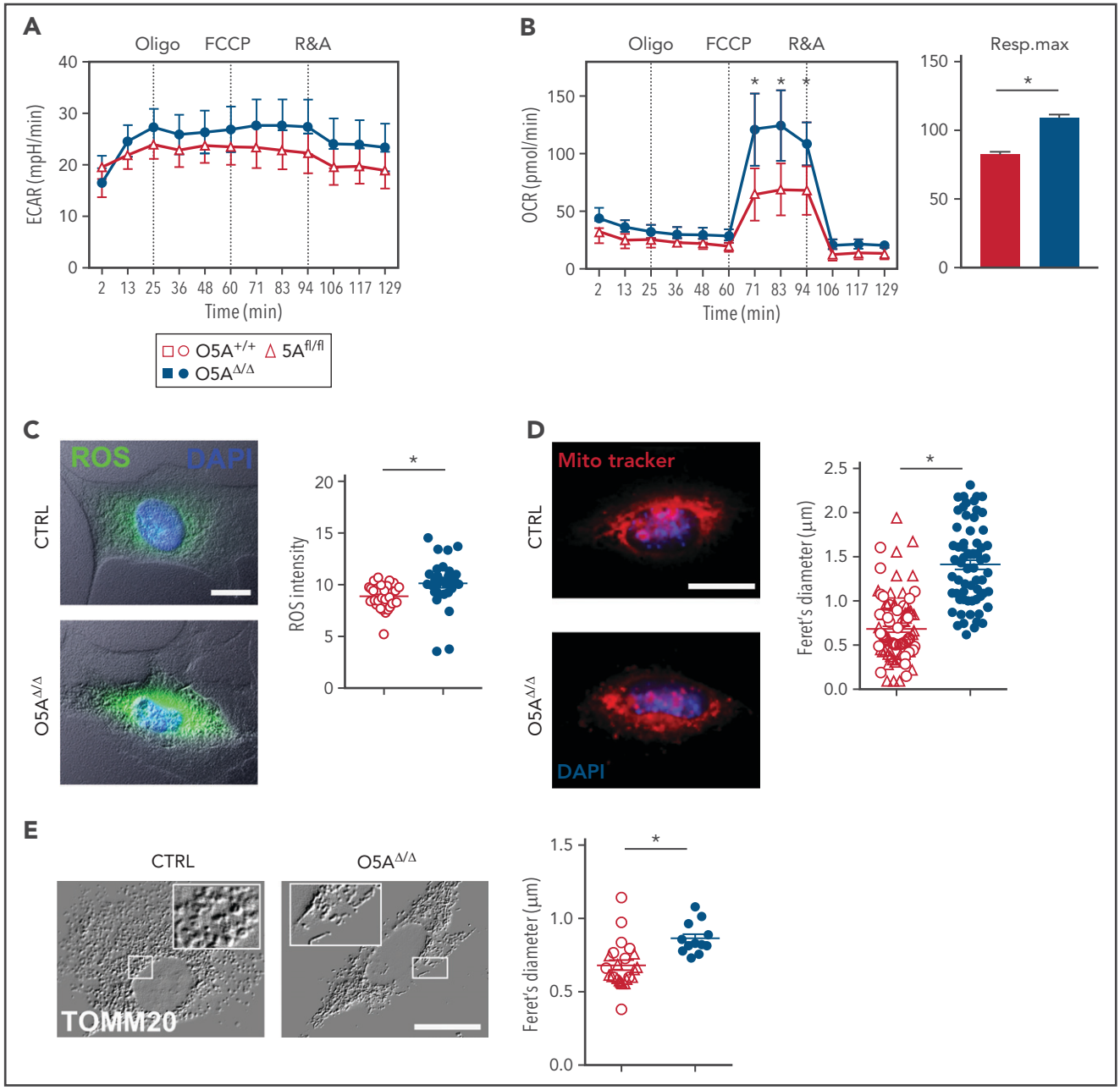

Figure 4. Mitochondria and mitochondrial function in MSPCs (p4) from 5-FU-treated O5A$^{\Delta/\Delta}$ and control mice. (A-B) Graphs showing 1 experiment out of 2 as an example for extracellular acidification rate (ECAR) (A) and OXPHOS levels measured by oxygen consumption rates (OCR) (B), in cultured MSPCs, respiration maximum (right panel) is shown for MSPCs from both experiments; oligo, oligomycin; FCCP, *p*-trifluoromethoxyphenylhydrazone; R&A, rotenone and antimycin. (C) Fluorescent microscopy images and intensity of reactive oxygen species (ROS = DCFDA, green) levels and DAPI (blue) in MSPCs. Graph showing pixel intensity measured by ImageJ software. (D) Fluorescent microscopy images and diameter of mitochondria designated as feret's diameter measured by ImageJ software (MitoTrackerRed, red) and DAPI (blue) in MSPCs. (E) Fluorescent microscopy images of mitochondria (TOMM20) in MSPCs illustrated as relief image (Adobe Photoshop: v21.1.1/filter relief) and diameter of mitochondria designated as feret's diameter measured by ImageJ software. Scale bars, 10 μm. *$P < .05$ (nonparametric Mann-Whitney test; A-E). The results of each panel represent 2 or 3 independent experiments. Data are represented as mean ± SEM. Open symbols and bars represent measurements of control (5A$^{fl/fl}$ and O5A$^{+/+}$). Closed symbols and bars represent measurements of O5A$^{\Delta/\Delta}$ MSPCs. Symbol legend shown in Figure 4A.

punctae, indicating autophagosome accumulation in both freshly sorted and cultured MSPCs from 5-FU-treated O5A$^{\Delta/\Delta}$ mice (Figure 3A-C; supplemental Figure 5A-C). In addition, accumulation of LAMP1^{+} lysosomes with larger diameters and reduced colocalization with LC3 in MSPCs from 5-FU-treated O5A$^{\Delta/\Delta}$ mice indicates associated reduced lysosomal degradation of autophagosomes (Figure 3D-E).

To assess autophagosome degradation, we performed autophagosome labeling with Cyto-ID and the degradation inhibitor chloroquine.[31] Here, we found a strongly reduced autophagic flux (ΔMFI) in MSPCs from 5-FU-treated O5A$^{\Delta/\Delta}$ mice (Figure 3F). Combined, these findings indicate that autophagosomes and lysosomes form, but autophagy fails in MSPCs from 5-FU-treated O5A$^{\Delta/\Delta}$ mice.

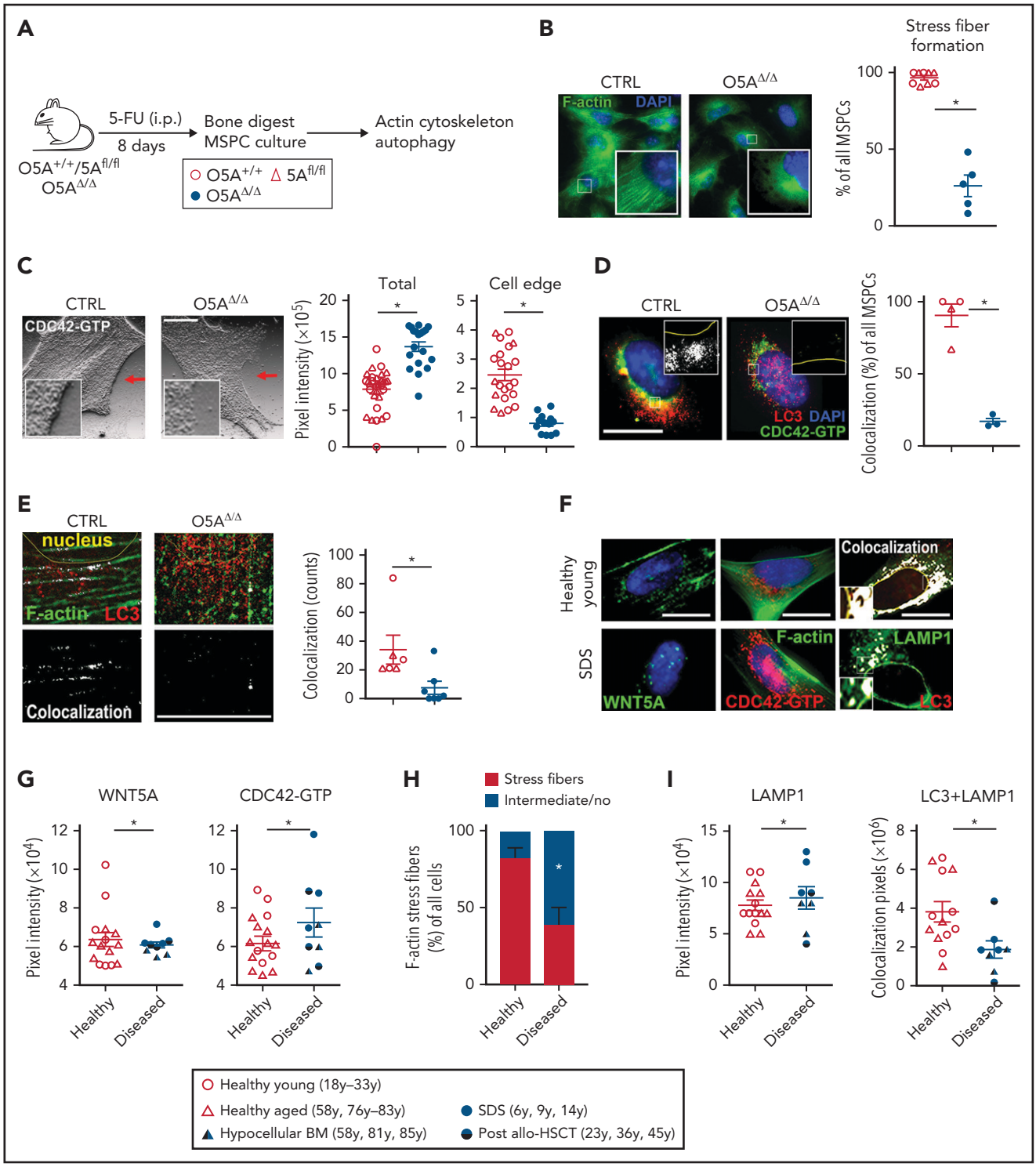

Figure 5. Actin- and CDC42-dependent autophagy in O5A$^{\Delta/\Delta}$ and human MSPCs. *Mouse samples*: (A) IP injection of 5-FU in the following genotypes: CTRL: O5A$^{+/+}$ n = 5, 5A$^{fl/fl}$ n = 7 and O5A$^{\Delta/\Delta}$ n = 10. Analysis of cytoskeleton-associated proteins and autophagy in compact bone-derived MSPCs, isolated 8 days after 5-FU-treatment and cultured until passage 4. (B) Fluorescent microscopy images of F-actin (Phalloidin/green) and DAPI (blue) staining. The graph shows the results of stress fiber formation in pooled MSPCs of 3 independent experiments. (C) Fluorescent microscopy images of CDC42-GTP in MSPCs illustrated as relief image (Adobe Photoshop: v21.1.1/filter relief). Graphs showing the total pixel intensity of CDC42-GTP (left panel) and the cell edge (right panel) as measured by ImageJ software. (D) Confocal images of CDC42-GTP (green), LC3 (red), and DAPI (blue) in MSPCs. Colocalization was measured by ImageJ software (plugin colocalization) and visualized in white. The graph shows the measurement of colocalization in pooled MSPCs. (E) Fluorescent microscopy images of F-actin (Phalloidin/green) and LC3 (red) in MSPCs. Colocalization was measured by ImageJ software (plug-in: colocalization) and visualized in white. *Human samples*: (F) Fluorescent microscopy images of cultured human MSPCs (P2) from healthy young donors and SDS patients. Fluorescent staining of WNT5A (green, left), F-actin (green, middle), CDC42-GTP (red, middle), DAPI staining (blue, left and middle), and colocalization of LAMP1 (green, right) and LC3 (red, right) measured by ImageJ software. (G) Graphs showing the protein content of WNT5A (left) and CDC42-GTP (right). (H) Evaluation of the orientation of F-actin stress fibers stained with phalloidin. Cells showing intermediate orientation (for instance, at the cell edge only) or no orientation were taken together (see

Enhanced oxidative mitochondrial activity in dysfunctional niche cells

Since damaged mitochondria are eliminated through autophagy,[32,33] we then studied whether mitochondria were altered in O5A$^{\Delta/\Delta}$ MSPCs. Our experiments show that glycolysis, as measured by the extracellular acidification rate (ECAR), is not affected. But the OCR is 1.7-fold higher in MSPCs from 5-FU-treated O5A$^{\Delta/\Delta}$ mice compared with controls (Figure 4A-B). Elevated OCR corresponded to high levels of ROS, not only in O5A$^{\Delta/\Delta}$ MSPCs (Figure 4C), but also in ECs and OBCs (supplemental Figure 5D-F). Furthermore, cultured O5A$^{\Delta/\Delta}$ MSPCs show alterations associated with oxidative stress, such as increased DNA damage (supplemental Figure 5G). But, these changes did not affect proliferation, apoptosis, or surface phenotype of MSPCs from 5-FU-treated O5A$^{\Delta/\Delta}$ mice (supplemental Figure 5H-J).

We then assessed whether elevated OCR and ROS are associated with a defective mitochondrial clearance in MSPCs from 5-FU-treated O5A$^{\Delta/\Delta}$ mice. Our experiments showed that mitochondrial mass, number, as well as diameter, in MSPCs from 5-FU-treated O5A$^{\Delta/\Delta}$ mice were increased (Figure 4D-E). In addition, staining for TOMM20 or the regulator of mitochondrial fission DRP1[34] showed significant elongation of the mitochondrial network in O5A$^{\Delta/\Delta}$ MSPCs (Figure 4E; supplemental Figure 5K). This indicates accumulation of mitochondria, reduced mitochondrial fission, and clearance.

Incorrect positioning of critical components of autophagy due to impaired F-actin stress-fiber orientation in MSPCs

The cytoskeleton is critical for correct autophagy.[11] Since deletion of *Wnt5a* in the microenvironment deregulates the cytoskeleton in HSCs,[10] we hypothesized that decreased autophagy is associated with deregulated F-actin orientation (Figure 5A). In addition, the GTPase CDC42 is an important regulator of cytoskeletal polymerization and polarization[8,10,19] and CDC42 is required for autophagy.[35] In line with our hypothesis, we found much less F-actin orientation and perinuclear localization in MSPCs from 5-FU-treated O5A$^{\Delta/\Delta}$ mice compared with controls (Figure 5B). Moreover, the expression of active GTP-binding CDC42 was strongly increased. Furthermore, while CDC42-GTP localized primarily to cell edges in control MSPCs, it localized mainly to perinuclear regions in MSPCs from O5A$^{\Delta/\Delta}$ mice (Figure 5C). These results indicate deregulation of F-actin orientation as well as CDC42-GTP localization in MSPCs of 5-FU-treated O5A$^{\Delta/\Delta}$ mice.

LC3 interacts with and regulates CDC42.[36] Thus, we explored whether LC3 colocalized with active CDC42-GTP and F-actin. Confocal images revealed punctate LC3 in the perinuclear regions of the O5A$^{\Delta/\Delta}$ MSPCs (Figure 3C). In O5A$^{\Delta/\Delta}$ MSPC, the LC3^{+} punctae are only marginally colocalized with either CDC42-GTP or F-actin compared with the MSPCs from control mice (Figure 5D-E), indicating diminished anchoring of LC3^{+} autophagosomes to the F-actin-cytoskeleton in O5A$^{\Delta/\Delta}$ MSPCs.

CDC42 activation and autophagy defects in MSPCs from human BM failure states

We then studied whether MSPCs from patients sharing features of peripheral cytopenias and hypocellular BM with the twice-5-FU-treated O5A$^{\Delta/\Delta}$ mice showed similar alterations in the cytoskeleton and autophagy. For this, MSPCs were cultured from BM samples from patients with different BM failure states, such as SDS, an inherited BM failure syndrome, hypocellular MDS, or severe aplastic anemia. We also included 3 samples from leukemia/lymphoma patients undergoing allogeneic HSCT. Two patients had previously been conditioned with total body irradiation, which may contribute to niche damage, and the third patient showed incomplete BM reconstitution HSCT (likely due to extensive pretreatment) (supplemental Table 2). Interrogation of published gene expression data in freshly isolated mesenchymal cells from MDS vs normal controls revealed that whereas all control BM samples (10 of 10) express *WNT5A*, it is not detected in 33 of 45 MDS BM samples, and some actin-regulating intermediates are reduced (supplemental Figure 6A).[37] In IF experiments, we subsequently found that expression of WNT5A or CDC42-GTP and colocalization of LC3/LAMP1 is similar in MSPCs from aged and young BM controls (supplemental Figure 6B), indicating their altered expression or colocalization is not due to aging. In comparison, staining of MSPCs from patients with the common features of peripheral cytopenia and BM hypocellularity revealed a slight but significant reduction of WNT5A, a clear increase of activated CDC42, and reduced F-actin stress fiber orientation (Figure 5F-H). Furthermore, LAMP1 is elevated with reduced LC3/LAMP1 colocalization (Figure 5I), indicative of cytoskeleton and autophagy defects.

Pharmacological attenuation of CDC42-GTP levels in vitro restores autophagy in MSPCs

Our data imply that cytostatic stress causes sustained CDC42 activation associated with deregulation of cytoskeleton-associated autophagy in MSPCs from cytopenic mice (Figure 5B-E). We consequently reasoned that inhibiting CDC42 activation would directly improve MSPC function. To test this hypothesis, we treated mouse MSPCs in vitro with the RhoGDI/CDC42 activation inhibitor CASIN (also described as Pirl1),[8,38-41] or the allosteric CDC42 inhibitor ML141[42,43] (supplemental Figure 7A-B). Both inhibitors reduced the cellular level of CDC42-GTP in O5A$^{\Delta/\Delta}$ MSPCs equally well. However, only CASIN restored CDC42-GTP localization at the cell edge and F-actin stress fibers in MSPCs from 5-FU-treated O5A$^{\Delta/\Delta}$ mice (supplemental Figure 7C-D).

To test whether CASIN improved autophagy, we compared treatments with CASIN, rapamycin, a known autophagy inducer, or chloroquine, a lysosomal lysis inhibitor (supplemental Figure 7E). These experiments showed that both rapamycin and CASIN increase LC3^{+} autophagosome formation without affecting LAMP1 expression (supplemental Figure 7F-H). Importantly,

Figure 5 (continued) supplemental Methods). (I) LAMP1 staining (left) and colocalization pixels of LAMP1 and LC3 (right) in MSPCs (P2) from healthy young individuals, n = 7, healthy aged individuals, n = 7, samples from hypocellular BM patients (P_1-3; see supplemental Table 2 for details), n = 3, SDS patients (P_7-9; see supplemental Table 2 for details), n = 3 and post-allo-HSCT patients (P_4-6; see supplemental Table 2 for details), n = 3. Scale bars 10 μm. *$P < .05$ (nonparametric Mann-Whitney test: B-E,G-I). The results represent 2 to 3 independent experiments. Data are represented as mean ± SEM. Symbol legends shown in Figure 5A and underneath Figure 5H-I.

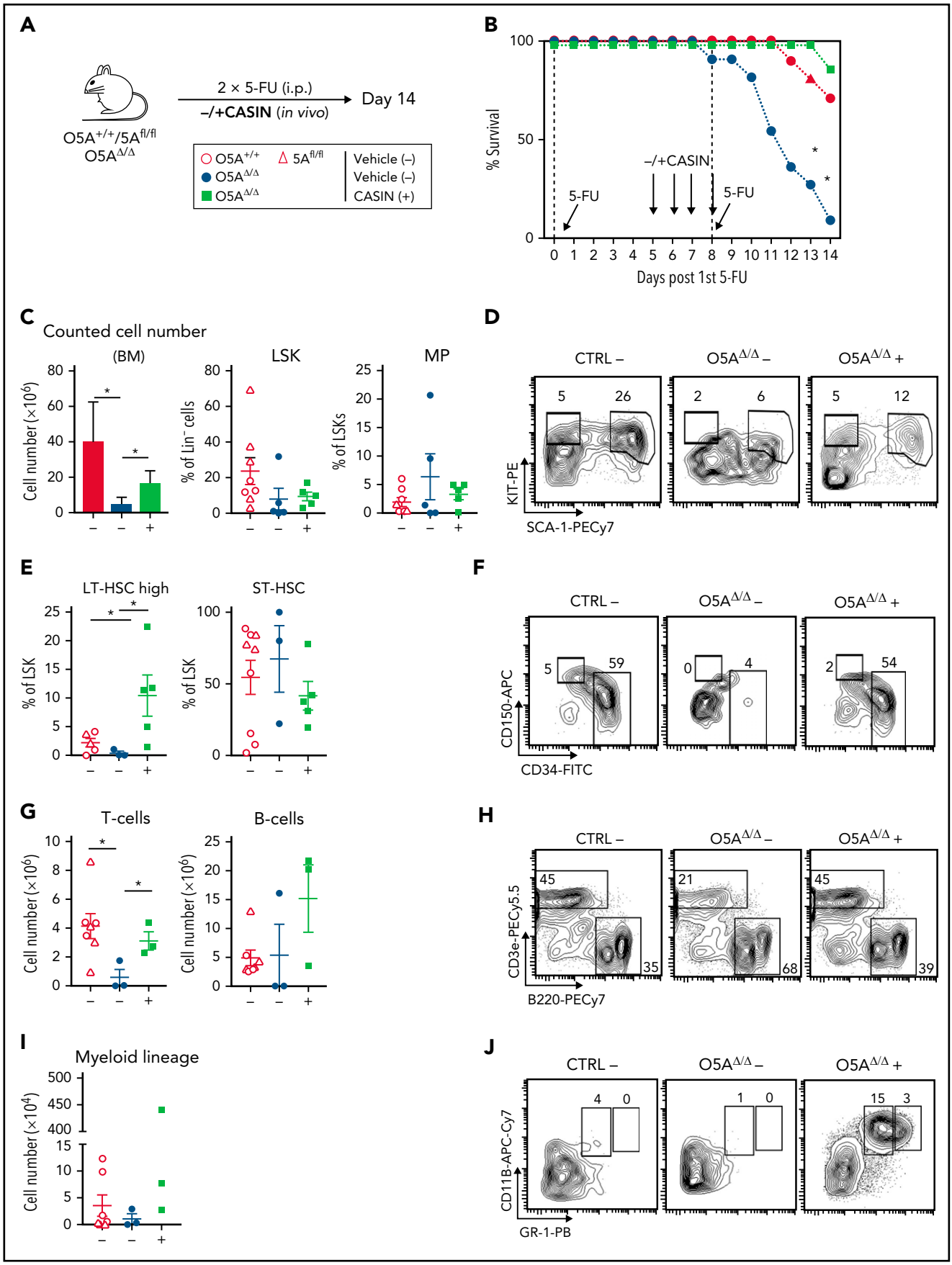

Figure 6. Attenuation of elevated CDC42 activity ensures survival. (A) Serial IP injection of 5-FU in the following genotypes: CTRL: O5A$^{+/+}$ n = 6, 5A$^{fl/fl}$ n = 7 and O5A$^{\Delta/\Delta}$ n = 7 at day 0 and day 8. Additional in vivo IP injection of CDC42-GTP inhibitor CASIN at day 5 through day 8. Analysis of animal survival, hematopoiesis (BM

both rapamycin and CASIN increase colocalization of LC3 and LAMP1 (supplemental Figure 7I), indicating CASIN directly stimulates autophagy in MSPCs.

To determine whether the extrinsic WNT5A signal similarly restores CDC42 activation, recombinant WNT5A was added to MSPC cultures. These experiments show that rWNT5A reduces both LC3 and LAMP1, as well as their colocalization (supplemental Figure S7J-M), indicating that rWNT5A also directly improves autophagy.

Pharmacological attenuation of CDC42-GTP levels in vivo protects against stress-induced mortality

To appraise whether attenuation of CDC42 activation also restores niche function and hematopoiesis in vivo, we serially treated O5A$^{\Delta/\Delta}$ and control mice with 5-FU on day 0 and day 8 and included an additional treatment with CASIN[41] (Figure 6A; supplemental Figure 8A). Strikingly, the application of CASIN protected O5A$^{\Delta/\Delta}$ mice from mortality induced by the second 5-FU-treatment (Figure 6B). In addition, we did not detect PB nor BM cytopenia with the rescue of both mature and immature hematopoietic cells (Figure 6C-J), particularly of LT-HSCs and BM T-cells (Figure 6E-G), in the CASIN-treated O5A$^{\Delta/\Delta}$ mice.

To find out whether in vivo attenuation of CDC42 activation maintains BM niche cell numbers and function, we found that the relative number of MSPCs was reverted to control levels in MSPCs from CASIN- and twice-5-FU-treated O5A$^{\Delta/\Delta}$ mice (supplemental Figure 8B-C). In addition, we observed similar MSPC differentiation in vitro (supplemental Figure 8D). In MSPCs from O5A$^{\Delta/\Delta}$ mice treated twice with 5-FU, CASIN treatment restored both CDC42-GTP localization to the cell edge and F-actin stress fiber orientation (supplemental Figure 8E-F).

Rescue of actin-guided autophagy and mitochondrial clearance in MSPCs

In experiments to determine whether in vivo attenuation of CDC42 activation prevents the decline of the F-actin-anchored autophagy in MSPCs prior to the second 5-FU treatment, we found that in vivo CASIN treatment reduces the levels and perinuclear localization of LC3 in O5A$^{\Delta/\Delta}$ MSPCs (Figure 7A-B) compared with controls (Figure 3B-C). Moreover, LC3 colocalizes with both CDC42-GTP and F-actin fibers (Figure 7C-D), indicating normalized cytoskeletal deregulation and actin cytoskeleton anchoring in MSPCs from 5-FU-treated O5A$^{\Delta/\Delta}$ mice. In experiments to determine whether the autophagy defects noted earlier (Figure 3) were also normalized, we found that both LAMP1 content and lysosome diameters were restored (Figure 7E). More importantly, LC3 and LAMP1 also colocalized (Figure 7F), indicating restored autophagy in MSPCs from 5-FU-treated O5A$^{\Delta/\Delta}$ mice. Indeed, we found that autophagic flux was substantially increased in MSPCs by prior in vivo CASIN treatment (Figure 7G). In addition, both reduction in ROS and MitoTracker Red levels and colocalization of LC3 and TOMM20 (Figure 7H; supplemental Figure 9A-C) indicate improved mitophagy after in vivo CASIN treatment.

Discussion

Understanding mechanisms involved in the hematopoiesis-supportive function of MSPCs is crucial for developing new treatments for debilitating hematologic diseases. Our present study shows that autophagy controlled by CDC42 is a critical factor for maintaining hematopoietic support by BM niche cells during stress. Furthermore, without *Wnt5a* in osteoprogenitors, CDC42 is constitutively active in MSPCs, which leads to secondary ineffective hematopoiesis and increased mortality after severe stress.

Our experiments show that regulation of CDC42 directly modulates F-actin and associated autophagic flux in niche cells. We found that only the RhoGDI/CDC42 association inhibitor CASIN, but not the allosteric inhibitor ML-141, restores cytoskeletal defects and CDC42-GTP localization. Thus, only RhoGDI/CDC42 attenuation effectively improves cellular processes resulting in healthier mice. Indeed, a similar 4-day treatment of aged mice with CASIN shows not only improved mouse health, it also extended their lifespan significantly.[44]

Interestingly, we found that similar changes in F-actin and autophagy also occur in MSPCs from patients sharing features of peripheral cytopenia and hypocellular BM, such as in different BM failure states, suggesting a possible role in their pathogenesis. Our findings add to reports showing that MSPCs from these diseases are defective in CFU-F content, show deregulated differentiation,[3,37,45,46] and demonstrate defects in maintaining HSCs and progenitor cells.[45,47-49] However, it remains elusive why and how CDC42 signaling, the cytoskeleton, or autophagy in MSPCs causes secondary ineffective hematopoiesis. Findings from SDS and like diseases showed that mutated SBDS and SRP54, which cause these syndromes, are both not only expressed by niche cells,[50] but these proteins also bind to F-actin and deregulate small GTPase activation.[51,52] Similar deregulation of these pathways may occur in MSPCs, also from other BM failure states. Alternatively, the processes mentioned may be linked indirectly through reduced mitophagy, causing oxidative injury[33] or deregulation of autophagy-dependent secretion of cytokines.[53,54]

In summary, autophagy, cytoskeletal orientation, and CDC42 activation in niche cells are possible targets for improving inefficient hematopoiesis after severe stress. Furthermore, we provide a rationale for extending our findings in the O5A$^{\Delta/\Delta}$ mouse model to human diseases featuring peripheral cytopenia and hypocellular BM. In addition, our work offers attenuation of CDC42 activation in vivo as a therapeutic strategy to improve the homeostasis of the hematopoietic BM niche.

Figure 6 (continued) from 4 flushed long bones), and compact bone-derived MSPCs at day 14. (B) Percentage of mice survival after serial 5-FU treatment. Graph shows the survival curve of CTRL and O5A$^{\Delta/\Delta}$ mice treated with CASIN (+) or vehicle (-). (C) Graph shows the total BM cell number (left) and relative number of LSK cells (middle) and MPs (right) at day 14 of CTRL mice with vehicle ([-]; O5A$^{+/+}$ n = 6, 5A$^{fl/fl}$ n = 7), O5A$^{\Delta/\Delta}$ mice with vehicle ([-]; n = 5, mice analyzed shortly before death) and O5A$^{\Delta/\Delta}$ mice with CASIN ([+]; n = 5). (D,F,H,J) Representative contour plots from BM populations. Graphs show relative number of LT-HSCs and ST-HSCs (E-F), T cells and B cells (G-H), and Gr1^{+} myeloid cells (I-J). *$P < .05$ (nonparametric Mann-Whitney test: C,E,G,I). The results represent 2 to 3 independent experiments. Data are represented as mean ± SEM. Symbol legend shown in Figure 6A.

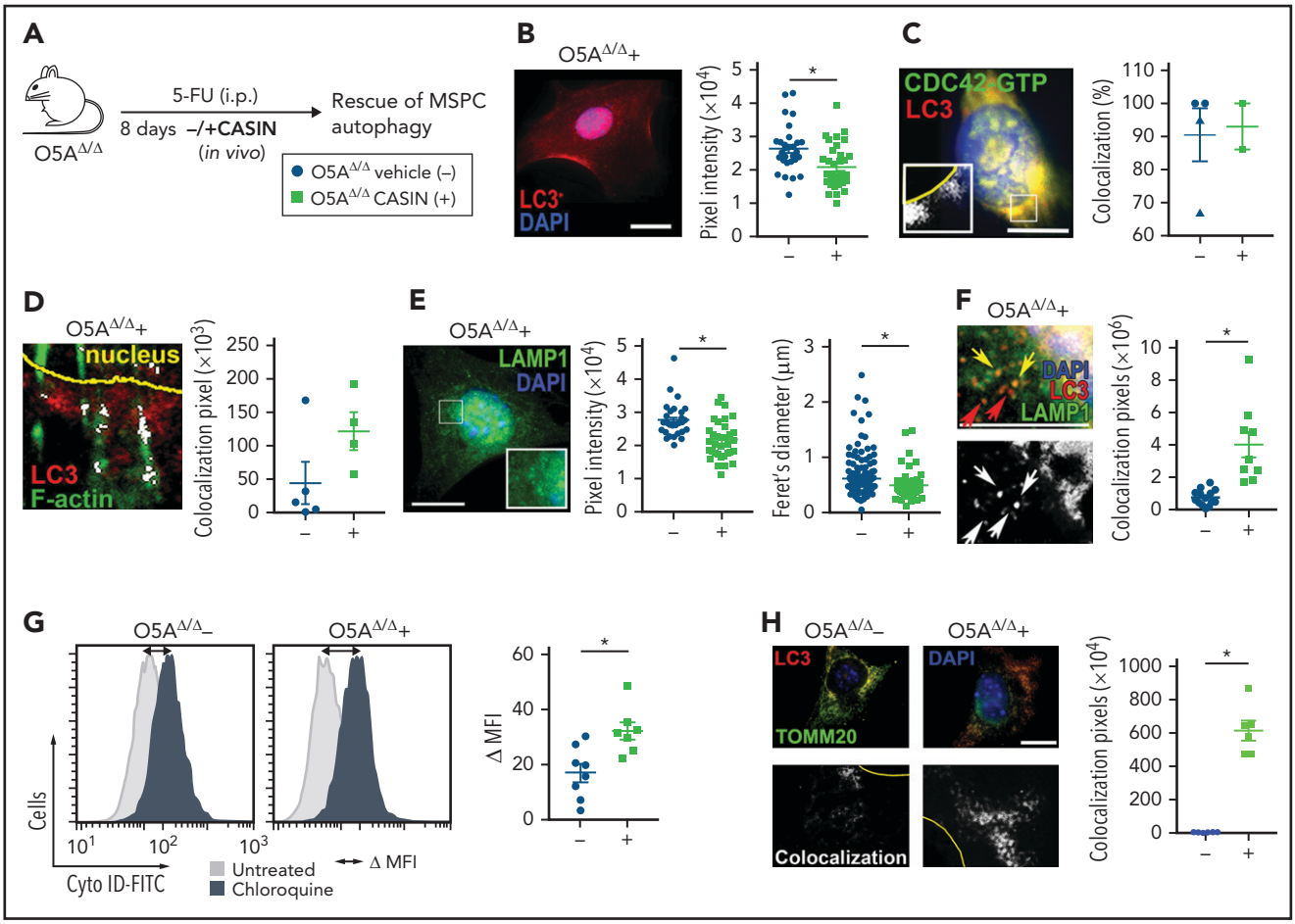

Figure 7. Attenuation of elevated CDC42 activity during auto/mitophagy. (A) IP injection of 5-FU in O5A$^{\Delta/\Delta}$ mice at day 0. Additional in vivo IP injection of vehicle ([-], n = 5) or CASIN ([+], n = 4) at day 5 through day 8. Rescue and analysis of autophagy relevant mechanisms in compact bone-derived MSPCs, isolated at day 8 and cultured until passage 4. (A-G) Shown are the results of O5A$^{\Delta/\Delta}$ mice with vehicle (-) and CASIN (+) treatment. CASIN-treated mice show the same phenotype as the control groups 5A$^{fl/fl}$ and O5A$^{+/+}$ (Figure 3). (B) Fluorescent microscopy images of LC3 (red) and DAPI (blue) staining. Graph shows the pixel intensity as measured by ImageJ software. (C) Fluorescent microscopy image of CDC42-GTP (green), LC3 (red), and DAPI (blue) staining. The graph shows the percentage of MSPCs with colocalization measured by ImageJ software (plugin colocalization) and visualized in white. (D) Fluorescent microscopy images of F-actin (Phalloidin/green) and LC3 (red) in MSPCs. Colocalization was measured by ImageJ software (plug-in colocalization) and visualized in white. The graph shows colocalization counted with ImageJ software. (E) Fluorescent microscopy images of LAMP1 (green) and DAPI (blue) staining. The pixel intensity (left graph) and feret's diameter (right graph) were measured by ImageJ software. (F) Fluorescent microscopy images of LAMP1 (green), LC3 (red), and DAPI (blue) staining. Yellow arrows show colocalized vesicle staining, red arrows depict LC3^{+} vesicles that did not colocalize with green LAMP1^{+} vesicles. Perinuclear colocalization of LAMP1 and LC3 measured by ImageJ software (plugin colocalization, depicted in white). (G) Representative FACS plots and quantification (graph) of Cyto-ID dye levels (DMFI: Cyto-ID dye level chloroquine treated, Cyto-ID dye level w/o treatment). (H) Fluorescent microscopy images of TOMM20 (green), LC3 (red), and DAPI (blue) staining. Colocalization was measured by ImageJ software (plugin colocalization) and visualized in the bottom row in white. Scale bars, 10 μm. *$P < .05$ (2-sided parametric Student's t test; B-H). The results represent 2 independent experiments. Data are represented as mean ± SEM. Symbol legend shown in Figure 7A.

Acknowledgments

The authors thank Hannah Kitzberger and Tommaso di Genio (Department of Internal Medicine III - Hematology/Oncology, Technical University of Munich) for excellent help in some of the experiments. The authors thank Christian Landspersky for graphical illustration of animals. The authors also thank L. Henkel, I. Andrä, C. Angerpointner, and S. Dürr (Institute of Microbiology, Immunology, and Hygiene, Technical University of Munich) for cell sorting and help with fluorescent microscopy. Furthermore, the authors thank H. Harz at the Center for Advanced Light Microscopy (CALM, Ludwig-Maximilian University) and Ritu Mishra (Cell Analysis Core Facility, TranslaTUM), as well as L. Chen and M.H.G.P. Raaijmakers (Department of Hematology, Erasmus University, Rotterdam, Netherlands) for sharing data. Special thanks to C. Peschel (Clinic and Policlinic for Internal Medicine III, Klinikum rechts der Isar, Technical University of Munich) for support of this project.

This work was funded by the German Research Foundation (DFG) grants FOR 2033 (A2 and B3), SFB 1243 (A01, A04, and A09), and OO 8/16 and 8/18.

Authorship

T.L., C.S., J.S.H., K.S.G., H.G., and R.A.J.O. designed research; T.L., C.S., M.S., E.H., K.B., F.H., R.I., S.R.M., J.R., J.S.H., R.L., M.G., M.B. and M.W. performed research and collected data; M.S., J.R., D.S., A.S., K.M., T.P.Y., M.K., H.L., F.B., K.S.G and H.G. contributed vital reagents and analyticaltools; T.L., M.S., C.S., J.R., J.S.H., K.S.G., and R.A.J.O. analyzed and interpreted data and performed statistical analyses; and T.L., C.S., and R.A.J.O. wrote the manuscript.

Conflict-of-interest disclosure: The authors declare no competing financial interests.

The current affiliation for R.I. is Technical University of Munich (TUM), School of Medicine, Department of Surgery, Munich, Germany.

ORCID profiles: J.R., 0000-0002-4680-2071; J.S.H., 0000-0002-1531-0517; K.B., 0000-0002-8719-2943; M.W., 0000-0002-4795-8086; J.R., 0000-0002-8381-3597; A.S., 0000-0002-4683-9958; K.M., 0000-0002-5528-4405; T.P.Y., 0000-0002-7452-4419; H.L., 0000-0002-5086-6449; K.S.G., 0000-0002-6276-8002; R.A.J.O., 0000-0002-4947-0412.

Correspondence: Christina Schreck, Technical University of Munich, Klinikum rechts der Isar, Department of Internal Medicine III, Ismaningerstrasse 22, 81675 München, Germany; e-mail: christina.schreck@tum.de; and Robert A. J. Oostendorp, Technical University of Munich, Klinikum rechts der Isar, Department of Internal Medicine III, Ismaningerstrasse 22, 81675 München, Germany; e-mail: robert.oostendorp@tum.de.

Footnotes

Submitted 22 March 2021; accepted 1 October 2021; prepublished online on *Blood* First Edition 17 October 2021. DOI 10.1182/blood.2021011775.

*C.S. and R.A.J.O. contributed equally to this study.

The online version of this article contains a data supplement.

There is a *Blood* Commentary on this article in this issue.

The publication costs of this article were defrayed in part by page charge payment. Therefore, and solely to indicate this fact, this article is hereby marked "advertisement" in accordance with 18 USC section 1734.

REFERENCES

1. Pronk E, Raaijmakers MHGP. The mesenchymal niche in MDS. *Blood*. 2019; 133(10):1031-1038.
2. Lin H, Sohn J, Shen H, Langhans MT, Tuan RS. Bone marrow mesenchymal stem cells: aging and tissue engineering applications to enhance bone healing. *Biomaterials*. 2019; 203:96-110.
3. Weickert MT, Hecker JS, Buck MC, et al. Bone marrow stromal cells from MDS and AML patients show increased adipogenic potential with reduced Delta-like-1 expression. *Sci Rep*. 2021;11(1):5944.
4. Hinge A, He J, Bartram J, et al. Asymmetrically segregated mitochondria provide cellular memory of hematopoietic stem cell replicative history and drive HSC attrition. *Cell Stem Cell*. 2020; 26(3):420-430.e6.
5. Ho TT, Warr MR, Adelman ER, et al. Autophagy maintains the metabolism and function of young and old stem cells. *Nature*. 2017;543(7644):205-210.
6. Liang R, Arif T, Kalmykova S, et al. Restraining lysosomal activity preserves hematopoietic stem cell quiescence and potency. *Cell Stem Cell*. 2020; 26(3):359-376.e7.
7. Loeffler D, Wehling A, Schneiter F, et al. Asymmetric lysosome inheritance predicts activation of haematopoietic stem cells. *Nature*. 2019;573(7774):426-429.
8. Florian MC, Dörr K, Niebel A, et al. Cdc42 activity regulates hematopoietic stem cell aging and rejuvenation. *Cell Stem Cell*. 2012;10(5):520-530.
9. Geiger H, de Haan G, Florian MC. The ageing haematopoietic stem cell compartment. *Nat Rev Immunol*. 2013; 13(5):376-389.
10. Schreck C, Istvánffy R, Ziegenhain C, et al. Niche WNT5A regulates the actin cytoskeleton during regeneration of hematopoietic stem cells. *J Exp Med*. 2016; 214(1):165-181.
11. Kast DJ, Dominguez R. The cytoskeleton-autophagy connection. *Curr Biol*. 2017; 27(8):R318-R326.
12. Moore AS, Wong YC, Simpson CL, Holzbaur EL. Dynamic actin cycling through mitochondrial subpopulations locally regulates the fission-fusion balance within mitochondrial networks. *Nat Commun*. 2016; 7(1):12886.
13. Miyoshi H, Ajima R, Luo CT, Yamaguchi TP, Stappenbeck TS. Wnt5a potentiates TGF-β signaling to promote colonic crypt regeneration after tissue injury. *Science*. 2012; 338(6103):108-113.
14. Rodda SJ, McMahon AP. Distinct roles for Hedgehog and canonical Wnt signaling in specification, differentiation and maintenance of osteoblast progenitors. *Development*. 2006;133(16):3231-3244.
15. Mizoguchi T, Pinho S, Ahmed J, et al. Osterix marks distinct waves of primitive and definitive stromal progenitors during bone marrow development. *Dev Cell*. 2014; 29(3):340-349.
16. Hecker JS, Hartmann L, Rivière J, et al. CHIP and hips: clonal hematopoiesis is common in hip arthroplasty patients and associates with autoimmune disease. *Blood*. 2021;138(18):1727-1732
17. Istvánffy R, Vilne B, Schreck C, et al. Stroma-derived connective tissue growth factor maintains cell cycle progression and repopulation activity of hematopoietic stem cells in vitro. *Stem Cell Reports*. 2015; 5(5):702-715.
18. Nakamura Y, Arai F, Iwasaki H, et al. Isolation and characterization of endosteal niche cell populations that regulate hematopoietic stem cells. *Blood*. 2010; 116(9):1422-1432.
19. Florian MC, Nattamai KJ, Dörr K, et al. A canonical to non-canonical Wnt signalling switch in haematopoietic stem-cell ageing. *Nature*. 2013;503(7476):392-396.
20. Saçma M, Pospiech J, Bogeska R, et al. Haematopoietic stem cells in perisinusoidal niches are protected from ageing. *Nat Cell Biol*. 2019;21(11):1309-1320.
21. Zhu H, Guo ZK, Jiang XX, et al. A protocol for isolation and culture of mesenchymal stem cells from mouse compact bone. *Nat Protoc*. 2010;5(3):550-560.
22. Cremer M, Brandstetter K, Maiser A, et al. Cohesin depleted cells rebuild functional nuclear compartments after endomitosis. *Nat Commun*. 2020;11(1):6146.
23. Sipol A, Hameister E, Xue B, et al. MondoA drives B-ALL malignancy through enhanced adaptation to metabolic stress. *Blood*. 2021; blood.2020007932.
24. Masamoto Y, Arai S, Sato T, et al. Adiponectin enhances quiescence exit of murine hematopoietic stem cells and hematopoietic recovery through mTORC1 potentiation. *Stem Cells*. 2017; 35(7):1835-1848.
25. Ndoye A, Budina-Kolomets A, Kugel CH III, et al. ATG5 mediates a positive feedback loop between Wnt signaling and autophagy in melanoma. *Cancer Res*. 2017; 77(21):5873-5885.
26. Jati S, Kundu S, Chakraborty A, Mahata SK, Nizet V, Sen M. Wnt5A signaling promotes defense against bacterial pathogens by activating a host autophagy circuit. *Front Immunol*. 2018;9:679.
27. Lock R, Kenific CM, Leidal AM, Salas E, Debnath J. Autophagy-dependent production of secreted factors facilitates oncogenic RAS-driven invasion. *Cancer Discov*. 2014;4(4):466-479.
28. Nakamura-Ishizu A, Ito K, Suda T. Hematopoietic stem cell metabolism during development and aging. *Dev Cell*. 2020; 54(2):239-255.
29. Dong S, Wang Q, Kao YR, et al. Chaperone-mediated autophagy sustains haematopoietic stem-cell function. *Nature*. 2021;591(7848):117-123.
30. Warr MR, Binnewies M, Flach J, et al. FOXO3A directs a protective autophagy program in haematopoietic stem cells. *Nature*. 2013;494(7437):323-327.
31. Guo S, Liang Y, Murphy SF, et al. A rapid and high content assay that measures cyto-ID-stained autophagic compartments and estimates autophagy flux with potential clinical applications. *Autophagy*. 2015; 11(3):560-572.
32. Fan P, Yu XY, Xie XH, et al. Mitophagy is a protective response against oxidative damage in bone marrow mesenchymal stem cells. *Life Sci*. 2019;229:36-45.

33. Ghanta S, Tsoyi K, Liu X, et al. Mesenchymal stromal cells deficient in autophagy proteins are susceptible to oxidative injury and mitochondrial dysfunction. *Am J Respir Cell Mol Biol*. 2017;56(3):300-309.

34. Cho HM, Ryu JR, Jo Y, et al. Drp1-Zip1 interaction regulates mitochondrial quality surveillance system. *Mol Cell*. 2019; 73(2):364-376.e8.

35. Till A, Saito R, Merkurjev D, et al. Evolutionary trends and functional anatomy of the human expanded autophagy network. *Autophagy*. 2015;11(9):1652-1667.

36. Chung YH, Yoon SY, Choi B, et al. Microtubule-associated protein light chain 3 regulates Cdc42-dependent actin ring formation in osteoclast. *Int J Biochem Cell Biol*. 2012;44(6):989-997.

37. Zambetti NA, Ping Z, Chen S, et al. Mesenchymal inflammation drives genotoxic stress in hematopoietic stem cells and predicts disease evolution in human pre-leukemia. *Cell Stem Cell*. 2016; 19(5):613-627.

38. Peterson JR, Lebensohn AM, Pelish HE, Kirschner MW. Biochemical suppression of small-molecule inhibitors: a strategy to identify inhibitor targets and signaling pathway components. *Chem Biol*. 2006; 13(4):443-452.

39. Sakamori R, Das S, Yu S, et al. Cdc42 and Rab8a are critical for intestinal stem cell division, survival, and differentiation in mice. *J Clin Invest*. 2012;122(3):1052-1065.

40. Lin Y, Zheng Y. Approaches of targeting Rho GTPases in cancer drug discovery. *Expert Opin Drug Discov*. 2015;10(9):991-1010.

41. Liu W, Du W, Shang X, et al. Rational identification of a Cdc42 inhibitor presents a new regimen for long-term hematopoietic stem cell mobilization. *Leukemia*. 2019; 33(3):749-761.

42. Hong L, Kenney SR, Phillips GK, et al. Characterization of a Cdc42 protein inhibitor and its use as a molecular probe. *J Biol Chem*. 2013;288(12):8531-8543.

43. Chen C, Song X, Ma S, et al. Cdc42 inhibitor ML141 enhances G-CSF-induced hematopoietic stem and progenitor cell mobilization. *Int J Hematol*. 2014; 101(1):5-12.

44. Florian MC, Leins H, Gobs M, et al. Inhibition of Cdc42 activity extends lifespan and decreases circulating inflammatory cytokines in aged female C57BL/6 mice. *Aging Cell*. 2020;19(9):e13208.

45. Medyouf H, Mossner M, Jann JC, et al. Myelodysplastic cells in patients reprogram mesenchymal stromal cells to establish a transplantable stem cell niche disease unit. *Cell Stem Cell*. 2014;14(6):824-837.

46. Hamzic E, Whiting K, Gordon Smith E, Pettengell R. Characterization of bone marrow mesenchymal stromal cells in aplastic anaemia. *Br J Haematol*. 2015; 169(6):804-813.

47. Wenk C, Garz AK, Grath S, et al. Direct modulation of the bone marrow mesenchymal stromal cell compartment by azacitidine enhances healthy hematopoiesis. *Blood Adv*. 2018;2(23):3447-3461.

48. Juneja HS, Gardner FH. Functionally abnormal marrow stromal cells in aplastic anemia. *Exp Hematol*. 1985;13(3):194-199.

49. Bardelli D, Dander E, Bugarin C, et al. Mesenchymal stromal cells from Shwachman-Diamond syndrome patients fail to recreate a bone marrow niche in vivo and exhibit impaired angiogenesis. *Br J Haematol*. 2018;182(1):114-124.

50. Dolgalev I, Tikhonova AN. Connecting the dots: resolving the bone marrow niche heterogeneity. *Front Cell Dev Biol*. 2021; 9:622519.

51. Orelio C, Kuijpers TW. Shwachman-Diamond syndrome neutrophils have altered chemoattractant-induced F-actin polymerization and polarization characteristics. *Haematologica*. 2009;94(3):409-413.

52. Bellanné-Chantelot C, Schmaltz-Panneau B, Marty C, et al. Mutations in the *SRP54* gene cause severe congenital neutropenia as well as Shwachman-Diamond-like syndrome. *Blood*. 2018;132(12):1318-1331.

53. Lee SG, Joe YA. Autophagy mediates enhancement of proangiogenic activity by hypoxia in mesenchymal stromal/stem cells. *Biochem Biophys Res Commun*. 2018; 501(4):941-947.

54. Cavalli G, Cenci S. Autophagy and protein secretion. *J Mol Biol*. 2020;432(8): 2525-2545.

REGULAR ARTICLE

blood advances

Targeting CDC42 reduces skeletal degeneration after hematopoietic stem cell transplantation

Theresa Landspersky,[1] Merle Stein,[2] Mehmet Saçma,[3] Johanna Geuder,[4] Krischan Braitsch,[1] Jennifer Rivière,[1] Franziska Hettler,[1] Sandra Romero Marquez,[1] Baiba Vilne,[5] Erik Hameister,[1] Daniel Richter,[2] Emely Schönhals,[1] Jan Tuckermann,[2] Mareike Verbeek,[1] Peter Herhaus,[1] Judith S. Hecker,[1] Florian Bassermann,[1] Katharina S. Götze,[1] Wolfgang Enard,[4] Hartmut Geiger,[3] Robert A. J. Oostendorp,[1,*] and Christina Schreck[1,*]

[1]School of Medicine, Department of internal Medicine III, Technical University of Munich, Munich, Germany; [2]Institute of Comparative Molecular Endocrinology, and [3]Institute of Molecular Medicine, Stem Cells, and Aging, Ulm University, Ulm, Germany; [4]Anthropology and Human Genomics, Faculty of Biology, Ludwig-Maximilians University, Munich, Germany; and [5]Bioinformatics Laboratory, Rīga Stradiņš University, Riga, Lettland

Key Points

- CDC42 activity regulates F-actin fiber alignment, mitochondrial function, and mitophagy in MSPCs in a bone marrow transplant setting.
- Attenuation of CDC42 activity improves MSPC quality to increase both bone volume and trabecular bone thickness.

Osteopenia and osteoporosis are common long-term complications of the cytotoxic conditioning regimen for hematopoietic stem cell transplantation (HSCT). We examined mesenchymal stem and progenitor cells (MSPCs), which include skeletal progenitors, from mice undergoing HSCT. Such MSPCs showed reduced fibroblastic colony-forming units frequency, increased DNA damage, and enhanced occurrence of cellular senescence, whereas there was a reduced bone volume in animals that underwent HSCT. This reduced MSPC function correlated with elevated activation of the small Rho guanosine triphosphate hydrolase CDC42, disorganized F-actin distribution, mitochondrial abnormalities, and impaired mitophagy in MSPCs. Changes and defects similar to those in mice were also observed in MSPCs from humans undergoing HSCT. A pharmacological treatment that attenuated the elevated activation of CDC42 restored F-actin fiber alignment, mitochondrial function, and mitophagy in MSPCs in vitro. Finally, targeting CDC42 activity in vivo in animals undergoing transplants improved MSPC quality to increase both bone volume and trabecular bone thickness. Our study shows that attenuation of CDC42 activity is sufficient to attenuate reduced function of MSPCs in a BM transplant setting.

Introduction

Osteoporosis and osteopenia are clinically well-documented long-term complications after allogeneic hematopoietic stem cell transplantation (allo-HSCT).[1,2] Myeloablation through chemotherapeutic treatment or irradiation remains a crucial preconditioning regimen for successful donor stem cell engraftment and regeneration of hematopoiesis in allo-HSCT. Osteoporosis is found in approximately half of HSCT recipients even 10 years after allo-HSCT, regardless of the type of the prior preconditioning regimen.[3,4] In addition, there are signs of senile osteoporosis in allo-HSCT recipients, which are independent of the age of the patient who received transplantation.[5] The observed bone degeneration in such patients suggests that the function of osteoprogenitors in the bone marrow (BM) niche is inefficient and/or incomplete after allo-HSCT or that the rate of osteodestruction is increased.

Submitted 7 February 2024; accepted 16 June 2024; prepublished online on *Blood Advances* First Edition 19 August 2024. https://doi.org/10.1182/bloodadvances.2024012879.

*R.A.J.O. and C.S. are joint senior authors.

Data are available on request from the corresponding author, Christina Schreck (christina.schreck@tum.de).

The full-text version of this article contains a data supplement.

The hematopoietic BM niche is an ecosystem of many different cell types that respond to external triggers and strive to restore and maintain optimal conditions for both hematopoiesis and bone remodeling.[6] The consequences of cellular stress and aging in HSCs, have been explored in several studies.[6,7] The impact of stress responses and aging on the function of BM niche cell populations is still largely unclear.[8-10] In previous work we showed that intermittent exposure to the cytostatic agent 5-fluorouracil leads to *Wnt5a*-dependent F-actin misalignment in BM-derived mesenchymal stem and progenitor cells (MSPCs), which is associated with incorrect positioning of autophagosomes and lysosomes.[11] Diminished autophagy is 1 of the hallmarks of aging,[12] which can also be found in MSPCs from aging individuals.[13] Furthermore, reduced autophagy is associated with reduced expression of selective autophagy receptors, such as optineurin (OPTN), Tax1-binding protein 1, or sequestosome 1.[14] In MSPCs, such changes reduce osteogenesis and favor adipogenesis, which contributes to degenerative bone loss (osteoporosis) with increasing age.[15]

Here, we identify cellular and molecular changes in MSPCs from mice undergoing HSCT. Our analyses showed clear signs of MSPC dysfunction: oxidative stress, reduced autophagy, and elevated activity of CDC42 compared with MSPCs of age-matched controls. Pharmacological attenuation of CDC42 activity restored function of MSPCs from mice undergoing HSCT in vitro and mitigated bone degeneration after HSCT upon in vivo treatment. Targeting dysfunctional MSPCs in the setting of allo-HSCT by attenuation of CDC42 activity might be a novel approach to ameliorate osteopenia and osteoporosis in patients receiving allo-HSCT.

Methods

Mice

For the transplantation experiments (HSCT group), we used 129Ly5.1 mice (3 months old) as donors, and 129Bl6 mice (3 months old) as recipients. Age-matched (no transplantation, middle-aged, up to 13 months) and young (129Ly5.1, 3 months old) mice were included in the experiments as control groups. To establish their age categories, we distinguished 3- to 6-month-old (young; Y) mice from 14-month-old (middle-aged; 13A) mice.[16] The mice were housed under specific pathogen–free conditions and experiments were conducted per approved ethical guidelines (Government of Upper Bavaria approvals Vet_02-14-112 et al). Further details are available in supplemental Materials.

Murine and human MSPC isolation and in vitro cell culture analysis assays

Murine long bones were flushed and crushed, followed by collagenase digestion as previously described.[11,17] After digestion, flushed or released endosteal cells were used for flow cytometry analysis and cell sorting. In the analysis and sorting of BM subpopulations we distinguished endothelial cells (ECs; $CD31^+$ $CD45/Ter119^-$), osteoblastic cells, (OBCs, $CD31^-$ $CD45/Ter119^-ALCAM^+$ $SCA1^-$), and MSPCs ($CD31^-$ $CD45/Ter119^-$ $ALCAM^{-/low}$ $SCA1^+$), as previously described.[18] The remaining bone fragments were plated (0.1% gelatin coating) and the adherent cells were cultured until passage 3 (p3; 80% confluency) in a humidified atmosphere, 5% CO_2 and at 37°C in minimal essential medium alpha with ribonucleic acids, GlutaMAX, 10% fetal calf serum, 1% penicillin-streptomycin, and 0.1% β-mercaptoethanol. Cell numbers were determined and reseeded (1×10^3 cells per cm^2) for different cell culture assays at p4, unless stated otherwise.

Human BM samples were collected with informed consent from healthy individuals (derived from the remains of stem cell transplantation bags or isolated from femoral heads after a hip surgery). Human BM samples were also obtained from allo-HSCT recipients with various malignant hematopoietic conditions. All data, both from healthy individuals and patients, were normalized and combined for analysis. Use of patient materials were approved by the institutional review board at the Technical University of Munich, School of Medicine, Munich, Germany (study TUM 538/16). Characteristics of healthy individuals and patient's treatment regimens used before allo-HSCT can be found in supplemental Table 4. Human MSPCs were cultured in low-glucose minimal essential medium alpha, supplemented with 2 mM L-glutamine, 10 U/L, and 20 U/ml penicillin-streptomycin. Freshly prepared pooled human platelet lysate, at a concentration of 10% (volume per volume), was added to the cell culture following previously described methods.[11,19]

All in vitro assays, such as fluorescence-activated cell sorting, treatment with pharmacological compounds, enumeration of CFU-F, senescence assay, immunofluorescence (IF) staining (confocal IF), as well as assessment of mitochondrial function, can be found in detail in supplemental Materials.

In vivo transplantation assay and in vivo treatment with pharmacological compounds

Whole BM cells (2.5×10^5) were IV transplanted into lethally irradiated (8.5 Gy) recipient mice, detailed in supplemental Materials. For in vitro assays, MSPCs (p4) were cultured with the Cdc42 activity-specific inhibitor (CASIN) or a vehicle (dimethyl sulfoxide) for 4 hours before starting cell culture assays. In vivo experiments were conducted using CASIN (2.4 mg/kg) or the vehicle (phosphate-buffered saline and 15% ethanol).[11] After HSCT, the compounds were administered via intraperitoneal (IP) injection every 24 hours for 4 consecutive days (day 5, 6, 7, and 8).

Micro-CT

Isolated bones were fixed in 4% paraformaldehyde in phosphate-buffered saline for 3 days and then stored in 70% ethanol. Microcomputed tomography (micro-CT) was performed and analyzed using the SkyScan1176 micro-CT scanner (supplemental Table 3). We additionally analyzed and evaluated the percent bone volume (BV) via the ratio of BV to total volume (BV/TV) by measuring only the areas that showed clear BV with ImageJ software. By setting a threshold, we focused exclusively on the dense, bright areas indicative of bone. This allowed us to selectively measure and quantify the characteristics of the bone structures.

Human BMD measurements

After allo-HSCT, patients underwent annual bone mineral density (BMD) measurements for a minimum of 5 years as per institutional guidelines. BMD was assessed via quantitative computed tomography of the lumbar spine. The quantitative CT PRO Mindways 6.1 software (https://www.qct.com/QCTPro.html) was used. Detailed

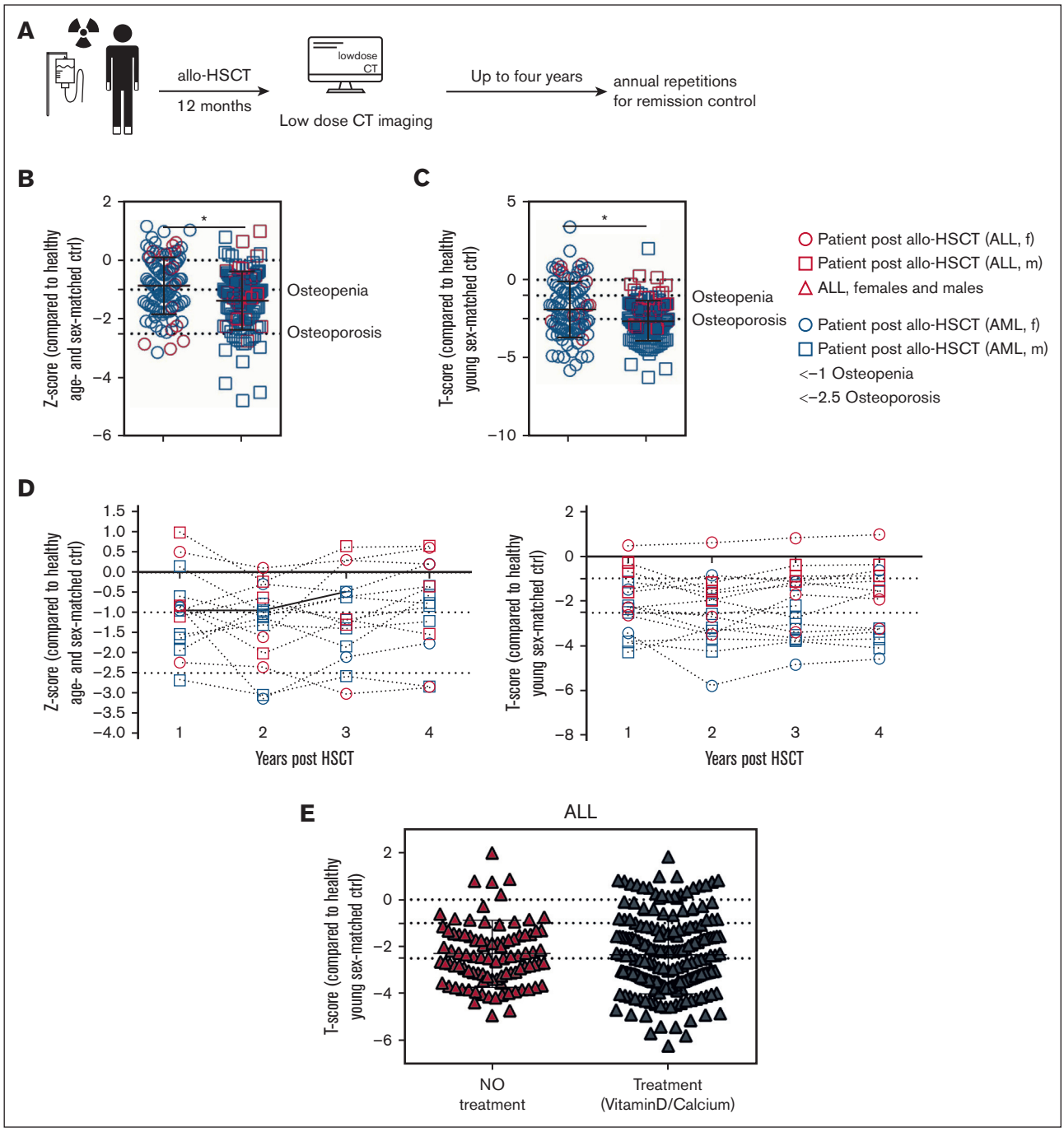

Figure 1. Human BMD measurements show induced osteoporosis after allo-HSCT. (A) Experimental design for human HSCT and myeloablation after allo-HSCT and analysis via CT 12 months after HSCT with annual repetitions for remission control (up to 4 years). Acute lymphoblastic leukemia (ALL; females, n = 17; males, n = 25) and acute myeloid leukemia (AML; females, n = 84; males, n = 97). (B) Z-score: comparison of the measured person's bone density with age- and sex-matched controls. (C) T-score: comparison of the measured person's density values with those of a healthy young adult (aged 20-30 years), comparison with peak bone density, sex matched. (D) Left graph: Z-score: comparison of the measured person's bone density with age- and sex-matched controls within the first 4 years after HSCT. Right graph: comparison of the measured person's density values with those of a healthy young adult (aged 20-30 years), comparison with peak bone density, sex-matched within the first 4 years after HSCT (right graph). (E) Analysis of differences in T-scores between vitamin D3–treated patients with Dekristol 20 0000 or calcium (calcium effervescent tablets of 500 mg) compared with untreated patients. The measurement of T- and Z-scores already incorporates BMD data across a wide age range (1-80 years) from healthy US Caucasian or Asian individuals, which constitutes a statistical analysis. *$P < .05$ (Kruskal-Wallis test: panels B,C). Data are represented as mean ± standard deviation (SD). ctrl, control; f, female; m, male.

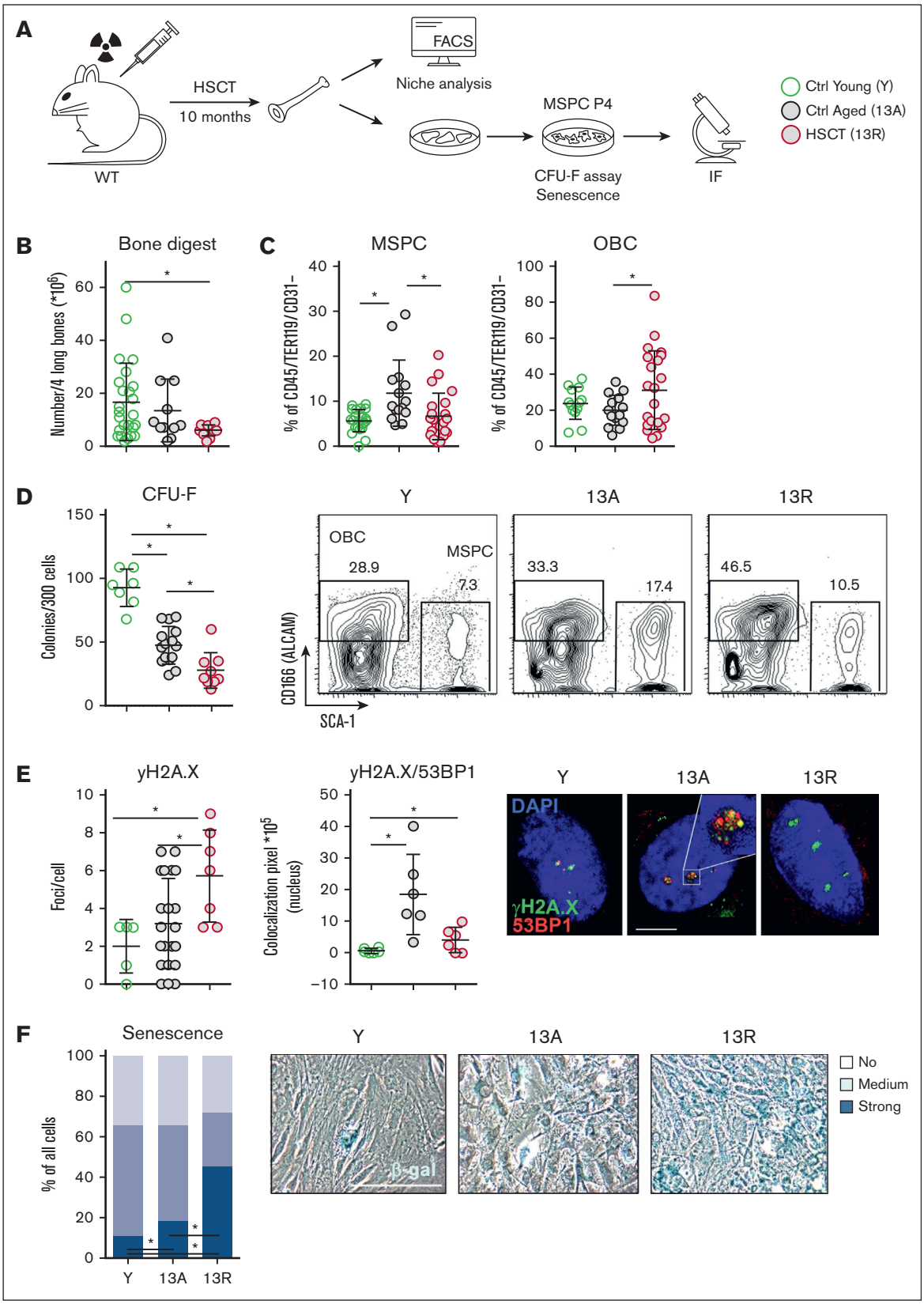

Figure 2. HSCT and permanent changes in the MSPCs. (A) Experimental design for HSCT into lethally irradiated 3-month-old wild-type mice (time point at the end of experiment: 13 months, 13R). Age-matched control group (13A) without treatment (HSCT). Analysis of the BM niche in 13-month-old mice (13A and 13R), and Y control group (3 months). Fluorescence-activated cell sorting (FACS) analysis of isolated stromal cells with subsequent cultivation of the MSPCs. (B) Graph shows the total cell number of 4

information can be found in supplemental Materials. T-scores and Z-scores were obtained retrospectively from patient records, with informed consent (ethics vote: 423/17 S).

A Z-score is used to compare an individual's bone density with the average for their age and sex, a T-score is used to compare bone density with the peak value observed in a healthy young adult. A score higher than or equal to −1 is considered normal. A value between −1 and −2.5 is referred to as osteopenia, a precursor of osteoporosis. Values lower than −2.5 is diagnosed as osteoporosis. In healthy young individuals, the Z and T-scores are typically close to 0, signifying that their bone density aligns with age and sex norms or corresponds to the peak bone density of a healthy young adult.

Bulk RNA-seq library preparation

RNA sequencing (RNA-seq) of BM MSPCs from Y, 13A, and (3 + 10) month old recipients (13R) mice was conducted using prime-sequencing based on molecular crowding SCRB-seq, with paired-end sequencing on an Illumina HiSeq1500. Detailed data processing and analysis are provided in supplemental Materials.

Statistics

Statistical analysis was conducted with Mann-Whitney tests for 2 groups, and Kruskal-Wallis tests for multiple groups, using Prism software. All statistical analyses were conducted using the Prism software package, and the results are presented as mean ± standard deviation. Detailed information can be found in supplemental Materials.

Results

A HSCT procedure results in permanent negative changes in BM-resident MSPCs

Osteoporosis is a commonly found complication in allo-HSCT.[1,2,20] More than 50% of female and 62% of male patients showed degenerative changes such as osteopenia or osteoporosis 1 year after allo-HSCT compared with healthy age- and sex-matched controls (Z-score; Figure 1A-B), and 86% of female and 91% of male allo-HSCT recipients showed clear bone loss compared with young controls (T-score; Figure 1C) in a patient cohort of the Technical University of Munich/University Hospital Klinikum rechts der Isar. Importantly, patients showed no significant improvement in bone density over time (Figure 1D) despite receiving standardized treatments such as vitamin D and calcium after transplantation, indicating that the osteoporotic changes due to HSCT may be difficult to revert (Figure 1E). To investigate the underlying mechanisms of transplant-associated long-term osteoporosis, we initially analyzed mice 10 months after the HSCT procedure.

HSCT was performed by transplanting BM cells in 3-month-old mice (young, Y) that received radiation as a preconditioning regimen. BM of the successfully reconstituted recipient animals was analyzed 10 months after HSCT (13R) to determine the long-term effect on bone-resident MSPCs ($CD31^-$ $CD45/Ter119^-$ $ALCAM^{-/low}$ $SCA1^+$) and compared with MSPCs of age-matched control mice (13A), which had not been preconditioned nor received HSCT (Figure 2A; supplemental Figure 1A). To assess the number and function of bone-forming cells after HSCT, $ALCAM^{-/low}$ MSPCs and $ALCAM^+$ $SCA1^-$ OBCs[18] were analyzed. The total number of cells from BM of 13R mice was lower than that of Y controls, whereas 13A controls were not significantly different from either Y or 13R (Figure 2B), implying successful but imperfect recovery/reconstitution of the BM in animals that underwent HSCT. Interestingly, BM showed a higher ALCAM-expressing OBC content in 13R mice than in 13A mice (Figure 2C). Next, we cultivated the MSPCs from these bones to determine their ability to generate CFU-F. The frequency of cells that were able to generate fibroblast-like colonies (CFU-F) was highest in Y MSPCs, with a diminished CFU-F frequency in the HSCT treatment and the age-matched control groups, suggesting the decline in CFU-F is time/aging related and additionally affected by HSCT (Figure 2D; supplemental Table 5). In addition, we found DNA damage in 13R MSPCs indicated by increased $\gamma H2AX^+$ double-strand break sites that are not colocalized with the DNA repair complex component 53BP1[21,22] (Figure 2E), as well as by a higher frequency of cells expressing senescence-associated β-galactosidase in 13R cultures (Figure 2F).

Altered mitochondrial quality control in MSPCs from mice undergoing HSCT

RNA-seq was performed on primary Y, 13A, or 13R MSPCs sorted from the BM (Figure 3A-B; supplemental Figure 2A-B). Comparisons between 13A and 13R MSPCs showed 257 differentially expressed genes (DEGs), 115 of which were downregulated in 13R cells (50 of those more than twofold) and 140 DEGs were upregulated (56 of which more than twofold; supplemental Figure 3C). Several of the DEGs downregulated in 13R MSPCs were genes coding for important proteins involved in mitophagy, selective autophagy, and guanosine triphosphate hydrolase (GTPase) signaling, such as ras homolog family member T1 (*Rhot1*), *Wasf2*, *Ddit3*, *Lamp1*, *Atg5*, *Tax1bp1* and *Gipc1* (Figure 3C). Further STRING (Search Tool for Retrieval of Interacting Genes/Proteins) analysis connected several of these DEGs to mitochondria-associated proteins, MYO6, parkin RBR E3 ubiquitin protein ligase (PRKN), PTEN-induced kinase 1 (PINK1), SQTSM1, and TOMM20, to possible regulation by CDC42 (Figure 3D; supplemental Figure 2D).

Figure 2 (continued) long BM flushed bones after collagenase digestion. (C) Relative numbers of immature MSPCs ($CD45/Ter119/CD31^-$ $Sca\text{-}1^+$ $Alcam^{-/low}$, left) and OBCs ($CD45/Ter1197CD31^-$ $Sca\text{-}1^-$ $Alcam^+$, right); FACS gating strategy in Landspersky et al.[11] Representative contour plots of collagenase-digested bones (below). (D) Number of colony-forming mesenchymal stem cells (CFU-F) of 300-plated cultured MSPCs (p4). (E) Graphs show foci/cell (left) and colocalization pixel of γH2A.X and 53BP1 in the nucleus of cultured MSPCs (p4; right). Representative IF images of γH2A.X (green) and 53BP1 (red) in compact bone-derived MSPCs (p4; below) counterstained with DAPI (4′,6-diamidino-2-phenylindole). (F) Average proportion of bluish β-galactosidase (β-gal)–stained compact bone–derived MSPCs (p4, left). White bar indicates cells with no detectable staining whereas light blue and dark blue refer to partially and strongly β-gal–stained cells, respectively; Y (n = 5), 13A (n = 6), and 13R (n = 4). The Kruskal-Wallis test was applied here between the 3 groups examined for each of the 3 β-gal staining concentrations (strong, medium, and no). Representative pictures of β-gal–stained MSPCs (right). The analysis represents 2-3 independent experiments. Scale bars, 5μm (E) and 20μm (F). $^*P < .05$ (Kruskal-Wallis test: panels B-F). Data are represented as mean ± SD. Ctrl, control.

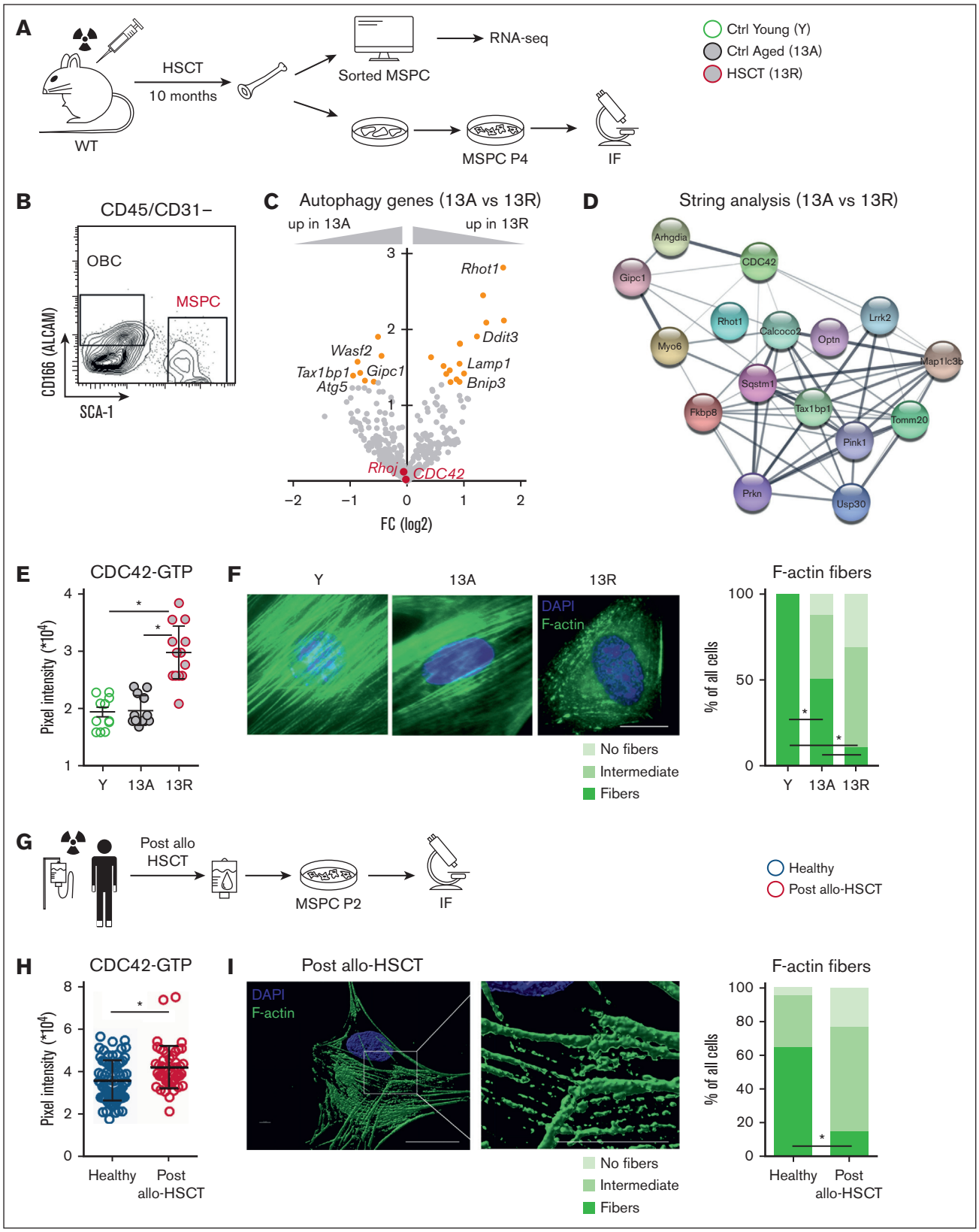

Figure 3. Impaired F-actin signaling. (A) Experimental design for HSCT into lethally irradiated 3-month-old wild-type mice (time point at the end of experiment: 13 months, 13R). Age-matched control group (13A) without HSCT. Analysis of the BM niche in 13-month-old mice (13A and 13R), and Y control group (3 months). RNA-seq analysis of sorted MSPCs (B) with subsequent cultivation of the MSPCs until p4 for analysis with IF assay. (C) Volcano plot showing differential protein expression of autophagy genes, with

The small GTPase CDC42 is a critical regulator of F-actin assembly and F-actin cages, targeting damaged mitochondria.[23,24] In addition, the fact that persistently elevated activation of CDC42 contributes to degenerative processes and aging in several different tissues,[11,25-27] led us to investigate CDC42 activity in MSPCs in more detail, first by anti–CDC42-GTP IF staining. The level of CDC42-GTP was indeed markedly upregulated in 13R MSPCs compared with both Y and 13A MSPCs (Figure 3E). In addition, MSPCs from 13R mice show significantly less elongated F-actin fibers compared with MSPCs from either Y or 13A controls (Figure 3F).

We also analyzed human MSPCs from patients with leukemia, 6 to 24 months after receiving allo-HSCT and who were within complete remission and compared them to MSPCs from hematologically healthy aged-matched controls (Figure 2G; supplemental Figure 1B). The allo-HSCT recipients were conditioned before transplantation, either by total body irradiation (2 patients) or by chemotherapy (5 patients; supplemental Table 4). As in mice, we found high levels of active CDC42-GTP as well as less elongated F-actin fibers in MSPCs from these donors compared with MSPCs from healthy age-matched controls (Figure 3H-I). In addition, also the human MSPCs from the transplant recipients showed a larger proportion of senescent cells (supplemental Figure 2F). In summary, also human MSPCs from patients that underwent allo-HSCT show changes associated with premature aging, like murine MSPCs in transplant recipients.

Damaged mitochondria are marked for mitophagy, but not cleared, in 13R MSPCs

Damaged mitochondria are targeted for mitophagy by F-actin.[23,24] Changes in the F-actin fiber length in MSPCs from transplant recipients (Figure 3I) might therefore affect mitophagy. Costaining of F-actin and mitochondria (via TOMM20, a protein localized on the outer membrane of mitochondria) revealed F-actin encapsulated mitochondria in 13A MSPCs, and even stronger in 13R MSPCs, whereas in Y MSPCs the mitochondria were not directly surrounded by F-actin fibers (Figure 4A-B). Furthermore, we detected increased reactive oxygen species (ROS) production in 13R MSPCs (supplemental Figure 3A-B), indicative of an increase in damaged mitochondria.[28] These findings are in line with a view that damaged mitochondria are encapsulated in 13R MSPCs but do not seem to be cleared. RHOT1 (also known as MIRO-1) identifies damaged mitochondria.[29] Colocalization experiments showed RHOT1 was strongly colocalized with TOMM20$^+$ mitochondria in both 13A and 13R MSPCs compared with Y controls (Figure 4C), indicating that damaged mitochondria are marked by RHOT1 in these cells. The motor-cargo protein MYO6 anchors mitochondria marked with RHOT1 to F-actin.[23,30] Our experiment showed that MYO6 colocalized at high levels with TOMM20$^+$ mitochondria in 13A and 13R MSPCs (Figure 4D), indicating that the RHOT1-MYO6 complex marked the damaged mitochondria. In contrast, MYO6 did not colocalize at all to F-actin in 13R but colocalization was detected in 13A MSPCs (Figure 4E; supplemental Figure 3C). Our results are consistent with a view that damaged mitochondria are recognized and encapsulated into F-actin cages in both 13A and 13R MSPCs, however, in 13R MSPCs, the mitochondria are not connected to F-actin for transport, a critical requirement for clearance of damage mitochondria.

The disruption of the final steps in mitophagy noted in 13R cells may also be relevant to MSPC fate. The selective autophagy receptors interact with MYO6,[23,31] and less OPTN has been associated with osteoporosis.[15] In our experiments, expression of OPTN is indeed reduced in 13R vs 13A MSPCs (Figure 4F).

Improving the regeneration of MSPCs by targeting CDC42 activation in vitro

Our data imply altered F-actin biology in 13R MSPCs, which are likely linked to altered clearance of mitochondria. We, and others, have shown that a defective F-actin fiber orientation in stressed cells is, at least partly, due to elevated activation of CDC42.[25-27] Attenuation of this CDC42 activation by a CASIN can restore the function of acutely stressed MSPCs.[11] Because CDC42-GTP levels were also elevated in both murine and human MSPCs from transplant recipients (Figure 3E-H), we therefore tested whether attenuation of CDC42 activity in HSCT MSPCs could rescue changes in the MSPCs, restore the transport of damaged mitochondria to mitophagosomes, and reverse the impaired function of 13R MSPCs.

In vitro treatment of 13R MSPCs with CASIN indeed restored alterations in the local environment, such as increased cell senescence and γH2A.X-directed DNA damage repair mechanisms (Figure 5A-C; supplemental Figure 4A-B). In addition, the in vitro treatment reduced CDC42-GTP levels and restored both F-actin levels and fiber formation, as well as mitochondrial diameter and actin cages (Figure 5D-F; supplemental Figure 4C-E). Treated MSPCs show a reconnection of F-actin and MYO6 (Figure 5G).

Figure 3 (continued) adjusted *P* values (false discovery rate [FDR]) plotted against $\log_2$ fold change (FC). 13A, n = 10 and 13R, n = 7. The dark dots show proteins that meet the FDR threshold for statistical significance (FDR < 0.05) and are considered differentially expressed. (D) Analysis of the DEGs using STRING (Search Tool for Retrieval of Interacting Genes/Proteins) for visualizing an interaction network. (E) Graph shows the protein content of CDC42-GTP in cultured MSPCs (p4). (F) Left: representative IF images of MSPCs (p4). IF staining of F-actin (green) counterstained with DAPI (blue). Right: evaluation of the orientation of F-actin fibers stained with phalloidin. Percentage of all cells showing fibers (bar in dark green), intermediate oriented fibers (bar in bright green), or no stress fibers (white bar). The Mann-Whitney test was applied here between the 3 groups examined for each of the 3 stress fiber orientations (fibers, intermediate, and no fibers). (G) Experimental design for human HSCT and myeloablation via chemotherapeutics (n = 5) or irradiation (n = 2) and analysis from 6 months up to 24 months after HSCT in human BM samples. Healthy donor samples as controls (n = 6). (H) Graphs show the protein content of CDC42-GTP measured by ImageJ software from healthy age-matched controls (n = 6) and allo-HSCT recipient (n = 7; left). (I) Left: representative IF staining of F-actin (green; right) counterstained with DAPI (blue) of a patient sample after allo-HSCT. Right: evaluation of the orientation of F-actin fibers stained with phalloidin. Percentage of all cells showing fibers (bar in dark green), intermediate oriented fibers (bar in bright green pattern), or no fibers (white bar). The Mann-Whitney test was applied here between the 3 groups examined for each of the 3 fiber orientations (fibers, intermediate, and no fibers). The analysis represents 2-3 independent experiments except for the RNA-seq analysis, which was performed once with a high number of samples (Y, n = 9; 13A, n = 10; and 13R, n = 7). Scale bars, 10 μm. *$P < .05$ (Kruskal-Wallis test, panel E,H; F-actin fibers/intermediate/no fibers were either present [value = 1], or not [value = 0]). Only the results for the presence of elongated F-actin fibers are presented in panels F and I and analyzed with the nonparametric Mann-Whitney test. Data are represented as mean ± SD.

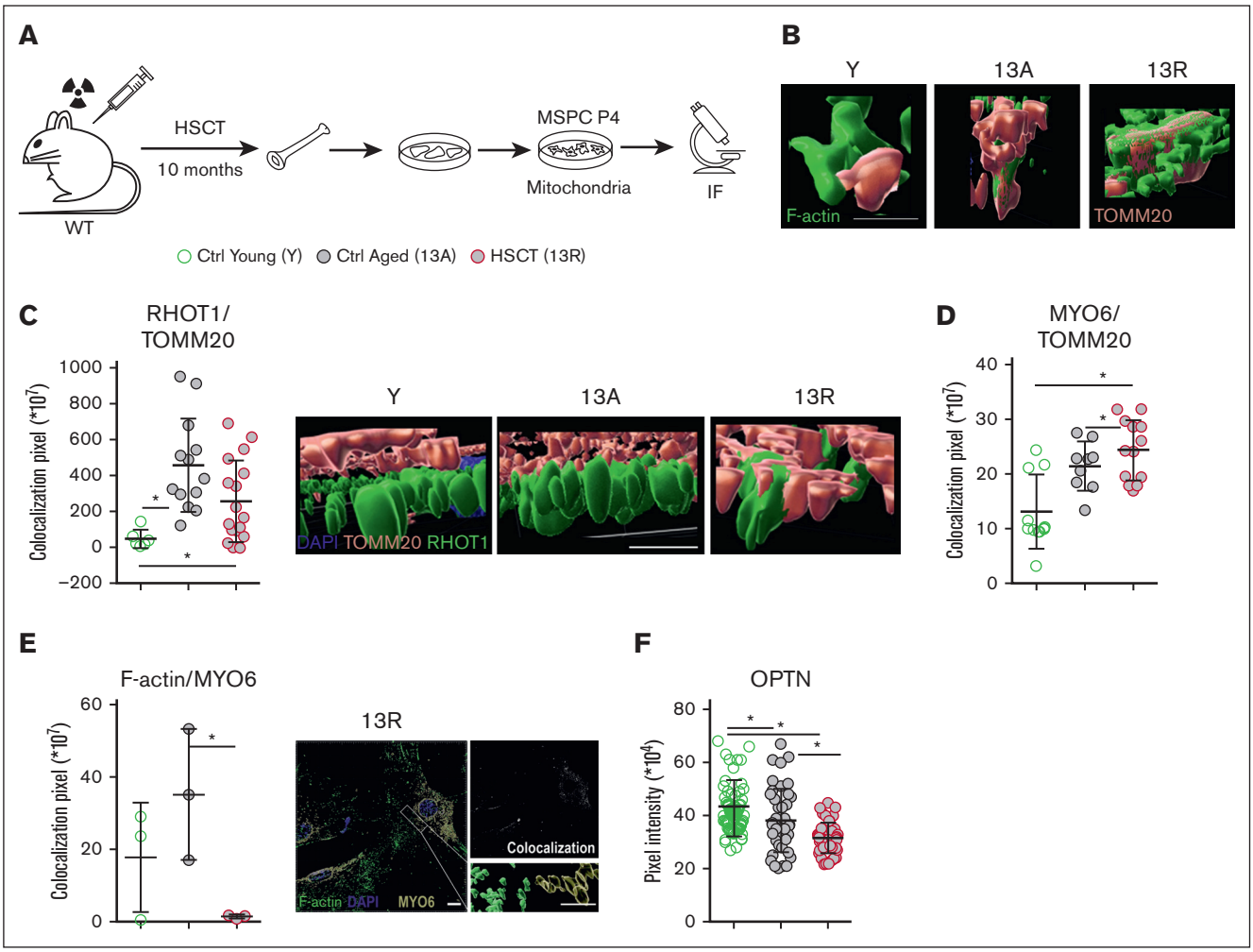

Figure 4. Damaged mitochondria in MSPCs of HSCT-mice. (A) Experimental design for HSCT into lethally irradiated 3-month-old wild-type mice (time point at the end of experiment: 13 months, 13R). Age-matched control group (13A) without HSCT. Analysis of the BM niche in 13-month-old mice (13A and 13R), and Y control group (3 months). Analysis of cultured MSPCs until p4 for analysis with IF assay. (B) Representative confocal microscopy images stained for F-actin (green) and TOMM20 (red) in MSPCs (p4). Image section of a mitochondrion with actin cages. (C) Colocalization pixel of RHOT1 and TOMM20 measured by ImageJ software (left) and representative confocal microscopy images of RHOT1 (green) and TOMM20 (red) counterstained with DAPI (blue, right). (D) Colocalization pixel of MYO6 and TOMM20 measured by ImageJ software. (E) Colocalization pixel of MYO6 and F-actin measured for 3 cells with Imaris software (left) and representative confocal microscopy images for F-actin (stained in green) and MYO6 (yellow) counterstained with DAPI (blue) with additional visualization of colocalization (white) in MSPCs of 13R mice (P4, right). (F) Protein content of OPTN of MSPCs (p4) measured by ImageJ software (the analysis represents 2-3 independent experiments). Scale bars (mitochondria), 0.2µm; scale bars (nucleus), 10 µm. *$P < .05$ (Kruskal-Wallis test: panels C-F). Data are represented as mean ± SD.

Conversely, where RHOT1 encapsulates mitochondria in 13R MSPCs (Figure 4C), CASIN treatment strongly reduces binding of RHOT1 to TOMM20 indicating either that the treatment interferes with RHOT1 binding or that mitochondria are normally cleared resulting in smaller and functional mitochondria (supplemental Figure 4F). These in vitro treatment experiments indicate that CASIN might repair mitochondrial quality control in 13R MSPCs by reconnecting MYO6 with now again elongated F-actin fibers. This suggests a reversal of the disrupted mitophagy process and suggests a return to a healthier, more functional state of mitochondria in 13R MSPCs after CASIN intervention. Additionally, we investigated whether RHOT1 colocalized with LAMP1, demonstrating that mitophagolysosome formation is possible in 13A and 13R after in vivo CASIN treatment. Whereas without treatment, we observed low levels of RHOT1/LAMP1 colocalization, CASIN treatment increased colocalization in 13A and 13R MSPCs compared with the Y control group (Figure 5H; supplemental Figure 4G). This finding supports the idea that CASIN treatment promotes the clearance of RHOT1-marked mitochondria via mitophagy in these experimental groups.

Attenuation of CDC42 activity in vivo after HSCT prevents osteoporotic changes

For testing the effects of attenuation of CDC42 activity in vivo in animals that underwent HSCT, we chose a treatment regimen in which CASIN was injected IP on 4 consecutive days on day 5 through 8 after HSCT (day 0), and animals were again monitored

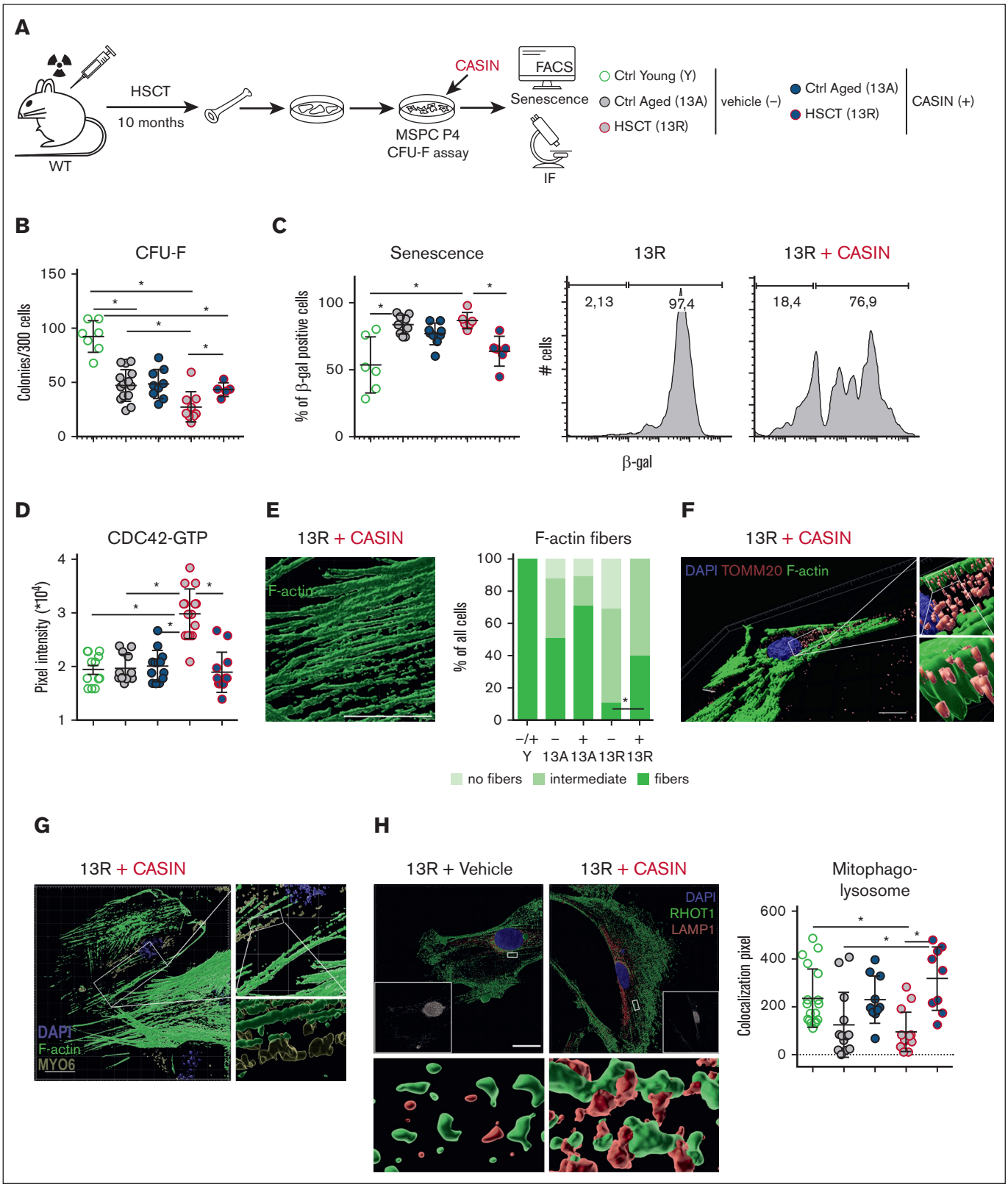

Figure 5. Pharmacological treatment rescues changes in the microenvironment and mitophagy in MSPCs in vitro. (A) Experimental design for HSCT into lethally irradiated 3-month-old wild-type mice (time point at the end of experiment: 13 months, 13R). Age-matched control group (13A) without HSCT. Analysis of the BM niche in 13-month-old mice (13A and 13R), and Y control group (3 months). MSPC culture and CASIN (blue filled symbols) or vehicle (dimethyl sulfoxide, gray-filled symbols) treatment in vitro at p4. (B) Number of colony-forming mesenchymal stem cells (CFU-F) of 300 plated cultured MSPCs (p4). (C) Average proportion of β-gal positive–stained compact

10 months after transplant (Figure 6A). In vivo application of CASIN reduces the activity of CDC42 in vivo in BM cells.[11] First, the elevated BM OBC numbers that were associated with 13R animals returned in 13R + CASIN mice to levels seen in 13A mice (Figure 6B). Functional assays show that 10 months after HSCT, MSPCs show an increase in damaged mitochondria, indicated by elevated ROS levels and low tetramethylrhodamine methyl ester staining (Figure 6C-D). Interestingly, by short in vivo CASIN treatment administered 10 months before analysis, ROS levels were significantly reduced, and the membrane potential recovered in MSPCs. Next, we analyzed femora to determine macro(cortical)- and micro(trabecular)-structural parameters using micro-CT (Figure 6A). This analysis showed that BV/TV was reduced in the femurs of HSCT animals. Importantly, CASIN administration in vivo markedly improved BV/TV to the levels of young and age-matched controls (Figure 6E). The trabecular and cortical microarchitecture was significantly improved in 13R + CASIN femora. Furthermore, there was significantly elevated trabecular thickness in 13R + CASIN animals than 13A and 13R bones, and significantly elevated cortical thickness in 13R + CASIN animals than 13A animals (Figure 6F-G). Interestingly, CASIN treatment within the age-matched control group showed the same effects (supplemental Figure 5A-D). In summary, pharmacological targeting of CDC42 activity in vivo after HSCTs might attenuate unwanted, likely preconditioning-associated, changes in MSPCs and bones.

Discussion

Our study highlights long-term effects of ablative conditioning with subsequent BM transplantation (HSCT). Although changes in bone remodeling and bone turnover induced by HSCT over time have been reported by others, details of the underlying mechanisms are incompletely understood. Our findings demonstrate that post-HSCT MSPCs show markedly reduced proliferation and increased number of committed MSPCs, coupled with cellular senescence, persisting DNA and mitochondrial damage, and reduced F-actin orientation. Although mitochondrial function has been described to be critical for the regenerative capacity of HSCs,[32,33] the role of such processes for the function of post-HSCT MSPCs is poorly studied.

Our results are in line with recent data showing that MSPC mitochondria respond to stressors by undergoing fusion, followed by fission, and finally mitophagy, which contributes to the osteogenic differentiation process.[34,35] This sequence of events is disrupted in 13R MSPCs, in which oxidative stress is elevated, fission and mitophagy are reduced, likely contributing to HSCT-associated osteoporosis. It appears from our experiments that HSCT aggravates mitophagy in such a manner that selective degradation of dysfunctional mitochondria is strongly reduced. In sum, these observations suggest that accumulation of damaged mitochondria and the accompanying oxidative stress supports the osteoporotic decrease in bone mass,[36] a hypothesis further supported by our evaluation of yearly checkup data from allo-HSCT patients. The patient data further show that in human allo-HSCT recipients, osteoporotic changes in bone mass persist, despite treatments of the secondary osteoporosis. These findings propose that osteoporotic remodeling after allo-HSCT is irreversible. Considering this, our experiments favor the point of view that initiating treatment prior to the diagnosis of osteopenia or osteoporosis, independent of risk factors, may be relevant for the clinical management of HSCT patients to prevent or repair anticipated osteoporotic changes.

We, and others, have found that attenuation of CDC42 activity has major effects on the F-actin[11,37] and tubulin[25] cytoskeleton. Both cytoskeletal components are critical for cellular maintenance processes, such as autophagy and vesicle transport. Clearance of damaged mitochondria is thought to be initiated by recognition of damaged mitochondria by a complex of RHOT1, PINK1, and PRKN,[38] which binds to selective autophagy receptors[39] as well as recruits so-called actin cages through binding to the MYO6 motorprotein.[23] CDC42 is involved in this process, because it triggers the necessary actin nucleation.[40] In our experiments, we found that in post-HSCT MSPCs, CDC42 is persistently overactivated and desensitized to stimuli, suggesting aging-like functional disruption as previously noted in HSCs[25] and other cell types.[26,27]

Previous studies found that both cytostatic- or irradiation-mediated myeloablation, causes bone loss.[41] To mitigate bone loss, therapies have been proposed to reduce osteoclast activity, or may increase osteoblast function.[42] Early studies showed that bisphosphonates, which are calcium-chelating molecules,[43] effectively inhibit osteoclast-mediated bone resorption.[44] Moreover, bisphosphonates also act to reduce prenylation and, by doing so, inhibit membrane trafficking of small GTPases, including CDC42,[45] as a result of which activated CDC42 may accumulate. The effects of bisphosphonates on HSCs or the hematopoietic niche are, however, controversially discussed, for which positive effects on CFU-F frequency,[46,47] no effects on HSCs,[41] as well as deleterious effects on HSCs,[48] B-lymphopoiesis,[49] and MSPCs have

Figure 5 (continued) bone–derived MSPCs (p4, left). Representative FACS plots for β-gal–positive 13R with or without CASIN MSPCs. (D) Protein content of CDC42-GTP measured with ImageJ software. (E) Left: representative F-actin staining in cultured 13R + CASIN MSPCs (phalloidin, green). Evaluation of the orientation of F-actin fibers stained with phalloidin. Right graph: percentage of all cells showing fibers (bar in dark green), intermediate oriented fibers (bar in bright green), or no fibers (white bar). The Mann-Whitney test was applied here between all groups examined for each of the 3 fiber orientations (fibers, intermediate, and no fibers). For a better overview, not all significant values are shown. Some of them (without/no CASIN treatment) are already shown in Figure 3F. In addition, the following groups are significant: *Y vs 13A+; Y vs 13R+; 13A+ vs 13R+. (F) Representative confocal microscopy images stained for F-actin (green) and TOMM20 (red) counterstained with DAPI (blue) of 13R MSPCs (p4) with and without CASIN treatment. Image section of mitochondria embedded in actin structure. (G) Representative confocal microscopy images for F-actin (stained in green) and MYO6 (yellow) in MSPCs of 13R mice (p4) with and without CASIN treatment. (H) Left: representative confocal microscopy images for RHOT1 (stained in green) and LAMP1 (red) in MSPCs of 13R mice (p4) with and without CASIN treatment. Colocalization is shown in white. Right graph: colocalization pixel of RHOT1 and LAMP1 measured by ImageJ software. The analysis represents 2-3 independent experiments. Scale bars (mitochondria), 0.2μm; Scale bars (nucleus), 10μm. *$P < .05$ (Kruskal-Wallis test: panels B,C,D,H; F-actin fibers/intermediate/no fibers were either present [value = 1], or not [value = 0]). Only the results for the presence of elongated F-actin fibers are presented in panel E and analyzed with the nonparametric Mann-Whitney test. Data are represented as mean ± SD. Y, young; A+, aged 13 months with CASIN (=13A+); 13R+, regenerated 13 months with CASIN.

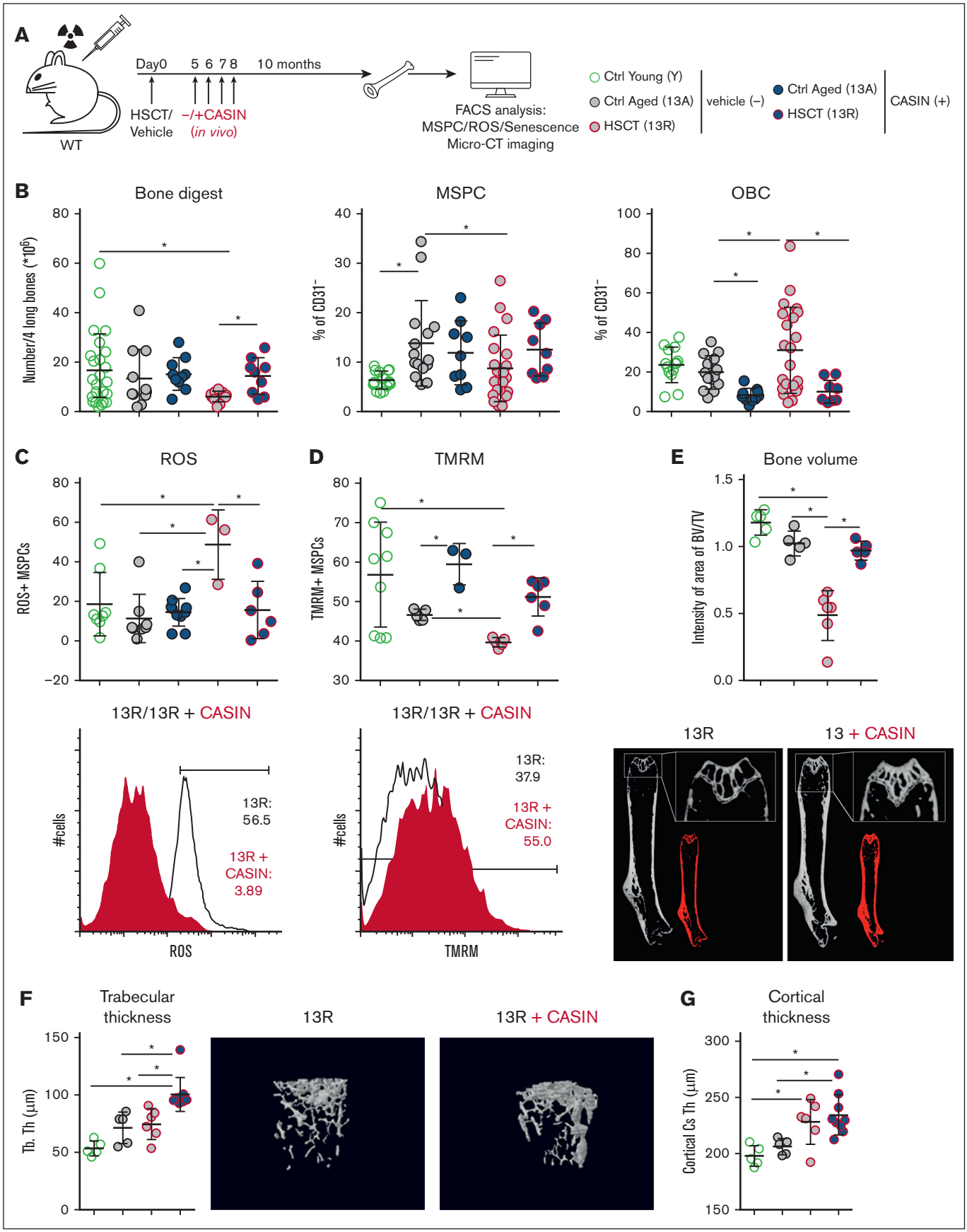
A
WT
Day0
5 6 7 8
10 months
HSCT/
Vehicle
–/+CASIN
(in vivo)
FACS analysis:
MSPC/ROS/Senescence
Micro-CT imaging
Ctrl Young (Y)
Ctrl Aged (13A)
HSCT (13R)
vehicle (–)
Ctrl Aged (13A)
HSCT (13R)
CASIN (+)
B
Bone digest
Number/4 long bones (*10^6)
MSPC
% of CD31−
OBC
% of CD31−
C
ROS
ROS+ MSPCs
D
TMRM
TMRM+ MSPCs
E
Bone volume
Intensity of area of BV/TV
13R/13R + CASIN
#cells
13R:
56.5
13R +
CASIN:
3.89
ROS
13R/13R + CASIN
#cells
13R:
37.9
13R +
CASIN:
55.0
TMRM
13R
13 + CASIN
F
Trabecular
thickness
Tb. Th (µm)
13R
13R + CASIN
G
Cortical
thickness
Cortical Cs Th (µm)

Figure 6.

been reported.[47,49] These side effects may limit the use of bisphosphonates in HSCT recipients, the recommended therapy for secondary osteoporosis after HSCT.[50]

Because osteoporotic changes are a frequent and seemingly irreversible complication, exacerbated in allo-HSCT because of more aggressive conditioning, chronic graft-versus-host disease (GVHD) and prophylactic steroid treatment,[51,52] research of additional therapeutics to treat secondary osteoporotic changes by stimulating osteogenic cells are being pursued.[53] Several of these agents have entered clinical trials, in which side effects such as gastrointestinal disorders, hypercalcemia, and osteonecrosis of the jaw are frequently noted.[53] Additional preclinical studies target myeloablation-induced senescence[54] using proteasome inhibition,[55,56] and our experiments add that early treatment to attenuate CDC42 activation positively affects both BV and trabecular thickness of femoral bones. Our studies may facilitate additional possibilities to treat osteoporotic changes after HSCT using a single agent or in combination with existing therapies.

Whereas bisphosphonates target prenylation and thereby act indiscriminately on many small GTPases, CASIN specifically inhibits the RhoGDI/CDC42 complex,[57] leaving other small GTPases unaffected. Considering that CDC42-GTP accumulates in different cell types with age, the use of CASIN may particularly benefit older HSCT recipients. We demonstrate that CDC42-GTP is upregulated in MSPCs, and reduced in CASIN-treated HSCT recipients. This appears to contradict reports in which bisphosphonates inhibit prenylation and promote CDC42-GTP accumulation in myeloid cells.[45] In contrast, because CDC42 is a central component of the noncanonical Wnt pathway, our findings support the use of anti-Wnt signaling therapies, such as antisclerostin therapy, which reduces osteoporosis by reducing osteoblast apoptosis after radiation.[58]

By administering CASIN immediately after HSCT, we adopted a treatment schedule that could feasibly be developed for HSCT protocols, with many patients being middle-aged to advance-aged and the treatment could be performed while stationary from the HSCT procedure. It is tempting to speculate that CASIN treatment either prevents osteoporotic changes or may partly reverse an already existing osteoporosis as well as further secondary side effects on MSPCs resulting from patient conditioning, not only in HSCT procedures but also in other cancer treatments.

Limitations of this study

Our in vitro and in vivo experiments focus on CDC42 activation as a therapeutic target for supporting osteogenic MSPCs. As such, we have not included an in-depth analysis of osteoclasts and their bone-resorbing activity. It is highly likely, however, that IP-injected CDC42 activity modulators will not only affect MSPCs of the BM but will also act on many other cells, including osteoclasts. In particular, bone resorption relies on the formation of actin rings, which, in turn, require CDC42 activation for assembly of the ARP2/3 actin nucleation complex.[59] Thus, it would be interesting to study in the future how the (dis)balance between bone formation by osteoblasts and bone resorption by osteoclasts is affected by attenuation of CDC42 activity in murine and human HSCT-derived cells.

Furthermore, congenic transplantation in mice does not match all aspects and complications in clinical allo-HSCT, and it is likely that immunosuppression, for example with corticosteroids, and GVHD, contribute to disrupted bone homeostasis in humans. In addition, osteoporotic changes after allo-HSCT are, in general, more severe than those observed in autologous HSCT.[51,52] However, late toxicities of autologous HSCT are driven by the drugs used for conditioning, which historically include busulfan and, for acute lymphoblastic leukemia, also total body irradiation, indeed similar to allo-HSCT. Indeed, 1 study finds that reduced BMD is found with similar incidence and severity in autologous HSCT and allo-HSCT in the absence of steroid use.[60]

In our view, these reported findings further highlight the potential benefit of CASIN treatment for preventing or reducing osteogenic degeneration, particularly in allo-HSCT recipients with GVHD and/or prolonged immunosuppressive therapy. Examining the additional role of GVHD and immunosuppression in mediating the observed effects is, however, beyond the scope of our study but will certainly need to be considered in future translational work with GVHD mouse models.

Acknowledgments

The authors thank Matthias Schiemann, Lynette Henkel, Immanuel Andrä, Corinne Angerpointner, and Susanne Dürr (Flow Cytometry Core Unit Technical University of Munich) for cell sorting. The authors also thank Ann-Engel Timm and Linda Cäsar for helping with experiments.

Figure 6. In vivo pharmacological treatment accompanying transplantation process rescues bone biology in mice. (A) Experimental design for HSCT into lethally irradiated 3-month-old wild-type mice (time point at the end of experiment: 13 months, 13R). Age-matched control group (13A) without HSCT. In vivo injection of CASIN (IP, blue filled symbols) at days 5, 6, 7, and 8 after HSCT (13R). Vector injection (phosphate-buffered saline and 15% ethanol, gray-filled symbols) at the same time points. Analysis of the BM niche of 13-month-old mice (13R with or without CASIN and 13A with or without CASIN) and Y control group (3 months, no HSCT; no CASIN and/or vehicle treatment). CT imaging of young and 13-month-old mice (13R + CASIN, 13R + vehicle, and 13A (13A no HSCT; no CASIN and/or vehicle treatment). (B) Graph shows the total cell number out of 4 long BM flushed bones after collagenase digest with CASIN or vehicle treatment (left graph) and relative numbers of immature MSPCs (CD45/Ter119/CD31$^-$ Sca-1$^+$ Alcam$^{-/low}$, middle left) and OBCs (CD45/Ter119/CD31$^-$ Sca-1$^-$ Alcam$^+$, middle right). (C) Graph shows ROS (reactive oxygen levels) staining measured with FACS analysis in cultured MSPC (p4) with representative FACS plot (right). 13R + vehicle, black; 13R + CASIN, red. (D) Graph shows tetramethylrhodamine methyl ester (mitochondrial membrane potential) staining measured with FACS analysis in cultured MSPC (p4) with representative FACS plot (right). 13R + vehicle, black; 13R + CASIN, red. (E) Micro-CT image of 1 dissected long bone (femur) per mouse (all males). Percentage of BV relative to total volume (TV, graph left) measured with ImageJ software and representative micro-CT images of 13R + CASIN (right). (F) Trabecular thickness analyzed with micro-CT imaging with representative micro-CT image of trabecular structures in mouse femur of 13R + CASIN (right). (G) Cortical thickness analyzed with micro-CT imaging. The analysis represents 2-3 independent experiments. The micro-CT imaging was performed once. *$P < .05$ (Kruskal-Wallis test: panels B-G). Data are represented as mean ± SD. Cs.Th, cortical thickness; PB, peripheral blood; Tb.Th, trabecular thickness.

This study was funded by the German Research Foundation (DFG; grants FOR 2033 [project B3], OO 8/18 and OO 8/21 [R.A.J.O.]). K.S.G received funding from the European Research Council under the European Union's Horizon 2020 Marie Sklodowska-Curie Innovative Training Network (grant agreement no. 953407).

Authorship

Contribution: T.L., J.G., R.A.J.O., and C.S. designed experiments and interpreted results; T.L., J.G., M. Saçma, M. Stein, K.B., J.S.H., F.H., S.R.M., E.S., and C.S. performed experiments and collected data; J.R., E.H., D.R., J.T., F.B., M.V., P.H., K.S.G., H.G., and W.E. contributed vital reagents and analytical tools; T.L., J.G., M. Saçma, M. Stein, J.R., B.V., R.A.J.O., and C.S. analyzed and interpreted data and performed statistical analyses; and T.L., R.A.J.O., and C.S. wrote the manuscript.

Conflict-of-interest disclosure: The authors declare no competing financial interests.

ORCID profiles: T.L., 0009-0001-7323-5113; M.S., 0000-0003-2926-6219; J.G., 0000-0002-5070-3404; K.B., 0000-0003-4028-5357; J.R., 0000-0002-4680-2071; B.V., 0000-0002-1084-7067; J.T., 0000-0003-3691-275X; J.S.H., 0000-0002-1531-0517; K.S.G., 0000-0002-6276-8002; W.E., 0000-0002-4056-0550; H.G., 0000-0002-5794-5430; R.A.J.O., 0000-0002-4947-0412; C.S., 0000-0002-0377-1412.

Correspondence: Christina Schreck, Department of Internal Medicine III, Klinikum rechts der Isar, Technische Universität München, Ismaningerstrasse 22, 81675 München, Germany; email: christina.schreck@tum.de; and Robert A. J. Oostendorp, Department of Internal Medicine III, Klinikum rechts der Isar, Technische Universität München, Ismaningerstrasse 22, 81675 München, Germany; email: robert.oostendorp@tum.de.

References

1. Schimmer AD, Mah K, Bordeleau L, et al. Decreased bone mineral density is common after autologous blood or marrow transplantation. *Bone Marrow Transplant*. 2001;28(4):387-391.
2. Schimmer AD, Minden MD, Keating A. Osteoporosis after blood and marrow transplantation: clinical aspects. *Biol Blood Marrow Transplant*. 2000;6(2A):175-181.
3. Savani BN, Donohue T, Kozanas E, et al. Increased risk of bone loss without fracture risk in long-term survivors after allogeneic stem cell transplantation. *Biol Blood Marrow Transplant*. 2007;13(5):517-520.
4. Inamoto Y, Lee SJ. Late effects of blood and marrow transplantation. *Haematologica*. 2017;102(4):614-625.
5. Qadir A, Liang S, Wu Z, Chen Z, Hu L, Qian A. Senile osteoporosis: the involvement of differentiation and senescence of bone marrow stromal cells. *Int J Mol Sci*. 2020;21(1):349.
6. Frobel J, Landspersky T, Percin G, et al. The hematopoietic bone marrow niche ecosystem. *Front Cell Dev Biol*. 2021;9:705410.
7. Cai Y, Song W, Li J, et al. The landscape of aging. *Sci China Life Sci*. 2022;65(12):2354-2454.
8. Zhong L, Yao L, Tower RJ, et al. Single cell transcriptomics identifies a unique adipose lineage cell population that regulates bone marrow environment. *Elife*. 2020;9:e54695.
9. Mo C, Guo J, Qin J, et al. Single-cell transcriptomics of LepR-positive skeletal cells reveals heterogeneous stress-dependent stem and progenitor pools. *EMBO J*. 2022;41(4):e108415.
10. Zhang H, Liesveld JL, Calvi LM, et al. The roles of bone remodeling in normal hematopoiesis and age-related hematological malignancies. *Bone Res*. 2023;11(1):15.
11. Landspersky T, Sacma M, Riviere J, et al. Autophagy in mesenchymal progenitors protects mice against bone marrow failure after severe intermittent stress. *Blood*. 2022;139(5):690-703.
12. Lopez-Otin C, Blasco MA, Partridge L, Serrano M, Kroemer G. Hallmarks of aging: an expanding universe. *Cell*. 2023;186(2):243-278.
13. Ma Y, Qi M, An Y, et al. Autophagy controls mesenchymal stem cell properties and senescence during bone aging. *Aging Cell*. 2018;17(1):e12709.
14. Gatica D, Lahiri V, Klionsky DJ. Cargo recognition and degradation by selective autophagy. *Nat Cell Biol*. 2018;20(3):233-242.
15. Liu ZZ, Hong CG, Hu WB, et al. Autophagy receptor OPTN (optineurin) regulates mesenchymal stem cell fate and bone-fat balance during aging by clearing FABP3. *Autophagy*. 2021;17(10):2766-2782.
16. Colom Díaz PA, Mistry JJ, Trowbridge JJ. Hematopoietic stem cell aging and leukemia transformation. *Blood*. 2023;142(6):533-542.
17. Zhu H, Guo ZK, Jiang XX, et al. A protocol for isolation and culture of mesenchymal stem cells from mouse compact bone. *Nat Protoc*. 2010;5(3):550-560.
18. Nakamura Y, Arai F, Iwasaki H, et al. Isolation and characterization of endosteal niche cell populations that regulate hematopoietic stem cells. *Blood*. 2010;116(9):1422-1432.
19. Weickert MT, Hecker JS, Buck MC, et al. Bone marrow stromal cells from MDS and AML patients show increased adipogenic potential with reduced Delta-like-1 expression. *Sci Rep*. 2021;11(1):5944.
20. Rachner TD, Link-Rachner CS, Bornhauser M, Hofbauer LC. Skeletal health in patients following allogeneic hematopoietic cell transplantation. *Bone*. 2022;158:115684.

21. Bartova E, Legartova S, Dundr M, Suchankova J. A role of the 53BP1 protein in genome protection: structural and functional characteristics of 53BP1-dependent DNA repair. *Aging (Albany NY)*. 2019;11(8):2488-2511.
22. Olivieri F, Albertini MC, Orciani M, et al. DNA damage response (DDR) and senescence: shuttled inflamma-miRNAs on the stage of inflamm-aging. *Oncotarget*. 2015;6(34):35509-35521.
23. Kruppa AJ, Kishi-Itakura C, Masters TA, et al. Myosin VI-dependent actin cages encapsulate parkin-positive damaged mitochondria. *Dev Cell*. 2018;44(4):484-499499.e6e486.
24. Kruppa AJ, Buss F. Actin cages isolate damaged mitochondria during mitophagy. *Autophagy*. 2018;14(9):1644-1645.
25. Florian MC, Dorr K, Niebel A, et al. Cdc42 activity regulates hematopoietic stem cell aging and rejuvenation. *Cell Stem Cell*. 2012;10(5):520-530.
26. Nalapareddy K, Zheng Y, Geiger H. Aging of intestinal stem cells. *Stem Cell Rep*. 2022;17(4):734-740.
27. Tiwari RL, Mishra P, Martin N, et al. A Wnt5a-Cdc42 axis controls aging and rejuvenation of hair-follicle stem cells. *Aging (Albany NY)*. 2021;13(4):4778-4793.
28. Gomes LC, Di Benedetto G, Scorrano L. During autophagy mitochondria elongate, are spared from degradation and sustain cell viability. *Nat Cell Biol*. 2011;13(5):589-598.
29. Konig T, Nolte H, Aaltonen MJ, et al. MIROs and DRP1 drive mitochondrial-derived vesicle biogenesis and promote quality control. *Nat Cell Biol*. 2021;23(12):1271-1286.
30. de Jonge JJ, Batters C, O'Loughlin T, Arden SD, Buss F. The MYO6 interactome: selective motor-cargo complexes for diverse cellular processes. *FEBS Lett*. 2019;593(13):1494-1507.
31. Tumbarello DA, Waxse BJ, Arden SD, Bright NA, Kendrick-Jones J, Buss F. Autophagy receptors link myosin VI to autophagosomes to mediate Tom1-dependent autophagosome maturation and fusion with the lysosome. *Nat Cell Biol*. 2012;14(10):1024-1035.
32. Ho TT, Warr MR, Adelman ER, et al. Autophagy maintains the metabolism and function of young and old stem cells. *Nature*. 2017;543(7644):205-210.
33. Harada K, Yahata T, Onizuka M, et al. Mitochondrial electron transport chain complex II dysfunction causes premature aging of hematopoietic stem cells. *Stem Cell*. 2023;41(1):39-49.
34. Wan MC, Tang XY, Li J, et al. Upregulation of mitochondrial dynamics is responsible for osteogenic differentiation of mesenchymal stem cells cultured on self-mineralized collagen membranes. *Acta Biomater*. 2021;136:137-146.
35. Li Q, Gao Z, Chen Y, Guan MX. The role of mitochondria in osteogenic, adipogenic and chondrogenic differentiation of mesenchymal stem cells. *Protein Cell*. 2017;8(6):439-445.
36. Zhang C, Li H, Li J, Hu J, Yang K, Tao L. Oxidative stress: a common pathological state in a high-risk population for osteoporosis. *Biomed Pharmacother*. 2023;163:114834.
37. Schreck C, Istvanffy R, Ziegenhain C, et al. Niche WNT5A regulates the actin cytoskeleton during regeneration of hematopoietic stem cells. *J Exp Med*. 2017;214(1):165-181.
38. Safiulina D, Kuum M, Choubey V, Hickey MA, Kaasik A. Mitochondrial transport proteins RHOT1 and RHOT2 serve as docking sites for PRKN-mediated mitophagy. *Autophagy*. 2019;15(5):930-931.
39. Qiu Y, Wang J, Li H, et al. Emerging views of OPTN (optineurin) function in the autophagic process associated with disease. *Autophagy*. 2022;18(1):73-85.
40. Fung TS, Chakrabarti R, Kollasser J, et al. Parallel kinase pathways stimulate actin polymerization at depolarized mitochondria. *Curr Biol*. 2022;32(7):1577-1592.e8.
41. Quach JM, Askmyr M, Jovic T, et al. Myelosuppressive therapies significantly increase pro-inflammatory cytokines and directly cause bone loss. *J Bone Miner Res*. 2015;30(5):886-897.
42. Weilbaecher KN. Mechanisms of osteoporosis after hematopoietic cell transplantation. *Biol Blood Marrow Transplant*. 2000;6(2A):165-174.
43. D'Souza AB, Grigg AP, Szer J, Ebeling PR. Zoledronic acid prevents bone loss after allogeneic haemopoietic stem cell transplantation. *Intern Med J*. 2006;36(9):600-603.
44. Russell RG. Bisphosphonates: mode of action and pharmacology. *Pediatrics*. 2007;119(suppl 2):S150-S162.
45. Dunford JE, Rogers MJ, Ebetino FH, Phipps RJ, Coxon FP. Inhibition of protein prenylation by bisphosphonates causes sustained activation of Rac, Cdc42, and Rho GTPases. *J Bone Miner Res*. 2006;21(5):684-694.
46. Tauchmanova L, Ricci P, Serio B, et al. Short-term zoledronic acid treatment increases bone mineral density and marrow clonogenic fibroblast progenitors after allogeneic stem cell transplantation. *J Clin Endocrinol Metab*. 2005;90(2):627-634.
47. Sweeney-Ambros AR, Biggs AE, Zimmerman ND, Mann KA, Damron TA, Oest ME. Orchestrated delivery of PTH [1-34] followed by zoledronic acid prevents radiotherapy-induced bone loss but does not abrogate marrow damage. *J Orthop Res*. 2022;40(12):2843-2855.
48. Lymperi S, Ersek A, Ferraro F, Dazzi F, Horwood NJ. Inhibition of osteoclast function reduces hematopoietic stem cell numbers in vivo. *Blood*. 2011;117(5):1540-1549.
49. Mansour A, Anginot A, Mancini SJ, et al. Osteoclast activity modulates B-cell development in the bone marrow. *Cell Res*. 2011;21(7):1102-1115.
50. Pundole X, Cheema HI, Petitto GS, Lopez-Olivo MA, Suarez-Almazor ME, Lu H. Prevention and treatment of bone loss and fractures in patients undergoing a hematopoietic stem cell transplant: a systematic review and meta-analysis. *Bone Marrow Transplant*. 2017;52(5):663-670.

51. Ebeling PR, Thomas DM, Erbas B, Hopper JL, Szer J, Grigg AP. Mechanisms of bone loss following allogeneic and autologous hemopoietic stem cell transplantation. *J Bone Miner Res*. 1999;14(3):342-350.

52. Serio B, Pezzullo L, Fontana R, et al. Accelerated bone mass senescence after hematopoietic stem cell transplantation. *Transl Med UniSa*. 2013;5(4):7-13.

53. Ukon Y, Makino T, Kodama J, et al. Molecular-based treatment strategies for osteoporosis: a literature review. *Int J Mol Sci*. 2019;20(10):2557.

54. Chandra A, Lagnado AB, Farr JN, et al. Targeted clearance of p21- but not p16-positive senescent cells prevents radiation-induced osteoporosis and increased marrow adiposity. *Aging Cell*. 2022;21(5):e13602.

55. Mukherjee S, Raje N, Schoonmaker JA, et al. Pharmacologic targeting of a stem/progenitor population in vivo is associated with enhanced bone regeneration in mice. *J Clin Invest*. 2008;118(2):491-504.

56. Chandra A, Wang L, Young T, et al. Proteasome inhibitor bortezomib is a novel therapeutic agent for focal radiation-induced osteoporosis. *FASEB J*. 2018;32(1):52-62.

57. Peterson JR, Lebensohn AM, Pelish HE, Kirschner MW. Biochemical suppression of small-molecule inhibitors: a strategy to identify inhibitor targets and signaling pathway components. *Chem Biol*. 2006;13(4):443-452.

58. Chandra A, Lin T, Young T, et al. Suppression of sclerostin alleviates radiation-induced bone loss by protecting bone-forming cells and their progenitors through distinct mechanisms. *J Bone Miner Res*. 2017;32(2):360-372.

59. Touaitahuata H, Blangy A, Vives V. Modulation of osteoclast differentiation and bone resorption by Rho GTPases. *Small GTPases*. 2014;5:e28119.

60. Yao S, Smiley SL, West K, et al. Accelerated bone mineral density loss occurs with similar incidence and severity, but with different risk factors, after autologous versus allogeneic hematopoietic cell transplantation. *Biol Blood Marrow Transplant*. 2010;16(8):1130-1137.